2016

Oscillating Heat Pipe Performance with Evaporator Section Modifications

Mitchell Hoesing
South Dakota State University

OSCILLATING HEAT PIPE PERFORMANCE WITH EVAPORATOR SECTION MODIFICATIONS

BY

MITCHELL HOESING

A thesis submitted in partial fulfillment of the requirements for the

Master of Science

Major in Mechanical Engineering

South Dakota State University

2016

OSCILLATING HEAT PIPE PERFORMANCE WITH EVAPORATOR SECTION MODIFICATIONS

This thesis is approved as a creditable and independent investigation by a candidate for the Master of Science in Mechanical Engineering degree and is acceptable for meeting the dissertation requirements for this degree. Acceptance of this does not imply that the conclusions reached by the candidates are necessarily the conclusions of the major department.

Gregory Michna, Ph.D.
Thesis Advisor Date

Kurt Bassett, Ph.D.
Head, Department of Mechanical Engineering Date

Dean, Graduate School Date

ACKNOWLEDGEMENTS

I would like to thank the Mechanical Engineering faculty at SDSU for the constant help and support throughout my academic career. In particular, I would like to express my great appreciation to Dr. Gregory Michna, who allowed so many doors to be opened in my life. I also want to thank Dr. Stephen Gent, Dr. Jeffery Doom, and Dr. Brain Graeb for being on my graduate committee and their thoughtful feedback.

I also wish to thank Maddy Sullivan for her support during the failures and successes of this project. I also thank my family whose love and support allowed me to get where I am today. Finally I want to thank Howard Hoesing, whose never ending encouragement and guidance will be greatly missed. Miss you and love you always Dad.

TABLE OF CONTENTS

LIST OF FIGURES vii

LIST OF TABLES x

NOMENCLATURE xi

ABSTRACT xii

Chapter 1 – MOTIVATION 1

Chapter 2 – LITERATURE REVIEW 3

2.1 - Extruded-Fin Heat Sinks 3

2.2 - Liquid Cooling 4

2.3 - Immersion Cooling 6

2.4 - Spray Cooling 6

2.5 - Heat Pipes 7

2.6 - Oscillating Heat Pipes 8

2.6.1 – Oscillating Heat Pipe Operational Dependence 11

2.7 - OHP Designs 22

2.7.1 -Open Loop/Closed Loop 22

2.7.2 - Check Valves 24

2.7.3 - Three-Dimensional Geometries 26

2.7.4 - Varying Channel Diameter 28

2.7.5 - Wicking OHP 29

2.7.6 - Other Configurations 30

2.8 - Modeling 31

2.9 – Research Objective 32

Chapter 3 - METHODOLOGY 33

2.1 - Apparatus 33

2.3 – Geometric Variations 39

2.4 – Data Reduction 43

2.5 - Heat Loss Experiment 44

2.6 - Test Metric 45

Chapter 4 – RESULTS 47

3.1 - Performance 47

3.1.1 – Straight-Channel OHP 47

3.1.2 – Pin-and-Cavity OHP 51

3.1.3 – Recessed-Cavity OHP 54

3.1.4 – Wavy-Channel OHP 58

3.2 - Geometry Comparison 61

3.3 – Effective Heat Transfer Coefficient 75

Chapter 5 – CONCLUSIONS 77

Chapter 6 – FUTURE WORK 80

LITERATURE CITED ii

Appendix A – ERROR PROPAGATION..... vii

LIST OF FIGURES

Figure 1: Approximate range of heat transfer coefficients of selected cooling technologies [3]. 4

Figure 2: Left: Example of indirect liquid cooling, Right: Example of direct liquid cooling [4]. 5

Figure 3: Cold plate from LYTRON® [5]. 5

Figure 4: Immersion cooling schematic with forced convection [4]. 6

Figure 5: Spray cooling [9]. 7

Figure 6: Oscillating heat pipe (OHP) schematic [19]. 10

Figure 7: Left: Open loop oscillating heat pipe, Right: Closed loop oscillating heat pipe [18]. 23

Figure 8: Oscillating heat pipe with check valves [55]. 24

Figure 9: Oscillating heat pipe with ball type check valve [57]. 25

Figure 10: Tesla-type check valve [20]. 26

Figure 11: Staggered channels in three-dimensional OHP [58]. 27

Figure 12: Section A-A showing channel of uniform diameter and Section B-B showing non-uniform diameter (crushed) channel [63]. 29

Figure 13: Left: U-shaped oscillating heat pipe, Right: L-Shaped oscillating heat pipe.. 30

Figure 14: Cross section view of OHP showing relevant geometry (Units: mm). 34

Figure 15: Schematic of OHP apparatus. 35

Figure 16: Thermocouple locations. 36

Figure 17: The assembled test apparatus, showing the valve manifold used for charging and degassing. 38

Figure 18: Straight-channel geometry (Units: mm). 40

Figure 19: Pin-and-cavity geometry (Units: mm). 41

Figure 20: Reentrant-cavity geometry (Units: mm). 42

Figure 21: Wavy-channel geometry (Units: mm). 43

Figure 22: Heat loss experimental data and best fit line presenting Q_{loss} as a function of the difference between evaporator and ambient temperatures. 45

Figure 23: Area of heat transfer 46

Figure 24: Straight-channel OHP performance, 0° inclination angle. 48

Figure 25: Straight-channel OHP evaporator temperature, 0° inclination angle. 49

Figure 26: Straight–channel OHP performance, 45° inclination angle. 50

Figure 27: Straight-channel OHP performance, 90° inclination angle. 51

Figure 28: Pin-and-cavity OHP performance, 0° inclination angle. 52

Figure 29: Pin-and-cavity OHP performance, 45° inclination angle. 53

Figure 30: Pin-and-cavity OHP performance, 90° inclination angle. 54

Figure 31: Recessed-cavity OHP performance, 0° inclination angle. 55

Figure 32: Recessed-cavity OHP performance, 45° inclination angle. 57

Figure 33: Recessed-cavity OHP performance, 90° inclination angle. 58

Figure 34: Wavy-channel OHP performance, 0° inclination angle. 59

Figure 35: Wavy-channel OHP performance, 45° inclination angle. 60

Figure 36: Wavy-channel OHP performance, 90° inclination angle. 61

Figure 37: Performance comparison, 35% fill ratio with 90° inclination angle. 62

Figure 38: Performance comparison, 55% fill ratio with 90° inclination angle. 63

Figure 39: Performance comparison, 75% fill ratio with 90° inclination angle. 64

Figure 40: Performance comparison, 35% fill ratio with 45° inclination angle. 65

Figure 41: Performance comparison, 55% fill ratio with 45° inclination angle. 66

Figure 42: Performance comparison, 75% fill ratio with 45° inclination angle. 67

Figure 43: Performance comparison, 35% fill ratio with 0° inclination angle. 68

Figure 44: Performance comparison, 55% fill ratio with 0° inclination angle. 69

Figure 45: Performance comparison, 75% fill ratio with 0° inclination angle. 70

Figure 46: Average thermal resistance of each geometry. 72

Figure 47: Average thermal resistance comparison for each geometry in each case. 73

Figure 48: Average thermal resistances, excluding 0° inclination angle. 74

Figure 49: Heat transfer coefficient comparison of various cooling technologies [3]..... 76

LIST OF TABLES

Table 1: Channel size ranges for commonly used heat pipe working fluids. 13

Table 2: Working fluid properties of significance to OHP operation. 16

Table 3: Design of experiment. 39

Table 4: Average thermal resistance for each case, averaged over all heating input levels. 71

Table 5: Maximum heat transfer rate for each case. 75

NOMENCLATURE

a	Adiabatic Coefficient
A_{xs}	Cross Sectional Area, m^2
B	Bulk Modulus, N/m
Bo	Bond Number.
D_h	Hydraulic Diameter, m
D_{max}	Maximum Hydraulic Diameter, m
g	Gravity, m/s^2
k	Thermal Conductivity, W/m-K
P_{in}	Power Input, W
Q_{loss}	Heat Loss from OHP, W
Q_{OHP}	Heat Transfer through OHP, W
R	Gas Constant, J/kg-K
R_{th}	Thermal Resistance, K/W
T	Temperature, K
T_C	Condenser Temperature, °C
T_E	Evaporator Temperature, °C
T_{ave}	Time-average Temperature, K
We	Weber Number, -
ρ_l	Liquid Density, kg/m^3
ρ_v	Vapor Density, kg/m^3
σ	Surface Tension, N/m

ABSTRACT

OSCILLATING HEAT PIPE PERFORMANCE WITH EVAPORATOR SECTION MODIFICATIONS

MITCHELL HOESING

2016

The continuous development of electronic components to become faster and smaller has led to an increasing problem with thermal management. Thermal management ensures that the component operating temperatures are within a safe range, which maintains performance and improves reliability and lifespan. Traditional thermal management devices, such as the extruded-fin heat sink, are incapable of maintaining the safe operating temperature range for current and future high heat flux cooling applications. A device that has the capability to meet this growing need is the oscillating heat pipe.

Oscillating heat pipes (OHPs) are passive, two-phase cooling devices that have been shown to transfer very large amounts of thermal energy over large distances, resulting in low thermal resistances. OHPs consist of two main sections: the condenser and evaporator that are interconnected by looping channels. The channels are filled with a two-phase mixture of acetone, which acts as the heat transfer medium for the system.

In this study, geometric features in the evaporator section are compared to determine operational effects. Four OHP evaporator geometries are compared: traditional straight-channels, pin-and-cavity channels, recessed-cavities, and wavy-channels. Each

OHP is constructed from a flat aluminum plate with 22 interconnected 2-mm × 2-mm square channels. These geometries were tested at 35%, 55%, and 75% fill ratios and at vertical, 45°, and horizontal inclination angles.

It was found that the wavy-channel, straight-channel, recessed-cavity, and pin-and-cavity OHPs had an overall thermal resistance of 0.32 K/W, 0.49 K/W, 0.37 K/W, and 0.60 K/W, respectively. This corresponds to a 41% and 28% improvement for the wavy-channel and recessed-cavity OHPs, and a 30% reduction in performance for the pin-and-cavity OHP. The wavy–channel OHP was the only geometry that was fully functional in the horizontal orientation, achieving an average thermal resistance of 0.17 K/W with a 55% fill ratio. The recessed-cavity OHP preformed the best above horizontal, where an average thermal resistance of 0.18 K/W was found. The best thermal resistance was 0.11 K/W by the recessed-cavity OHP at vertical orientation and 35% fill ratio.

The wavy-channel and recessed-cavity OHPs both showed significant improvements over straight-channel and pin-and-cavity geometries. This indicates that geometric variations can be integrated into OHP designs to improve system performance.

CHAPTER 1 – MOTIVATION

The miniaturization and improvement in performance of electronics has led to thermal management becoming a major limiting factor in future development. Therefore, there is a need for devices that can effectively dissipate very high heat fluxes and maintain acceptable operating temperatures [1]. High heat fluxes are encountered in numerous applications including performance supercomputers, electric vehicles, and advanced military electronics [2]. Conventional cooling methods are either incapable of maintaining the operational temperature at these high heat fluxes or are not practical for the application.

The growing demand on thermal management has led to a push to develop new cooling technologies. From this push, the oscillating heat pipe (OHP) has shown great potential to be a viable heat transfer device for high heat flux cooling applications. The OHP has several advantages over other thermal devices such as passive operation, low complexity, and lower price.

An OHP is a simple device consisting of multiple interconnected channels that loop back and forth between the evaporator and condenser sections. The channels are filled with a two-phase working fluid that is the heat transfer medium. The temperature difference between the evaporator and condenser sections leads to the force that drives the fluid flow, ultimately creating a passive cooling device.

In order for the OHP to become a viable option for cooling applications, the fundamental operating principles of an OHP must be further understood. By using theoretical modeling and experimentation there has been substantial progress in understanding the operating behavior and performance of OHPs in recent years. Yet, there are still several areas that need to be explored further to fully understand the capability of the OHP as a thermal management device.

One area of study that has a deficiency in the understanding is how geometric variations affect performance of the OHP. There have been several studies which look at variations in channel size and count, but the effect of adding various features to the channel geometry is unknown. The purpose of this paper is to begin to fill this void of knowledge by experimentally investigating the behavior of three unique geometries and a traditional straight-channel OHP and comparing performance between the four OHPs.

The three unique geometries were developed to increase contact area with the working fluid and to increase the turbulence within the system. Both properties should result in better heat transfer characteristics over a traditional straight-channel OHP; however, by adding these features, a pressure drop penalty is incurred. At this point, it is understood that pressure drop does play an important role in OHP operation, but how significant of a role is not well understood.

This study will investigate how geometric features affect OHP performance. Further understanding of OHP operating principles is needed to meet the growing thermal management needs of future technologies.

CHAPTER 2 – LITERATURE REVIEW

2.1 - Extruded-Fin Heat Sinks

The most common thermal management device is the extruded-fin heat sink. Extruded-fin heat sinks are designed to transfer heat to air, with the fin structures increasing the surface area available for heat transfer. The increased surface area allows these heat sinks to be effective heat transfer devices when transferring heat to air, a poor thermal fluid. Generally, heat sinks are made of aluminum or copper, but other high conductive materials or alloys may be used. Heat sinks can come in a variety of shapes, configurations, fin lengths, colors, etc. The variability of a heat sinks allows it to be designed for particular cooling applications such as central processing unit (CPU), electro-mechanical, and light emitting diodes (LEDs) cooling for example.

Heat sinks will fall into two primary categories: natural (passive) and forced convection. Passive heat sinks rely on the buoyancy of the fluid to create fluid motion that drives heat transfer. This type of heat sink requires no external energy source to function and is very simple and inexpensive. A major drawback of passive heat sinks is the limited obtainable heat transfer rate. When air is used as the working fluid, approximately 10 W/m^2-K (.06 W/cm^2 assuming 60 °C temperature difference) is achievable (Figure 1).

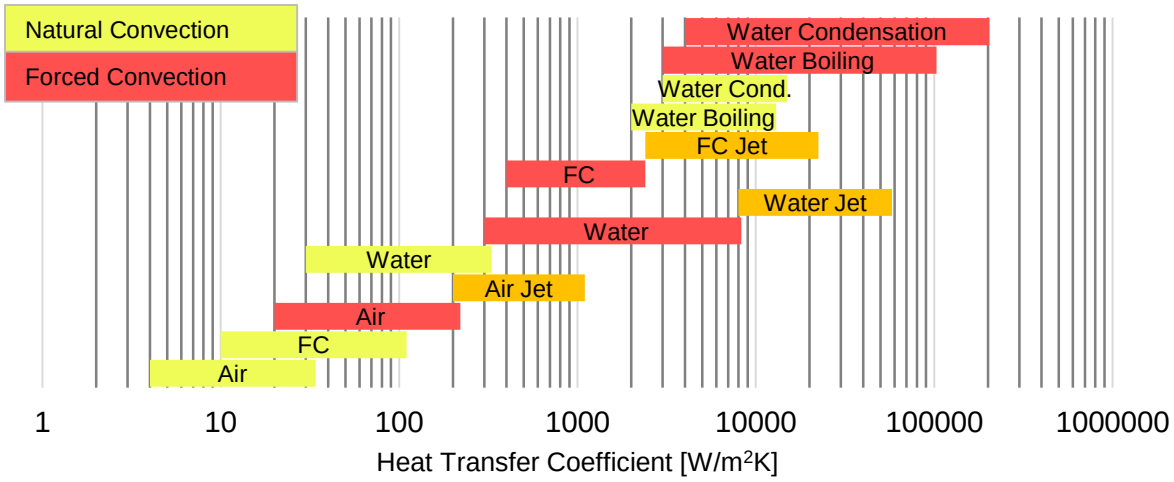

Figure 1: Approximate range of heat transfer coefficients of selected cooling technologies [3].

To increase the cooling capacity of heat sinks, it is common to mount a fan to induce forced convection heat transfer. As a result, the heat transfer coefficient improves, but a maximum heat transfer coefficient of approximately 200 W/m^2-K is the upper limit for air [3]. The primary disadvantages of these systems are the limited heat flux and the requirement for an external power source, which may not be practical to integrate into the system and increases operating cost.

2.2 - Liquid Cooling

Generally, liquid cooling of electronics is divided into two types: direct and indirect cooling. In direct liquid cooling, the fluid comes into direct contact with the components. Conversely, in indirect cooling, the fluid does not directly contact any of the components (Figure 2). An example of indirect cooling is a cold plate.

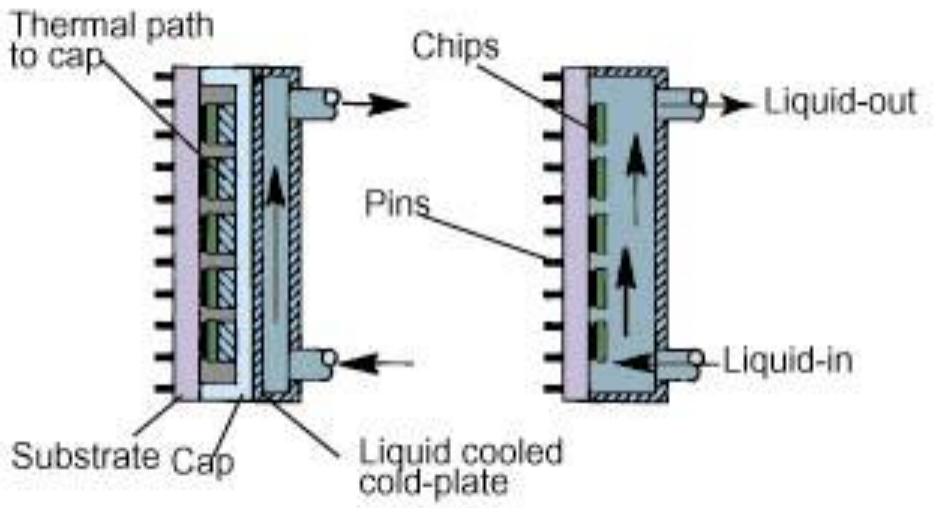

Figure 2: Left: Example of indirect liquid cooling, Right: Example of direct liquid cooling [4].

Cold plates are heat sinks that use liquid instead of air for the heat transfer medium. In a cold plate, liquid is pumped through channels (Figure 3) where it absorbs heat and transfers it away from the device. This type of cooling device is commonly used when air-cooling is insufficient due to heat transfer or space limitations. Cold plates have been used in data centers, medical equipment, electronics, and other high heat transfer applications.

Figure 3: Cold plate from LYTRON® [5].

2.3 - Immersion Cooling

Immersion cooling is a direct cooling method in which the components are submerged in a dielectric cooling fluid such as FC-72 or other Flourinerts. Natural convection or forced convection (Figure 4) can be used, as well as pool boiling or flow boiling. Natural convection with FC-72 can produce equivalent heat fluxes to that of forced convection using air (Figure 1). Typical heat fluxes for pool boiling range from 10 to 15 W/cm^2, while for flow boiling the heat flux is in the range of 25 to 30 W/cm^2[6]. The limiting factor in immersion cooling with boiling is the critical heat flux, where vapor bubbles become so prevalent that liquid access to the surface is restricted. As a result, the heat transfer coefficient rapidly decreases and the device temperature increases drastically.

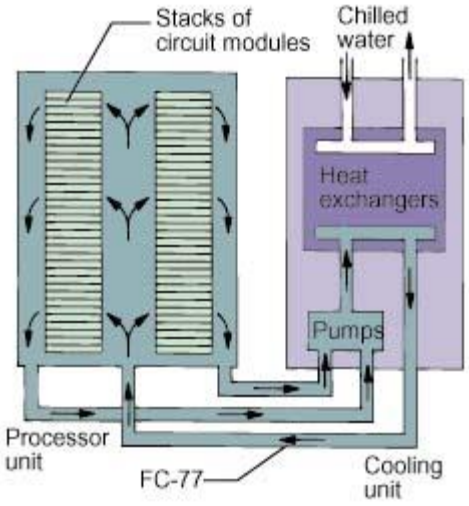

Figure 4: Immersion cooling schematic with forced convection [4].

2.4 - Spray Cooling

In spray cooling (Figure 5), liquid is forced through a small orifice and is dispersed to form small droplets that contact a heated surface. The droplets then evaporate or form a thin film on the surface. Due to the phase change during evaporation and single phase convection effects, large amounts of heat are transferred. Spray cooling can achieve

higher rates of heat transfer than pool boiling. It has produced heat fluxes in the range of 50 W/cm^2-60 W/cm^2, but these heat fluxes can vary based on surface enhancements, nozzle, and fluid velocity [7]. Spray cooling is advantageous because of the possibility for uniform cooling, no overshoot, and low impact velocity of droplets. Disadvantages include the need for a pump and filters and to transport excess liquid and vapor to a condenser [7]. The fluid can also be propelled at a high velocity at a surface, this is called jet impingement. The use of jet impingement has produced heat fluxes in excess of 100 W/cm^2 [8].

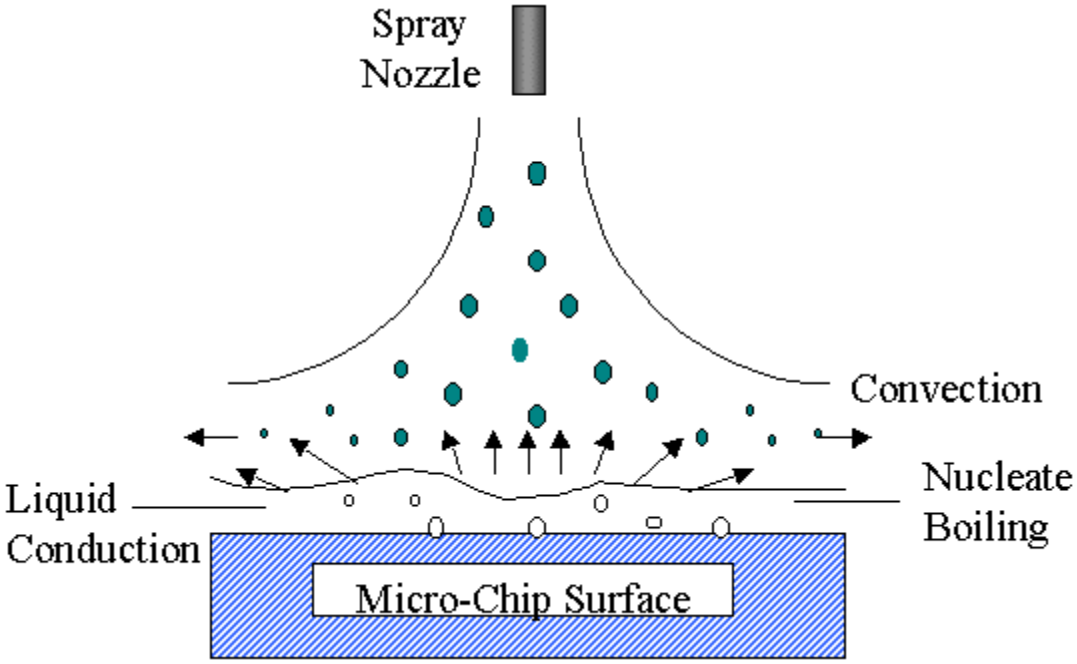

Figure 5: Spray cooling [9].

2.5 - Heat Pipes

Heat pipes are two-phase heat transfer devices that take advantage of latent heat transfer to reduce thermal resistance. A heat pipe is a fluid-filled tube with a wicking structure along the inside perimeter. There are two primary regions, the evaporator and condenser sections, with an adiabatic section between being optional.

Heat is input to the evaporator section of a traditional heat pipe. This changes the working fluid to a vapor, and the vapor is then transferred to the condenser section. In the condenser section, heat is removed and the fluid condenses into the liquid phase. Wicking structures next to the inner walls of the heat pipe transfer the fluid back to the evaporator section. The wicking structure acts as a capillary pump to bring the liquid back to the evaporator section. The wicking structure also enhances heat transfer due to the additional surface area [10].

Heat pipes in production can handle heat transfer rates up to 50 W/cm^2 [11]. Axial grooves have also been used instead of the wicking structure for heat pipes. With this set up the heat pipe can handle heat fluxes up to 40 W/cm^2 [12]. Heat pipes have several advantages over other electronic cooling devices including large equivalent thermal conductance, excellent packaging flexibility, passive operation, and high reliability [10].

The main limitation of traditional heat pipes is the capillary limit. Capillary action within a heat pipe causes the fluid to circulate from condenser to evaporator. If a large heat input is applied, the capillary force may not be able to return the fluid to the evaporator before dry-out occurs[13]. Due to this limitation, an alternative heat pipe, known as an oscillating heat pipe (OHP) is being researched and developed.

2.6 - Oscillating Heat Pipes

Oscillating Heat Pipes (OHPs) were first developed by Akachi et al. [14, 15] in the early 1990s. In recent years, research efforts have been increased to develop the OHP into a viable thermal management device. The primary applications for OHPs are electronics,

including the special applications of satellite and laser cooling systems [16]. Other possible applications include preheating air in a dryer proposed by Rittidech et al. [17]. In this application, the heat from the outlet hot air from a dryer is transfer to the cool inlet air using an OHP. This improves the efficiency of the system by preheating the air coming into the system with heat that would otherwise be wasted.

OHPs, like traditional heat pipes, are two-phase heat transfer devices. However, unlike traditional heat pipes, latent heat transfer is used primarily to drive the fluid flow while sensible heat transfer is the primary (95%) heat transfer mechanism [18]. It has been shown that because OHP's channels are on the capillary scale, the working fluid in the OHP can be moved from the condenser to evaporator sections without the wicking structure required in traditional heat pipes.

An OHP consists of three primary regions: the evaporator, condenser, and adiabatic sections. These sections are interconnected by several looping channels (Figure 6). The channels are filled with a two-phase working fluid, which acts as the heat transfer medium.

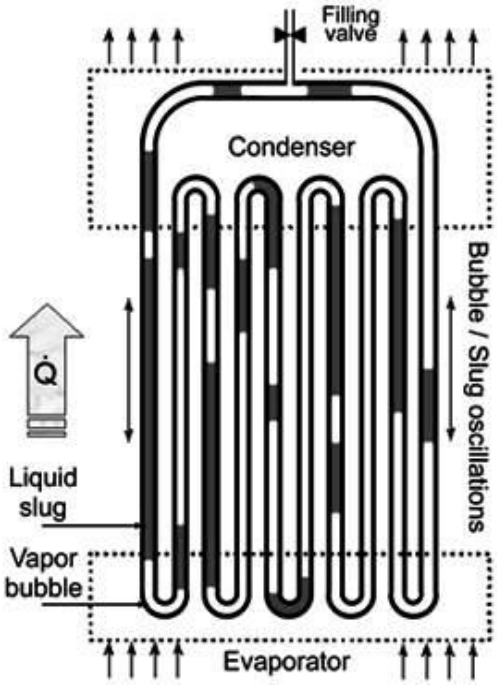

Figure 6: Oscillating heat pipe (OHP) schematic [19].

Effective operation depends on the working fluid being circulated continuously, thus certain operational limits dictate when the OHP will function properly. A minimum temperature difference, and a corresponding pressure difference, is required between the evaporator and condenser sections to begin the fluid oscillation. If the minimum temperature difference is not met, there will not be a sufficient pressure differential to drive the fluid flow. The minimum temperature difference is dependent on the fluid, but ranges from only a few degrees to around 15 ºC for water. The upper operating limit is caused by the boiling limit of the fluid [13]. When the evaporator temperature becomes so hot that the fluid vaporizes before reaching the evaporator wall, the result is dry-out, causing temperature spikes. If either of these limits is met, an OHP will not function effectively.

As heat is inputted into the evaporator, small temperature instabilities are created between each channel. This causes pressure differentials that drive the fluid motion through the system. OHPs are inheritably unstable and must be to operate. If channels were at the same temperatures across the transverse direction, there would be no net driving force in the system, and the fluid would become stagnant. By utilizing multiple interconnected channels and system instabilities, the working fluid is moved from the evaporator and condenser sections, thus removing the need for the wicking structure in traditional heat pipes.

By removing the wicking structure, OHPs are simpler, lighter devices that can be easier and cheaper to manufacture than traditional heat pipes, while having a wider range of form factors and fewer operating limits such as temperature range and heat transfer rate [20]. Increased heat transfer capability is attributed to the majority of the heat transfer being caused by forced convection and the transfer of sensible heat, unlike in traditional heat pipes where heat transfer is dominated by latent heat exchange [18]. Also, OHPs have been shown to be gravity and inclination independent above a critical heat flux, especially when channel counts exceed 80 turns [15, 16] . This strengthens the case for their application in aerospace cooling.

2.6.1 – Oscillating Heat Pipe Operational Dependence

The design of OHPs includes the selection of several different parameters to ensure proper operation. The primary considerations are geometry, fill ratio, working fluid, heat input, and inclination angle. By varying these parameters, an OHP’s performance can be adjusted to meet a specific application.

2.6.1.1 - Geometry

One of the design parameters that has the greatest effect on overall performance is the geometry of the OHP. The geometry includes channel size, count, shape, length, and the size of the evaporator and condenser sections.

Channel size is an important parameter that directly links to the working principles of the OHP. Because OHPs work on the principle of capillary forces, the channels must be sized appropriately so that the working fluid can create vapor bubbles separated by liquid slugs due to surface tension. A useful dimensionless parameter commonly used to determine the appropriate range of size for the channels is the Bond number. The Bond number is a dimensionless parameter that relates the magnitude of surface tension forces to body forces. Equation 1 shows the Bond number for terrestrial applications [16].

$$Bo = \frac{D^2 g(\rho_l - \rho_v)}{\sigma} \quad (1)$$

The Bond number is used to determine the maximum channel size by determining what channel diameters the capillary force of the fluid equals the gravitational force. An upper limit of the Bond number for proper operation is considered to be between 3.39 and 4. A lower limit has also been proposed between 0.36 and 0.49 [16]. Outside of these ranges, the working fluid will be unable to form vapor bubbles and pulsate.

An alternative equation proposed by Gu et al. [21] for determining the maximum channel size in microgravity environments is shown in Equation 2. Gu et al. proposed this

equation by stating that a stable slug/plug flow is achieved if the liquid's kinetic energy per unit volume is less than the slug's surface energy per unit volume

$$D_{max} \leq \frac{4\sigma}{\rho_l v^2} \tag{2}$$

This can also be represented using the Weber number (Equation 3). The Weber number is a dimensionless parameter that relates fluid inertia to surface tension and is commonly used in multiphase flow. Combining the Weber number and Equation 2, Equation 3 can be derived.

$$We = \frac{\rho_l v^2 D_h}{\sigma} \tag{3}$$

$$We \leq 4 \tag{4}$$

Table 1 shows the maximum and minimum channel diameters for commonly used working fluids. These values were determined using Equations 1 and 2. The fluid properties were evaluated at 70 °C, and the fluid velocity was assumed to be 0.1 m/s. The velocity was determined from a study conducted by Xu et al. [22], where a high speed visual flow analysis was conducted. The maximum diameter for microgravity applications is approximately five times greater than terrestrial application under these conditions.

Table 1: Channel size ranges for commonly used heat pipe working fluids.

	D_{min}, mm	D_{max}, mm	D_{max} μg, mm
Water	1.81	4.67	26.38
Acetone	1.09	2.79	9.37
Ethanol	1.11	2.86	9.89
Methanol	1.11	2.86	9.94

According to Equation 2, the maximum channel size diameter for microgravity applications will be reduced as the velocity of the fluid is increased. This relationship impacts the geometric configuration of an OHP in microgravity applications. The number of turns, distance between evaporator and condenser, and maximum heat input may vary from terrestrial OHPs. In general, smaller diameter OHPs will require larger heat inputs [16, 23]. Likely, an optimal relationship exist between inertial, surface tensions, and viscous forces that will allow for operation over a wide range of gravitational conditions [16].

Channel shape can also have effects on OHP performance. Studies by Yang et al. [24] and Khandekar et al. [25] indicate that thermal resistance can be reduced when square channels have low fill ratios and are vertically heated. This is due to the sharp edges of the channels acting as a capillary structure, effectively creating a gravity-assisted thermosyphon. OHPs with high fill ratios and/or circular channels will not see this effect.

2.6.1.2 - Fill Ratio

Fill ratios between 25-75% are considered the operation range of OHPs with commonly used working fluids such as water, acetone, and refrigerants [24-26]. Fill ratios outside of this range could negatively affect the performance of the OHP. When the fill ratio is less than 25%, it is possible the evaporator section will dry-out, resulting in much higher temperatures. Similarly, if the fill ratio is greater than 75%, the high fluid volume may dampen the oscillatory motion by limiting the amount of fluid that can be in the vapor phase. Less fluid in the vapor phase means that there will be a reduction in driving force within the OHP as more fluid will require a larger pressure drop, resulting in higher

evaporator temperatures [18]. Yin et al. [27] developed a numerical model, Equation 5, which can be used to predict the maximum fill ratio. This model was verified with experimental data, and correlated well with findings from Groll et al. [28] for maximum fill ratio.

$$\phi_{max} = \frac{1}{1+\left(\frac{aRT\rho}{B}\right)^{\frac{1}{2}}} \tag{5}$$

2.6.1.3 - Working Fluid

Another important parameter is the working fluid. The two-phase working fluid is the heat transfer medium. The selection of the working fluid is dependent on many criteria: compatibility with wall material, good thermal stability, latent heat, surface tension, thermal conductivity, liquid and vapor viscosities, vapor pressure over operating temperature range, and wettability of wall materials [29]. Because there are several criteria for selecting a working fluid, various fluids have been studied to determine operating characteristics.

Table 2 presents four commonly used working fluids in heat pipe technology and their values for those properties that have been determined to have significant impact on performance. The first property listed is latent heat of vaporization (LHV). This property is important as it can give an indication to how much energy will be required to cause the necessary phase change of the fluid for proper operation. It is ideal to have lower values, as this means oscillations can begin with less energy required.

Low dynamic viscosity is also ideal. With lower viscosity less force will be required to generate flow. Surface tension is also closely related to force requirements. If there is a

significant difference in surface tension between fluids, then according to the Bond number, the channel will have to be reduced in sized for operation. This will then increase the pressure drop within in the system.

Since OHPs have been found to primarily transfer heat via sensible heat, specific heat capacity is also important. The larger the specific heat capacity of the fluid, the more thermal energy that can be transferred per unit mass for a given temperature difference. Finally, the change in saturation pressure with temperature is very important, as this is the primary driving force behind the OHP operation. In this case, the largest change of saturation pressure with changes in temperature will result in oscillations at lower temperature differences.

Table 2: Working fluid properties of significance to OHP operation.

	Deionized Water	Methanol	Ethanol	Acetone
Liquid Density (kg/m^3)	998	791	789	792
Specific Heat (Liquid) (kJ/kg-°C)	4.18	2.48	2.39	2.35
Latent Heat of Vaporization (LHV) (kJ/kg)	2257	1101	846	523
(dp/dT) @80° (Pa/°C)	1.92×10^{-3}	6.45×10^{-3}	4.23×10^{-3}	6.27×10^{-3}
Dynamic Viscosity (Pa-s)	1.01×10^{-3}	0.60×10^{-3}	1.15×10^{-3}	0.32×10^{-3}
Surface Tension (N/m)	72.8×10^{-3}	72.6×10^{-3}	22.8×10^{-3}	23.7×10^{-3}

Properties at standard ambient conditions unless otherwise noted.

From this, the ideal fluid would have a low LHV, low viscosity, low surface tension, high specific heat capacity, and high dp/dT. The underlined values in Table 2 correspond to the best values for each property. Acetone has the best fluid property characteristics for two of the parameters: LHV and viscosity. This indicates that acetone will have better start up characteristics. Methanol has the best dp/dT, only slightly better than acetone. Water has by far the best specific heat capacity, indicating it may be well suited for high heat transfer applications.

OHPs are applicable to a wide array of cooling applications, largely due to the variety of working fluids. A particular application will dictate which working fluid will be best suited. For example, in cryogenic applications neon and nitrogen have been used [30, 31]. The characteristics of these fluids make them well suited for the temperature range (below -150 °C) associated with cryogenic applications. It was found that even at these low temperatures that the OHP was able to transfer 380W, indicating it operated well in sub-zero temperatures required for cryogenic cooling [31].

Hathaway and Ma et al. [32] studied an OHP using acetone and water as working fluids. It was observed that the acetone began oscillating sooner than water for the same power input. Acetone also had a much lower temperature difference between evaporator and condenser. Water was found to have a greater heat transfer capacity at higher heating powers than acetone. Top heating was studied to determine gravity dependence, here again acetone obtained operation sooner than water.

Maydanik et al. [33] studied an OHP used as a compact cooler for electronics. Three fluids were investigated: water, methanol, and R-141b. It was observed that water required the largest power input to cause pulsations, followed by methanol, and then R-141b.

Han et al. [34] studied the effects of different fluids in an OHP. Water, methanol, ethanol, and acetone were used. It was found that for a given fill ratio, the fluid with the lower latent heat of vaporization is more likely to dry-out, in this case acetone. At high heat inputs, the specific heat and latent heat of vaporization of the fluid became the primary properties for overall performance. As the heat input increased, the thermal resistance of all fluids converged, indicating that a limit is reached in performance that is dependent on the OHP itself, i.e. material and structure. It was also observed that dynamic viscosity is a dominant fluid property for start-up.

Cui et al. [35] studied an OHP with water, methanol, ethanol, and acetone as working fluids. It was found as heat input was increased, that the performance of these fluids became similar as long as dry-out did not occur, agreeing with the study by Han et al. [34].

Nanofluids have gained much interest in recent years, due to the potential to have better heat transfer qualities than pure fluids. As a result, several studies have been conducted utilizing nanofluids in OHPs.

Qu and Wu [36] studied an OHP that used an aqueous nanofluid as the working fluid. The SiO_2/water mixture reduced the performance of the OHP when compared to pure water as the working fluid. Al_2O_3/water was shown to improve the performance of the OHP over pure water; a 25.7% reduction in thermal resistance was observed for this mixture. This improvement was attributed to a change in the surface condition of the channels in the evaporator and condenser sections. As the fluid was transferred though the OHP, the nanoparticles were deposited on the wall, creating nucleation sites.

Ma et al. [37, 38] studied an OHP with a diamond naoparticle/water mixture as the working fluid. It was found that oscillating motion of the fluid can suspend the particles in the fluid. As a result, the heat transport capacity of the nanofluid was increased. It was determined that using a nanofluid in an OHP can significantly increase the heat transfer capacity.

Peng et al. [39] studied an OHP that contained two layers of channels. Acetone, water, diamond/acetone, gold/water, and diamond water nanofluids were used as working fluids. When water was used as the base, or pure working fluid, greater heat transfer capacity was achieved over acetone. In general, it was observed that when nanofluids were used in low concentrations, thermal resistance decreased. However, in high concentrations, capacity was reduced because the particles were collecting in the turns, causing blockages.

2.6.1.4 - Heat Input

Heat input also affects performance. Several analyses of OHP performance indicate that as heat input is increased, the thermal resistance decreases [24, 40, 41]. It has also been shown that the heat removal rate from the condenser section by the cooling mechanism, i.e. cooling bath or air stream, can limit the minimum thermal resistance that can be achieved by the OHP [42].

Hu et al.[43] studied a flat plate OHP, focusing on start-up performance. It was found that start up is linked to heating power and filling ratio. It was also found that when heating orientation was varied, i.e. top heating and bottom heating, the optimal fill ratio changes. Bottom heating required less power for start-up and produced a lower thermal resistance when compared to top heating.

In a study by Lin et al. [44], an OHP was developed for LED cooling. It was found that as the condenser temperature was warmed, the thermal resistance of the OHP was reduced. The effect of condenser temperature decreased as heating power increased. It was also found that by increasing the number of the channels, the thermal resistance was reduced.

Similarly Hansen et al. [45] observed lower thermal resistance when a warmer condenser temperature was used. When the condenser temperature was set to 30 °C instead of 20 °C, a significant reduction in the thermal resistance was found, even at lower power inputs.

Jiansheng et al. [46] looked into the effects of how heat is applied. It was found that by varying the heating patterns, such that the heating pattern was non-uniform, could shorten start-up time. But non-uniform heating causes the thermal resistance to increase, so uniform heating should be used for steady-state operation.

2.6.1.5 - Inclination Angle

Orientation of the OHP plays a significant role in operation, although many modeling efforts have assumed that operation is not directly dependent on gravity [14, 15]. The thermal resistance of an OHP can depend on the inclination angle. Several apparatuses were non-operational in the horizontal and/or top heat configurations [19, 47-49]. By increasing the inclination angle to a threshold level above horizontal, the OHP would begin to operate, although at a reduced performance level compared to vertical orientation.

In a studies by Charoensawn et al. [23, 25], it was determined that a minimum number of channels is required for operation in the horizontal orientation. In the vertical orientation, thermal resistance was decreased as channel count increased. It was theorized that by increasing the channel count the inhomogeneity, or chaos, of the system would increase. This increase in inhomogeneity results in a stronger driving force for fluid flow improving performance. In a study be Khandekar et al. [50], it was stated that a high heat flux is also needed for orientation-independent operation. A larger heat flux into the system will similarly increase the fluid driving force.

Mameli et al. [51] looked into the effects of varying gravitational force on an OHP. This was done by running tests on the 58th ESA Parabolic Flight Campaign. The vertical orientation was shown to be affected by the presence (or lack thereof) of gravity. When gravity was reduced to near zero, pulsations would slow and evaporator temperatures would rise. When the flight ascended and gravity returned, operation would return to high pulsations. It was also stated that because the flight time for the microgravity was short, approximately 20s, the transient effects were all that were being measured. It was determined that at least 180s is needed for complete transition for varying inclination angles.

2.7 - OHP Designs

Several different configurations of OHPs have been studied.

2.7.1 -Open Loop/Closed Loop

There are two primary categories of OHP: open-loop and closed-loop (Figure 7). The ends of open-loop OHPs are unconnected, and conversely a closed-loop OHP has its ends connected together to form a continuous channel. In general, closed-loop OHPs have lower thermal resistances due to the closed-loop OHP's ability to have bulk fluid flow (continuous flow in a single direction). In a study by Khandekar et al. [50], closed loop OHPs with bulk fluid flow showed an annular flow pattern. In an open loop OHP, only slug flow was observed. In slug flow, latent heat transfer is minimal. However, in annular flow the contribution of latent heat transfer increases, improving the OHP's performance [52].

In a similar study by Liu et al. [53], it was observed that the fluid flow in the OHP was not a simple slug/bubble flow. It can also consist of semi-annular, bubble and annular, or bubble flow patterns. For a closed-loop OHP, circulation is possible, which enhances the heat transport capability of the OHP. By promoting circulating flow, heat transfer is not only improved, but can make the system more predictable as a result, and design and implementation of the OHP can be simplified.

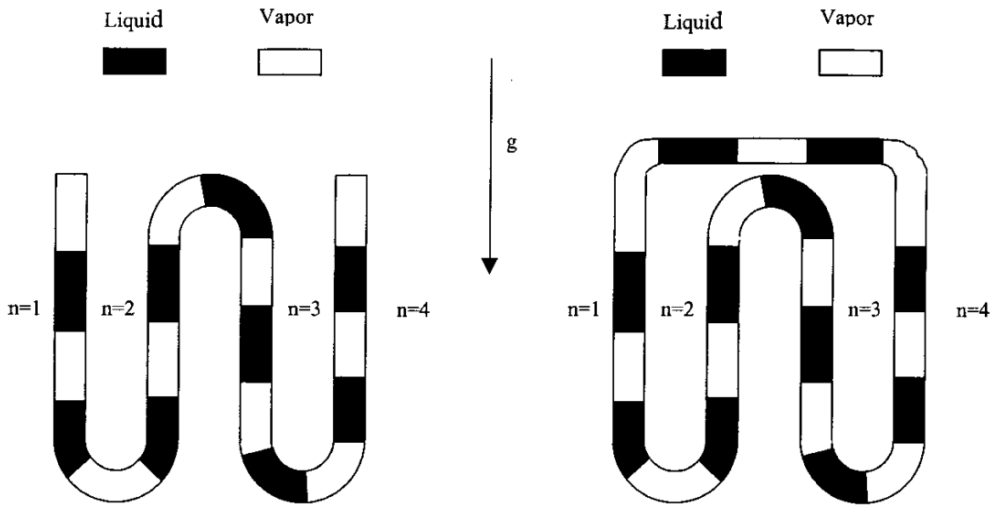

Figure 7: Left: Open loop oscillating heat pipe, Right: Closed loop oscillating heat pipe [18].

Wilson et al. [54] performed a study with four OHPs: two closed-looped and two open-looped using water and acetone. It was observed that the thermal amplitude for water was greater than that of acetone, meaning the temperature fluctuations were greater for water. It was also observed that higher oscillation frequency resulted in smaller thermal variation. Acetone was shown to pulsate at a higher frequency than water, and the temperature fluctuations were smaller at lower power. Higher condenser temperatures showed lower temperature differences, and the fluid was visually observed to have a higher velocity. When higher heat fluxes were used, water was shown to be the superior

working fluid, resulting in smaller average temperature differences between the evaporator and condenser sections. Similar trends were found for both the open- and closed-looped heat pipes. It was found that little fluid motion was observed in the interconnecting channel of the closed-looped OHP. This prevented flow circulation at times, and thus similar results were found for both types. Similar findings were presented by Shafi et al. [18], who studied both open-looped and closed-looped OHPs and found that both configurations performed comparatively.

2.7.2 - Check Valves

Check values can be used to regulate the flow direction of the working fluid in an OHP (Figure 8). By limiting the fluid to a single direction of flow, flow circulation may result in increased performance in closed-loop OHPs. Without check valves, it is common for local pulsations to only take place, i.e. pulsations within individual channels or small clusters of channels.

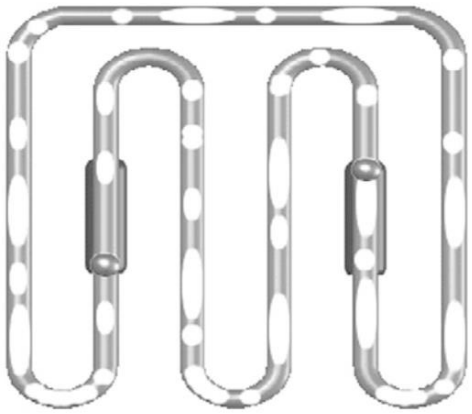

Figure 8: Oscillating heat pipe with check valves [55].

In a study conducted by Rittidech et al. [17, 56, 57], an OHP with ball type check valves were investigated that controlled fluid flow direction (Figure 9). Water, ethanol, and R123 were used as the working fluids. The effect of the number of check values on the performance was considered. It was found as the check valve ratio decreased, number of valves to number of turns, heat flux increased. This indicates that OHP performance is strongly dependent on the pressure drop between the evaporator and condenser sections. It was also shown that as the evaporator-to-condenser length ratio was increased, the heat transfer rate decreased.

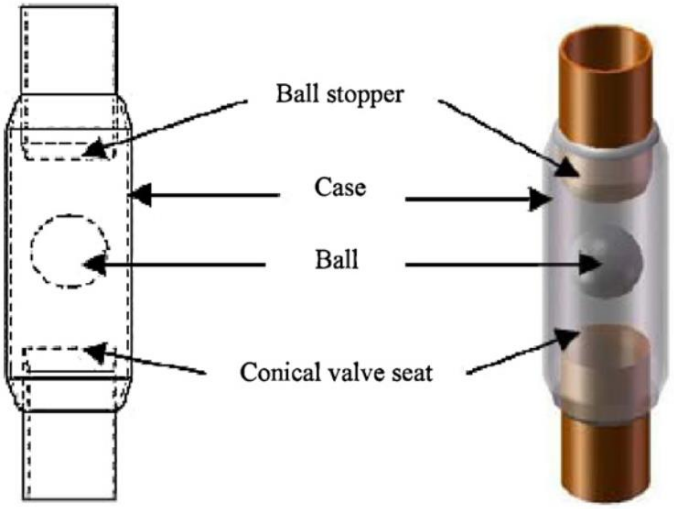

Figure 9: Oscillating heat pipe with ball type check valve [57].

Thompson et al. [20] developed an OHP with an integrated Tesla-type check valve (Figure 10). Unlike other check valves that used a ball to float and seal a channel, the Tesla-type check valve is integrated into the OHP structure easily. However, much more space between channels is required, reducing channel density. The Tesla-type check valve did help to promote bulk fluid flow in the desired direction. As a result, the OHP with the check valve decreased thermal resistance by approximately 15% compared to a standard OHP with the same channel density.

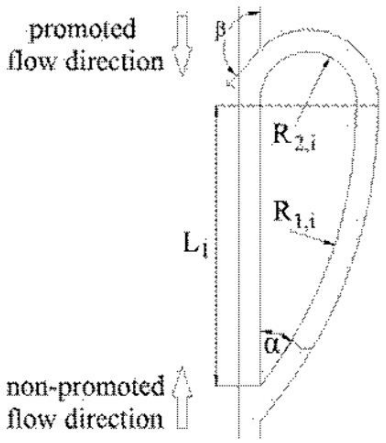

Figure 10: Tesla-type check valve [20].

2.7.3 - Three-Dimensional Geometries

One limitation of the OHP is channel density. As a result, research has been conducted to increase channel density by layering two-dimensional OHPs to create three-dimensional OHPs capable of high heat transfer while reducing the cross-sectional area.

Thompson et al. [58] studied a three-dimensional (3-D) OHP for an application in cooling of electromagnetic launchers (Figure 11). It was determined that the 3-D OHP could increase axial heat transfer by nearly 4000% when compared to pure copper. In another (3-D) OHP study by Thompson et al. [59], it was determined that thermal resistance will decrease as heat input increases for a constant heating area. In comparison, if the heating input is increased and the heating area is decreased (localized heating), the thermal resistance will increase. It was observed that channels located away from the localized heating area were shown to not be oscillating and did little to contribute to the heat transfer. Based on this, for localized heating applications the width of OHP should be

minimized. The 3-D OHP showed only a slight increase in thermal resistance in the horizontal orientation when compared to the vertical bottom heating orientation.

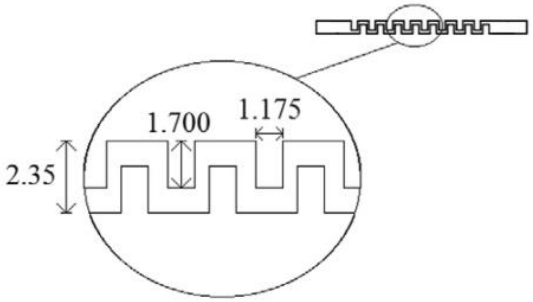

Figure 11: Staggered channels in three-dimensional OHP [58].

Hathaway and Ma et al. [32] studied a three-dimensional OHP which contained an uneven number of turns in the evaporator and condenser sections: 20 and 14 turns, respectively. The results of this study showed that the uneven-turn design can reduce the adverse effects of gravity on OHP performance.

Smoot and Ma [60] studied a three layer OHP that consisted of an inter-connected outer loop creating a two-layer, 23-turn OHP and a single layer independent 10-turn OHP in the middle. It was shown that increasing the number of layers resulted in a considerable increase in OHP performance compared to the single layer. The inter-connected two-layer OHP also showed the smallest sensitivity to orientation. This apparatus was tested by charging only the independent single layer, then only the two-layer portion, and finally with all three layers charged and operating. This allowed for distinctions to be made between operational characteristics of each channel system.

2.7.4 - Varying Channel Diameter

Liu et al. [53] conducted a study on three types of OHPs. One was a standard uniform channel diameter OHP, the second had non-uniform channels, and the third had thicker tubes. The results indicated that neither of the modified configurations reduced the thermal resistance when compared to the standard OHP. With a fill ratio between 20%-50%, all three apparatuses behaved similarly. Above this, the modified OHPs were unable to consistently form annular flow, and the overall heat transfer capacity was reduced.

Holley and Faghri [61] developed a model for an OHP which consisted of a capillary wick and varied channel diameter. The model was compared to data collected from similar apparatuses with wicking structures in place, and it was shown to have similar performance characteristics. Their models showed that by varying channel diameter, bubble pumping can be induced, which can increase fluid circulation. The channel diameters were varied from 1.6 to 1.4 mm. It was shown that if the channel diameter change was too extreme, fluid motion was reduced. This reduction was likely attributable to the increased pressure drop. Similar results were achieved if one parallel channel was a constant diameter and the neighboring channel was a varying diameter. It was found that the OHP with varying channel diameters have reduced heat transfer performance when compared to uniform channels. However, the varying-diameter channels were less dependent on inclination angle, and thus gravity. This conclusion is supported by Chein et al. [62], who also developed an OHP with varied channel diameters. It was determined that the non-uniform OHP performed better at lower inclination angles, whereas the uniform-diameter OHP was un-operational.

Tseng et al. [63] studied an OHP with non-uniform channels. These channels were crushed to form an oval shape (Figure 12). Water, methanol, and HFE-7100 were used as working fluids. When the OHP was in the horizontal orientation the non-uniform OHP had a lower thermal resistance and resulted in easier start-up. HFE-7100 easily starts up at low heat inputs, but at high heat inputs water was shown to be the best working fluid.

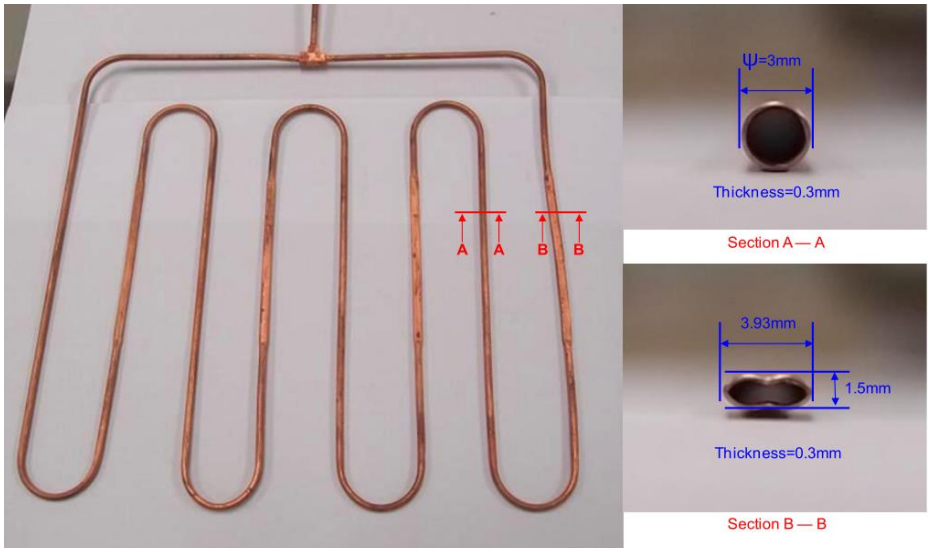

Figure 12: Section A-A showing channel of uniform diameter and Section B-B showing non-uniform diameter (crushed) channel [63].

2.7.5 - Wicking OHP

Smoot and Ma [64] studied a hybrid OHP which included of a wicking structure similar to conventional heat pipes and the meandering channels of the OHP. It was observed that vapor bubbles and liquid slugs did not form with a wicking structure. Pulsations were only observed in the evaporator section. It was believed that the wicking structure caused the liquid slug to disperse before it reached the condenser section. As a result, heat transfer was generally observed in the evaporator sections and in the adiabatic sections. Due to the limited fluid motion, the OHP was found to have significantly lower heat transfer rates than a typical OHP. It was also noted that as condenser temperature was

increased, so was the amplitude of oscillation in the evaporator. No oscillation was observed in the condenser.

2.7.6 - Other Configurations

In a study by Lin et al. [65], U-shaped and L-shaped OHPs (Figure 13) were integrated into a heat sink. It was found that the U-shaped OHP had better operational characteristics because it reduce the distance between evaporator and condenser and symmetry helped to distribute heat evenly. The L-shaped OHP performance was comparable to that of a standard flat plate OHP.

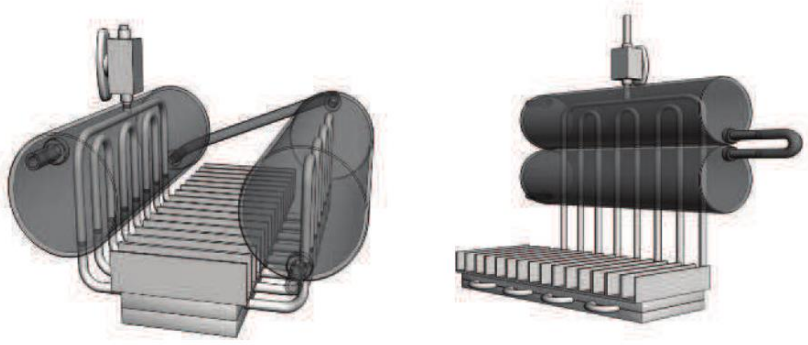

Figure 13: Left: U-shaped oscillating heat pipe, Right: L-Shaped oscillating heat pipe.

Iwata et al. [66] studied a variable conductance OHP (VC-OHP). A VC-OHP uses non-condensable gas with the working fluid to vary the conductance of the OHP. The non-condensable gas was in a reservoir, and the amount of non-condensable gas was controlled by regulating the temperature of the reservoir. This allowed the OHP to maintain set operating temperature even at lower power, a condition for which a regular OHP would simply have a lower evaporator temperature. This study showed that the evaporator temperature remained nearly equal to the temperature of the reservoir, even

when heat input was increased. It was shown that the VC-OHP can be controlled in multiple orientations, indicating that gravity had little effect and that it may function well in low or no gravity applications.

Taslimifar et al. [67] conducted studies on an OHP considering non-condensable gases, heat input, working fluid, inclination angle, and magnets. It was found that when using a magnetic field with a nanofluid, the ferrofluid particles were pull towards the wall, thus roughening the surface. The roughened surface may have improved boiling and latent heat transfer. The magnetic field was shown to enhance the ferrofluid's thermal conductivity. By adjusting the location of the magnetic field in the evaporator or condenser sections, the thermal resistance could be adjusted to maintain a desired evaporator temperature. It was found that middle inclination angles showed the best heat transfer performance. Higher concentrations of ferrofluid particles reduced the steady-state thermal performance.

2.8 - Modeling

One of the limiting factors for OHP implementation is the lack of effective design tools. As a result, efforts have been made to develop models that can be used to predict OHPs' performance. These models have also led to better understanding of how OHPs function.

Shaifi et al. [18] developed a thermal model for looped and unlooped OHPs. The model consisted of multiple vapor plugs and liquid slugs. The conclusions drawn from the model were that gravity does not significantly affect performance, heat transfer is mainly

due to sensible heat transfer, and by increasing diameter the average heat transfer increases.

Ma et al. [68] developed a mathematical model that predicts fluid motion and temperature drop in an OHP. This model accounted for forced convection due to oscillations, confined evaporating heating, and thin film condensation. It was concluded that oscillating motions significantly enhance heat transfer. In this work, an analytical model to represent the heat transfer capacity of an OHP was also developed. From the analysis, it was found that heat transfer is mainly due to sensible heat, agreeing with Khandekar et al. [19] and Zhang and Faghri [18, 69].

2.9 – Research Objective

From the literature review, it was observed that there is minimal information about geometric features and their effects on performance. The objective of this research is to fill this void in knowledge by determining how several geometric features in the evaporator section will effect operating performance. Insight into how to improve OHP performance will be gained through a thorough analysis comparing each geometry over comparable testing parameters. This study will show if improvements in OHP operation can be made by adjusting or modifying a traditional straight-channel OHP geometry.

CHAPTER 3 - METHODOLOGY

2.1 - Apparatus

A testing apparatus was designed and built that would allow testing parameters to be easily controlled. Independent parameters controlled included fill ratio, power input, condenser temperature, and inclination angle.

The OHP structure was machined into an aluminum plate, where the channels acted as the fluid passageway. Aluminum was selected due to its low cost, machinability, good thermal conductivity, and because it is already a commonly used material in cooling devices. The channel sizing was determined by looking to the Bond number. As discussed in Chapter 2, the Bond number is a dimensionless parameter that relates surface tension to fluid body forces. Square channels (2 mm × 2 mm) were selected. These channel dimensions produce a Bond number of 1.44 when acetone is used as the working fluid. It has been established that Bond number should fall between 4 and 0.5 in order for the OHP to operate properly [16]. This channel size was also selected to allow for other common fluids to be studied in the future.

$$Bo = \frac{D_h^2 g(\rho_l - \rho_v)}{\sigma} = \frac{(.002m)^2 \left(\frac{9.81m}{s^2}\right)\left(767.7\frac{kg}{m^3} - 1.309\frac{kg}{m^3}\right)}{\frac{0.02084N}{m}} = 1.44 \qquad (6)$$

Acetone was selected as the working fluid due to its compatibility with aluminum and its physical properties (low LHV and viscosity) that make it an ideal candidate for the OHP. A total of twenty-two channels were machined with eleven turns in the evaporator section and eleven turns in the condenser section including one large return bend. A cross-sectional view of the OHP base geometry is shown in Figure 14. The channels are 2 mm

x 2 mm square with a 2 mm spacing between each channel. In addition, there is a larger channel that surrounds the inner channels. This larger channel is an O-ring channel, used to create a seal between the aluminum plate and glass cover plate. The glass cover (6.35-mm thick) allows for flow visualization during operation. A polycarbonate cover (6.35-mm thick) was used to protect the glass cover from high stress points created by clamps that were used to secure the cover to the aluminum plate (Figure 15).

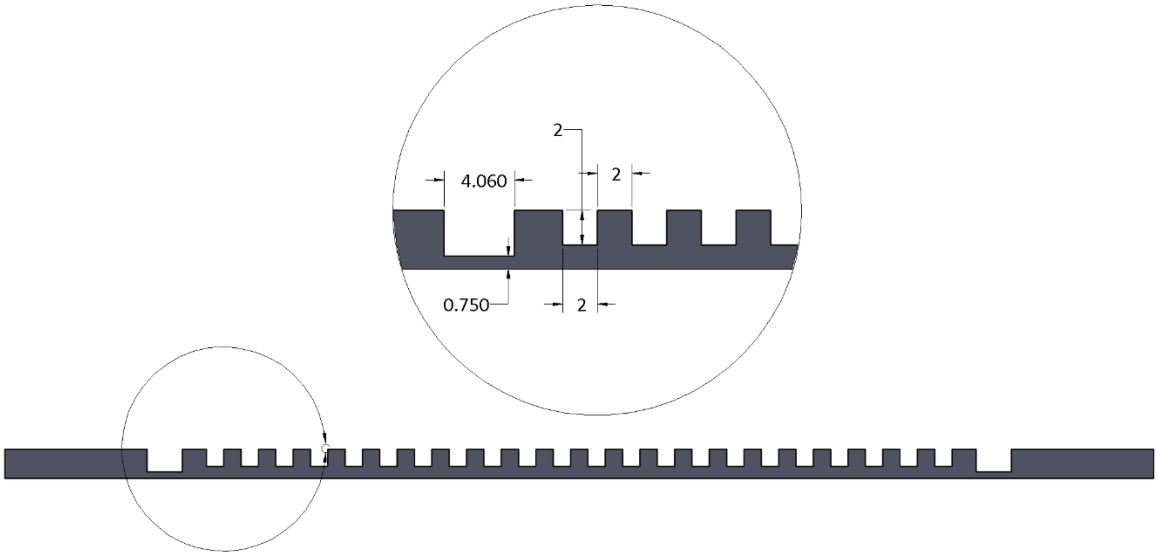

Figure 14: Cross section view of OHP showing relevant geometry (Units: mm).

A copper heating block was mounted to the evaporator section and used to provide the heat input into the system (Figure 15). The heating block consisted of four embedded 0.25 inch (6.35 mm)-diameter 100-W cartridge heaters. The block dimensions were 83 mm x 32 mm x 9.5 mm. A 120-VAC variable output transformer was used to regulate the power supplied to the heaters. Power was measured using an AC voltage transducer (CR Magnetics CR4510-150) and an AC current transducer (NK Technologies AT1-005-000-SP) with uncertainties of 0.5% and 1%, respectively.

A cooling block was secured to the backside of the condenser section of the OHP (Figure 15). The dimensions of the aluminum cooling block were 127 mm × 70 mm × 17 mm. The cooling block was constructed with a single inlet and single outlet connected by multiple cooling passages to ensure uniform cooling. A 50/50 volume percent water/ethylene glycol solution flowed through the cooling block, removing heat from the OHP. A thermostatic chiller circulated and regulated the temperature of the solution. High-density fiberglass insulation (2.54-cm-thick) surrounded the heating and cooling blocks, as well as the back of the OHP to minimize heat losses.

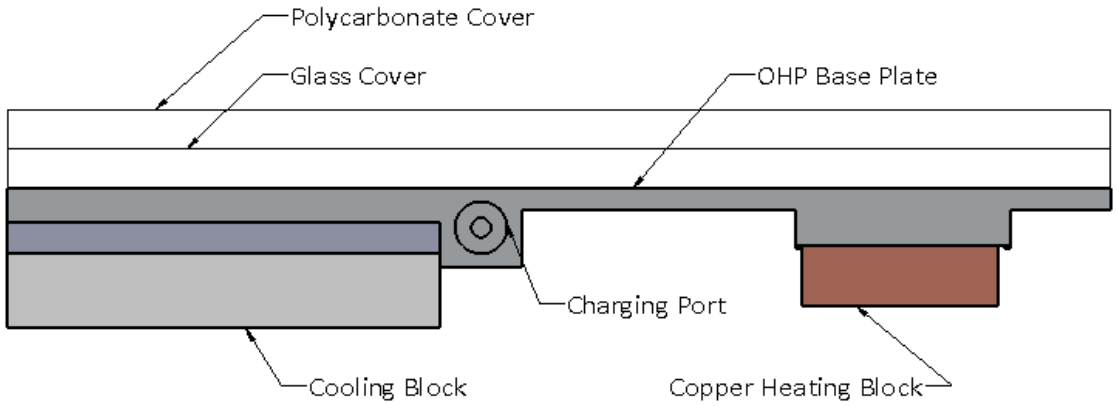

Figure 15: Schematic of OHP apparatus.

A small charging port was also machined into the side of the OHP aluminum plate (Figure 15). The system was degassed and charged with the working fluid through this port. To ensure the system remained degassed during charging, a valve/manifold system was made that would isolate certain areas, ensuring minimum leakage.

Temperature was measured using fifteen 30-gauge, T-type thermocouples. Five thermocouples were placed in each section (Figure 16). The thermocouples were calibrated to achieve an uncertainty of ±0.2 °C. Small channels were milled into the back

of the OHP to allow the thermocouples to be within 0.8 mm of the fluid-filled channels. The small channels were offset to obtain a better geometric average of the evaporator and condenser sections. A data acquisition system was used to record the data from the thermocouples and transducers at a rate of 1000 Hz.

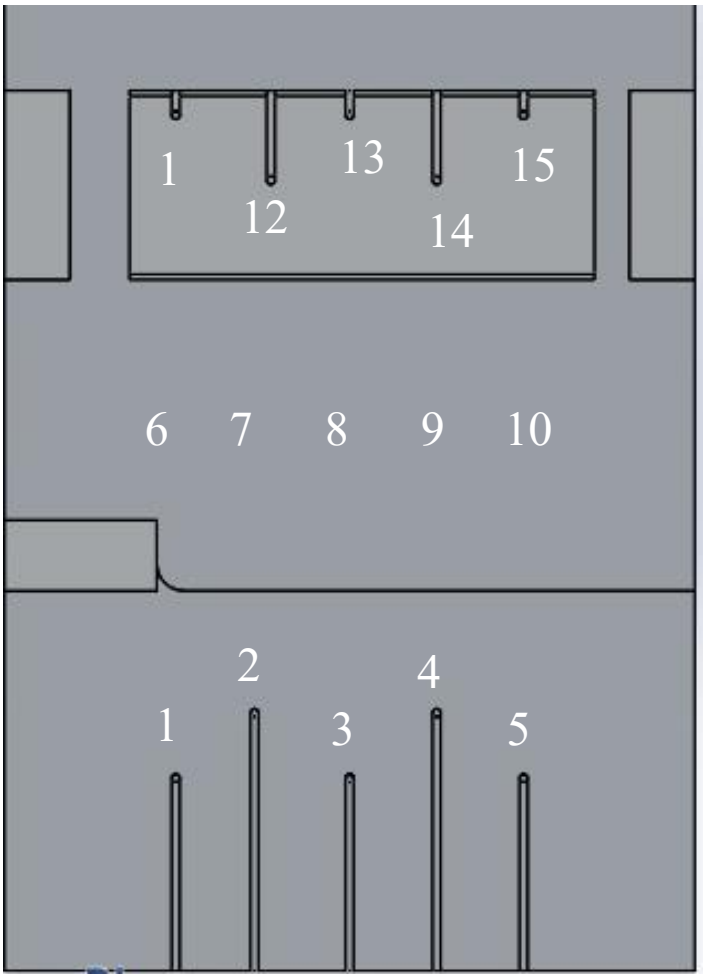

Figure 16: Thermocouple locations.

2.2 – Experimental Procedure

A good charge is extremely important for proper OHP operation. A good charge will evacuate all liquid and gases from the OHP volume and add a precise amount of working fluid to the OHP. To ensure that this was achieved, the following procedure for charging was developed.

To charge the OHP, a charging tube was filled with the appropriate amount of working fluid, degassed, and sealed via a valve. This charging tube was then connected to an inlet port, identified as (3) in Figure 17. A vacuum pump was then connected to outlet port (2). With the charging tube still sealed, the OHP was degassed using the vacuum pump. Once this was achieved, valve (2) was closed. Next, the charging tube was heated using a heat gun. Once the charging tube was heated to a sufficient temperature, the valve on the charging tube was opened. The combination of low pressure in the OHP channels and lower temperature of the OHP (which keeps saturation pressure low even after working fluid is present) served to draw the working fluid in. Once all working fluid was transferred to the OHP, valve (1) was closed, sealing the OHP. This process ensured accurate filling (±0.2 mL).

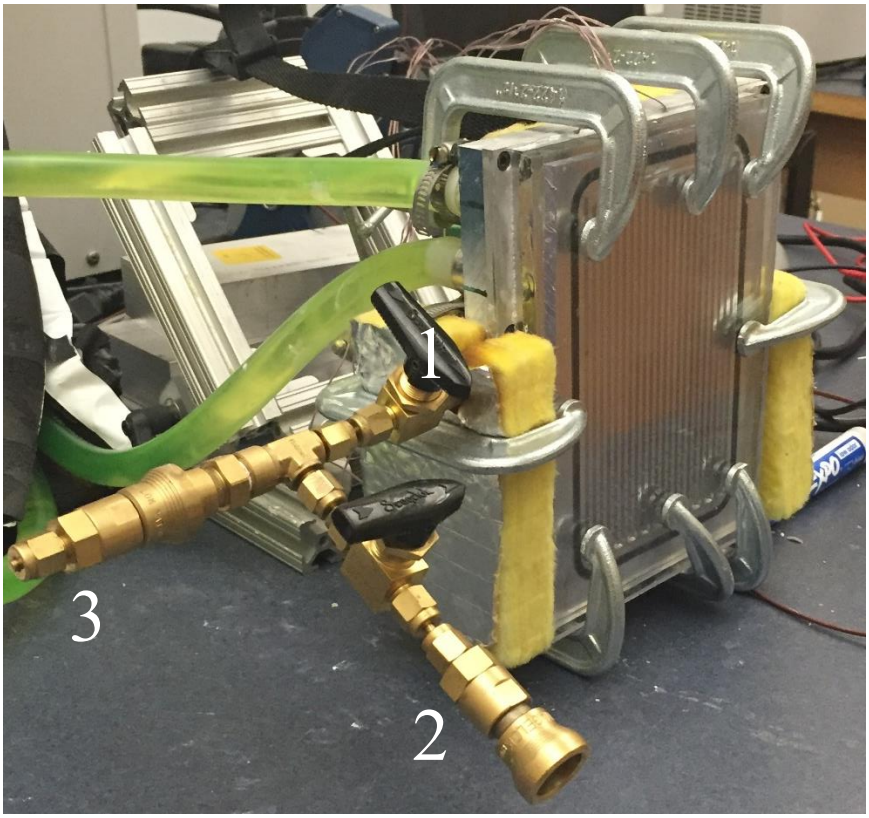

Figure 17: The assembled test apparatus, showing the valve manifold used for charging and degassing.

To test the OHP geometry, heat was supplied to the system in 25 W intervals from 25 W up to 400 W. At each interval, the OHP was allowed to reach steady state. Steady state was determined to have been reached if the standard deviation of the evaporator temperature was less than 0.5 °C over a five-minute period. Once steady state had been reached, five minutes of one-second average values of current, voltage, and temperature readings were recorded. The test runs were conducted until the maximum heat input of 400 W was achieved, dry-out occurred, or a maximum temperature of 90 °C was reached in the evaporator section. The maximum temperature of 90 °C was selected as this is a common maximum operating temperature for many types of electronics.

In addition to varying heat input, the inclination angle was also changed. After a full run from 25 W to 400 W had been completed, the inclination angle was changed. The inclination angles considered were vertical (90°), 45°, and horizontal (0°). Top-heating operation was not investigated. The fill ratio for each OHP would also be varied; fill ratios of 35%, 55%, and 75% were investigated. The setup of the experiment is shown in Table 3. This experiment was repeated for each geometry tested.

Table 3: Design of experiment.

Watt	Vertical			45°			Horizontal		
25	35%	55%	75%	35%	55%	75%	35%	55%	75%
50	35%	55%	75%	35%	55%	75%	35%	55%	75%
75	35%	55%	75%	35%	55%	75%	35%	55%	75%
100	35%	55%	75%	35%	55%	75%	35%	55%	75%
125	35%	55%	75%	35%	55%	75%	35%	55%	75%
150	35%	55%	75%	35%	55%	75%	35%	55%	75%
175	35%	55%	75%	35%	55%	75%	35%	55%	75%
200	35%	55%	75%	35%	55%	75%	35%	55%	75%
225	35%	55%	75%	35%	55%	75%	35%	55%	75%
250	35%	55%	75%	35%	55%	75%	35%	55%	75%
275	35%	55%	75%	35%	55%	75%	35%	55%	75%
300	35%	55%	75%	35%	55%	75%	35%	55%	75%
325	35%	55%	75%	35%	55%	75%	35%	55%	75%
350	35%	55%	75%	35%	55%	75%	35%	55%	75%
375	35%	55%	75%	35%	55%	75%	35%	55%	75%
400	35%	55%	75%	35%	55%	75%	35%	55%	75%

2.3 – Geometric Variations

Four different evaporator geometries were studied to analyze performance characteristics.

The baseline geometry is the traditional straight-channel configuration (Figure 18). Straight-channel geometry has been widely studied largely due to its simplicity, which

increases manufacturability and reduces cost. In this study, the straight-channel apparatus is used as a baseline against which the performance of the other geometries is compared. The channels run parallel to each other, and are spaced equally, 2 mm apart.

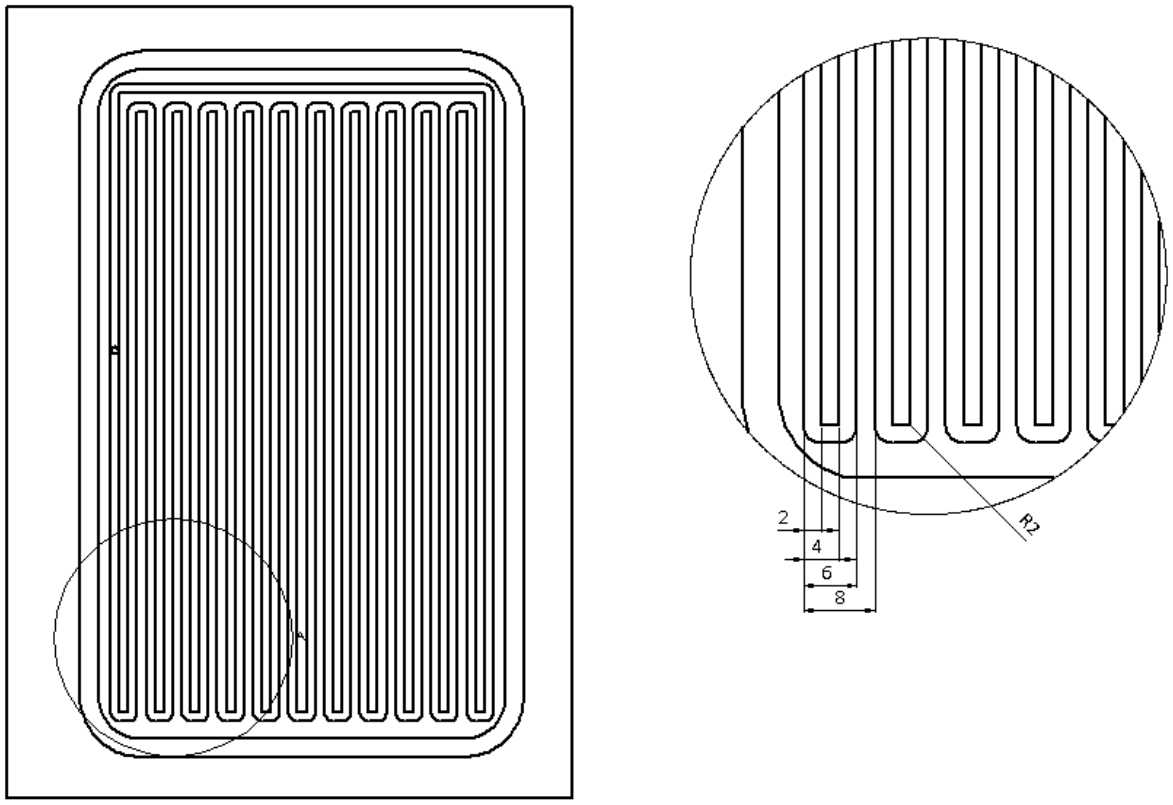

Figure 18: Straight-channel geometry (Units: mm).

The second geometry is the pin-and-cavity geometry (Figure 19). This geometry is being considered because it increases area and turbulence within the fluid channel, which could result in an increase in heat transfer performance over the baseline. This geometry consists of small pins centered in the channels with cavities surrounding the channels to reduce the fluid passage blockage caused by the fins. The pins are 1.25 mm in diameter with a height of 2 mm. The cavity has a diameter of 4 mm. The pins are staggered to increase density and to allow the channel spacing to be maintained 2 mm apart.

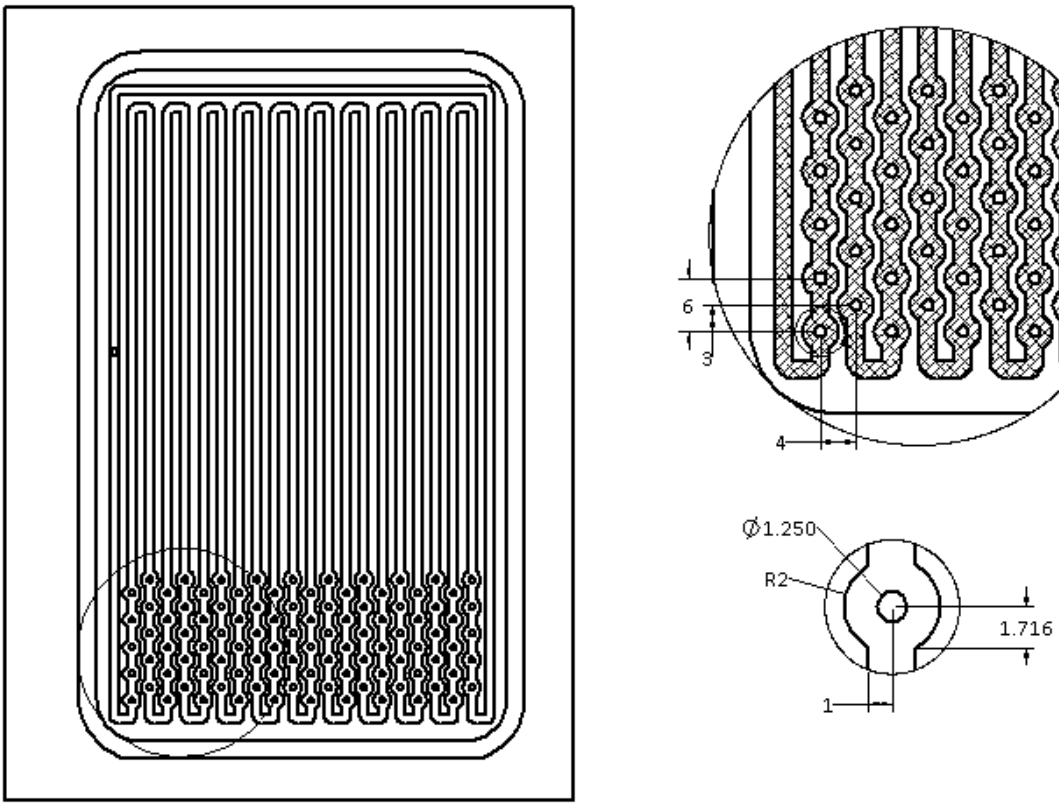

Figure 19: Pin-and-cavity geometry (Units: mm).

The next geometry is the reentrant-cavity geometry (Figure 20). This geometry utilizes small, 1-mm diameter cavities recessed into the channel walls. These small cavities are then connected to the main flow channel by a 0.508-mm x 1-mm channel. The connecting channels are placed at 35° angles to the main channels. The connecting channel directions are alternated from main channel to main channel. This is done to promote fluid flow in a single direction, similar to the research where check valves were used to improve performance by 15% compared to an OHP with no check valves [17, 20].

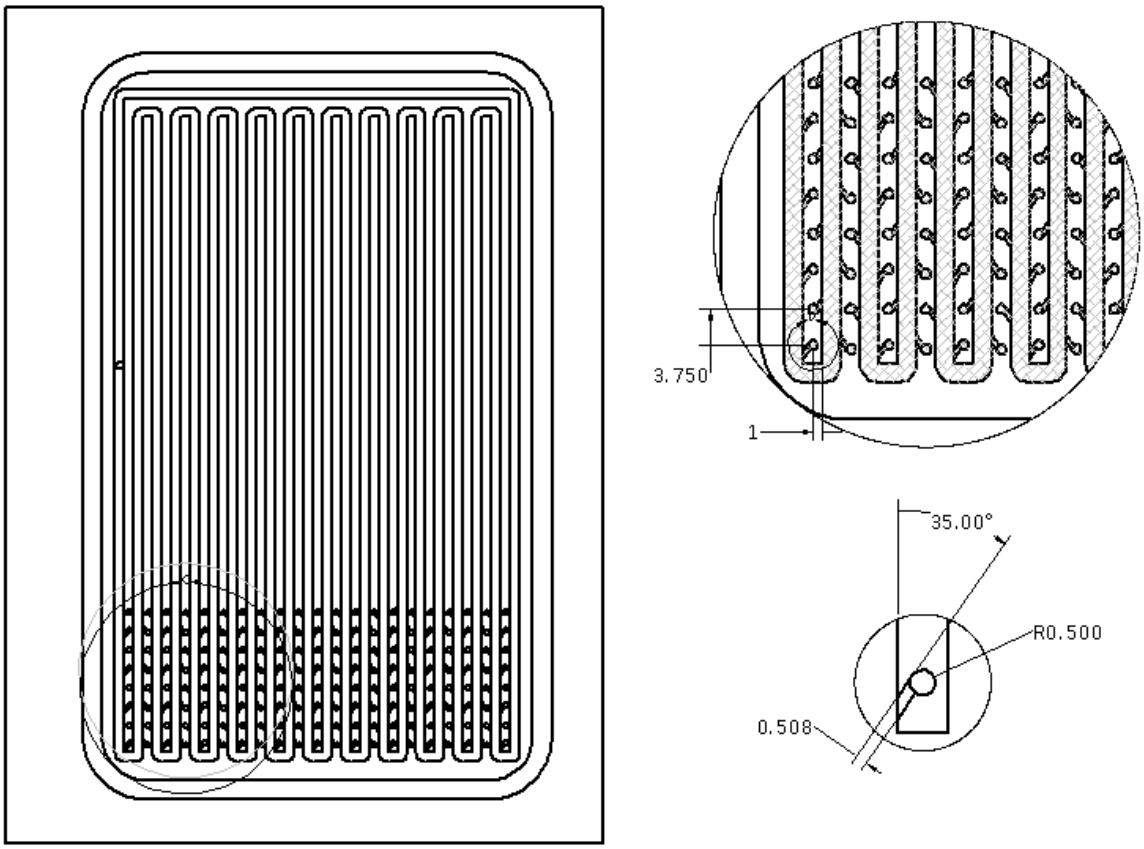

Figure 20: Reentrant-cavity geometry (Units: mm).

The final geometry considered was the wavy-channel geometry (Figure 21). This geometry replaces the straight main flow channels with wavy-channels in the evaporator section. The goal of this geometry modification was to increase turbulence in the fluid and slightly increase the heat transfer surface area while having a minimum increase in pressure drop.

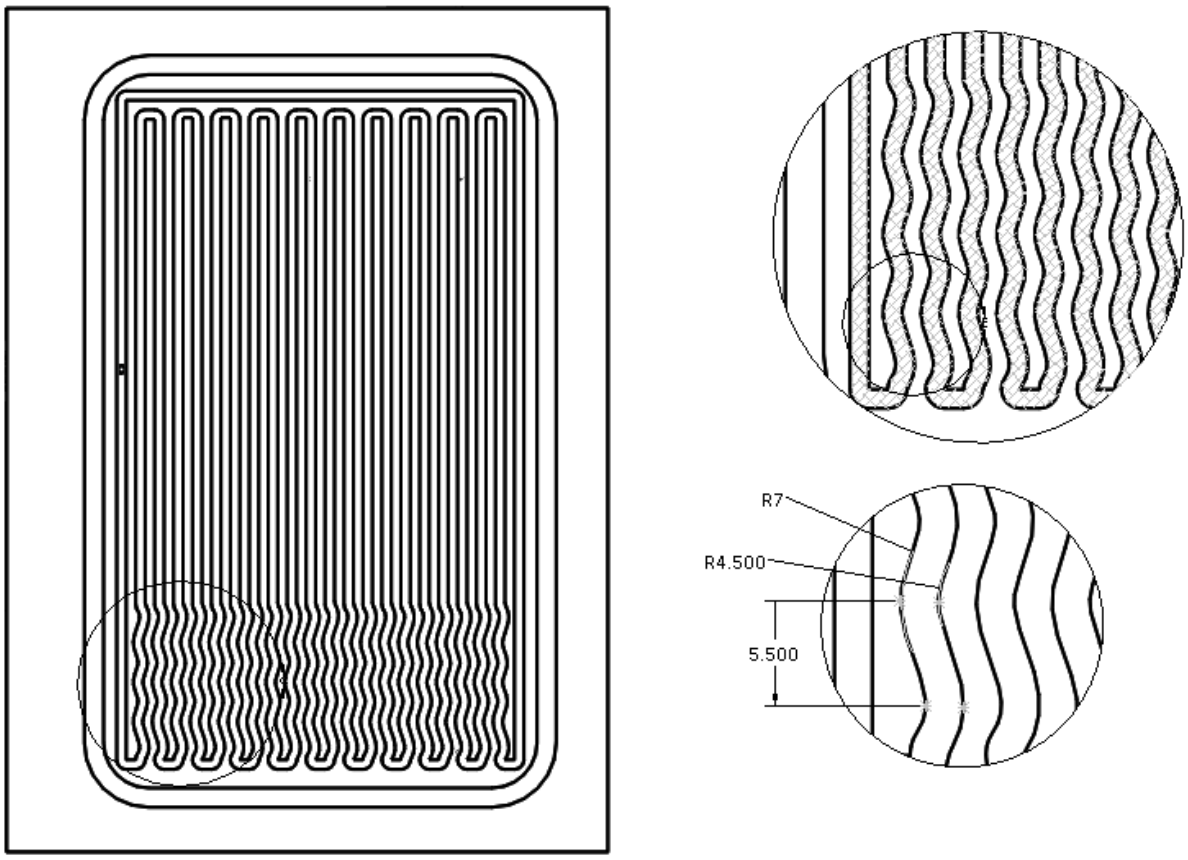

Figure 21: Wavy-channel geometry (Units: mm).

2.4 – Data Reduction

The average temperature from the evaporator and condenser sections were used to determine the temperature difference across the OHP. The equations used to determine average evaporator and condenser temperatures are shown in Equations 7 and 8, respectively. T_{ave} is defined as the time-averaged temperature of a single thermocouple.

$$T_E = \frac{1}{5} \sum_{i=1,2,3,4,5} T_{ave,i} \tag{7}$$

$$T_C = \frac{1}{5} \sum_{i=11,12,13,14,15} T_{ave,i} \tag{8}$$

The power input to the system was also determined. This was found by taking the product of the voltage and current values measured with transducers, Equation 9.

$$P = VI \tag{9}$$

2.5 - Heat Loss Experiment

To estimate the amount of heat loss to the environment while the OHP is operating, a heat loss test was conducted. This was done by testing an uncharged OHP. The condenser temperature was set and maintained at 30 °C. The heater power input was incrementally increased, while measuring evaporator temperature, condenser temperature, and ambient temperature. Using published thermal conductivity values of 6061-T651, the heat transfer rate due to conduction in the plate itself was estimated from Equation 10. Once the conduction heat transfer was known, the heat loss to the environment was found with Equation 11. From this a function of evaporator temperature and ambient temperature was developed that estimated the heat loss from the OHP during normal operation, which is shown in Equation 12 and in Figure 22.

$$Q_{cond} = \frac{(T_E - T_C)(A_{xs})(k)}{x} \tag{10}$$

$$Q_{loss} = P_{in} - Q_{cond} \tag{11}$$

$$Q_{loss} = 0.329(T_E - T_A) \tag{12}$$

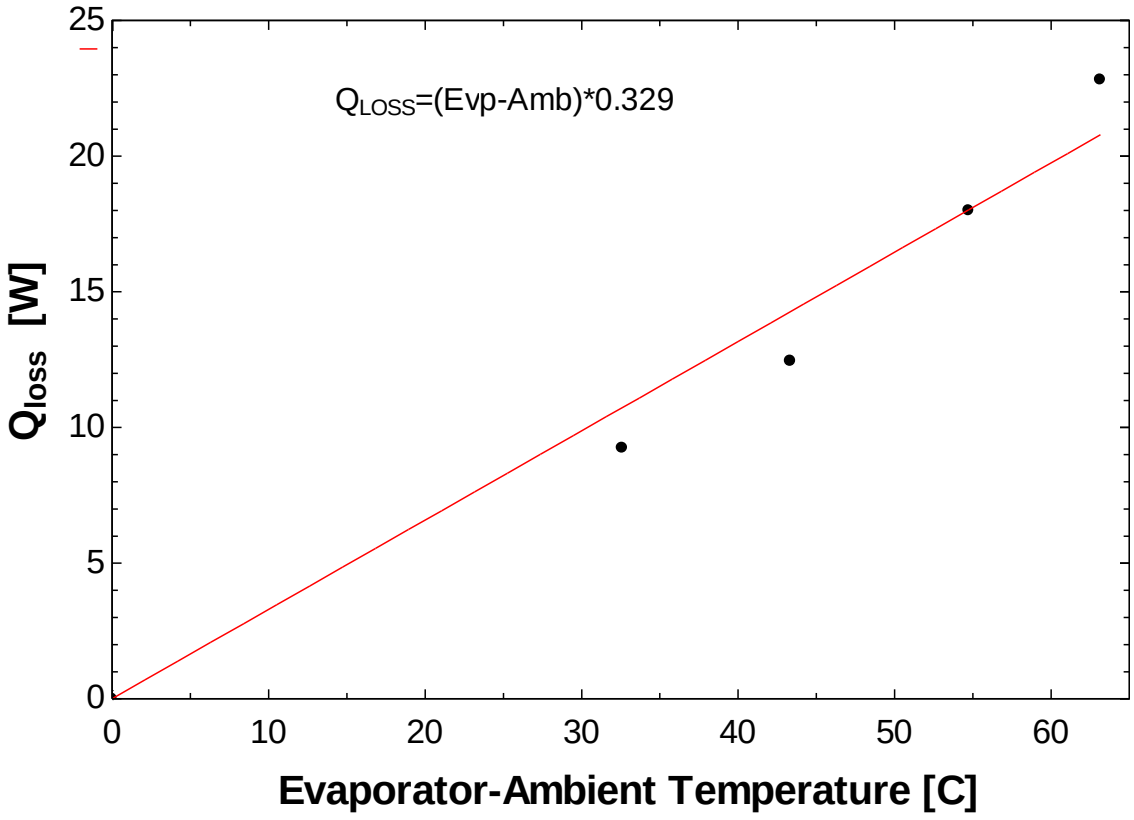

Figure 22: Heat loss experimental data and best fit line presenting Q_{loss} as a function of the difference between evaporator and ambient temperatures.

2.6 - Test Metric

The primary test metric used for comparison of the different geometries in this study was thermal resistance. Thermal resistance is the temperature difference between the evaporator and condenser section of the OHP required to drive a unit of heat transfer. Thus, lower values of thermal resistance are desirable, as this will reduce the evaporator temperature for a given heat load and condenser temperature. Thermal resistance is determined using Equation 14[1].

$$Q_{OHP} = P_{in} - Q_{loss} \tag{13}$$

[1] Uncertainty analysis presented in Appendix A, page 86.

$$R_{th} = \frac{T_E - T_C}{Q_{OHP}} \tag{14}$$

In addition to thermal resistance, the effective heat transfer coefficient (HTC) was also used as a performance parameter of interest. The HTC is the inverse of the thermal resistance times the area of heat transfer (Equation 15). The area of heat transfer is defined here as the area in which the OHP is contact with the cooling load. The area of heat transfer for the OHPs being tested in this study is shown in Figure 23. The HTC can be used to make qualitative comparisons of many different types of cooling technologies.

$$h_{eff} = \frac{1}{R_{th}A} \tag{135}$$

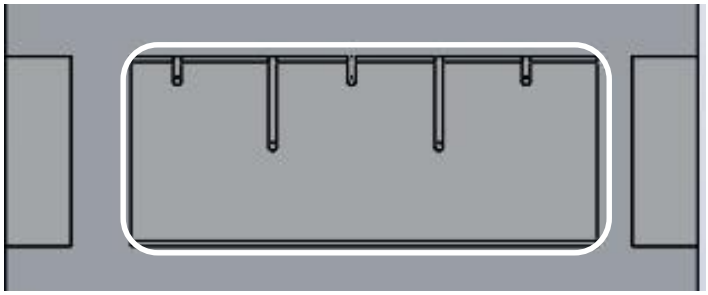

Figure 23: Area of heat transfer

Since all of the devices investigated in this study have the same heat transfer area, comparison of the HTC is equivalent to comparison of the thermal resistance. However, comparison of an effective HTC will allow comparison with OHPs of different geometries as well as other thermal management strategies.

CHAPTER 4 – RESULTS

3.1 - Performance

The four geometries were tested over identical parameter spaces. Fill ratios of 35%, 55% and 75% and inclination angles of 90°, 45°, and horizontal were tested. The performance of each of these trials is presented in the following sections.

3.1.1 – Straight-Channel OHP

The first geometry was the traditional straight-channel. It was found that OHP performance in the horizontal orientation is very dependent on geometric properties. In this case (Figure 24), similar conclusions can be made. The straight-channel OHP failed to ever fully develop the oscillatory motion characteristic of an OHP, thus little heat transfer improvement was observed when compared to an uncharged OHP at this inclination angle.

From the high thermal resistances and low maximum heating values, it is apparent that horizontal operation never occurred. It can also be seen that for the 35% and 55% fill ratios, as the heater power increased, the thermal resistance increased. This indicates that a large evaporator temperature increase occurred. This temperature increase can be seen in Figure 25. This large spike occurred because of evaporator dry-out. Since this OHP was in the horizontal position, all of the liquid working fluid collected in the condenser sections with only vapor present in the evaporator section. Due to this, the phase change, which provides the fluid driving forces in an OHP, was absent.

The 75% fill ratio test had a more consistent, yet high, thermal resistance. Since the working fluid occupied such a large volume of the channels, there was more fluid for conduction. No oscillations occurred, but conduction in the fluid in and near to the evaporator section allowed the heat to be dissipated through the acetone in additional to the aluminum plate.

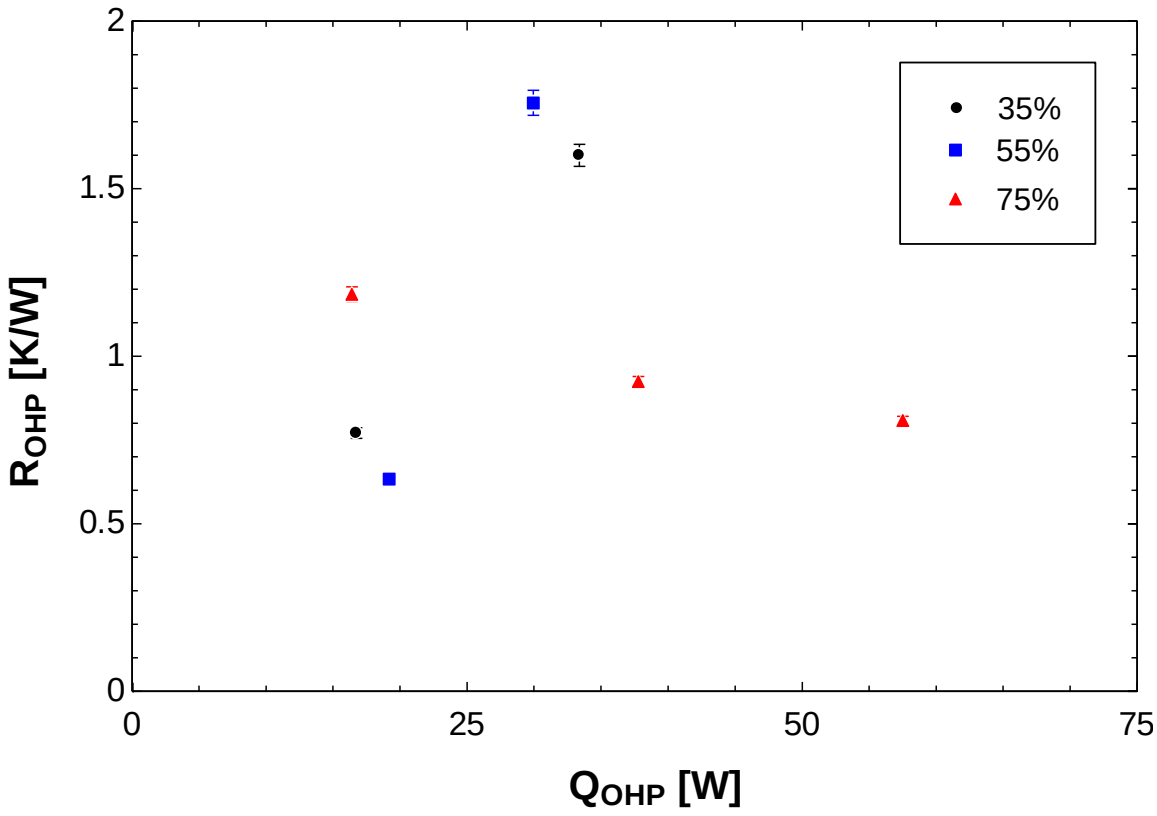

Figure 24: Straight-channel OHP performance, 0° inclination angle.

As noted above, as the heat input into the system increased, a subsequent increase in evaporator temperature was found. The temperatures for the 35% and 55% fill ratios increased at a nearly linear rate, further indicating that oscillations did not occur. It has been widely found that thermal resistance decreases exponentially as the heating power is increased to a nearly constant thermal resistance. From Figure 24 and Figure 25, it is apparent that this is not the case for this geometry in this orientation.

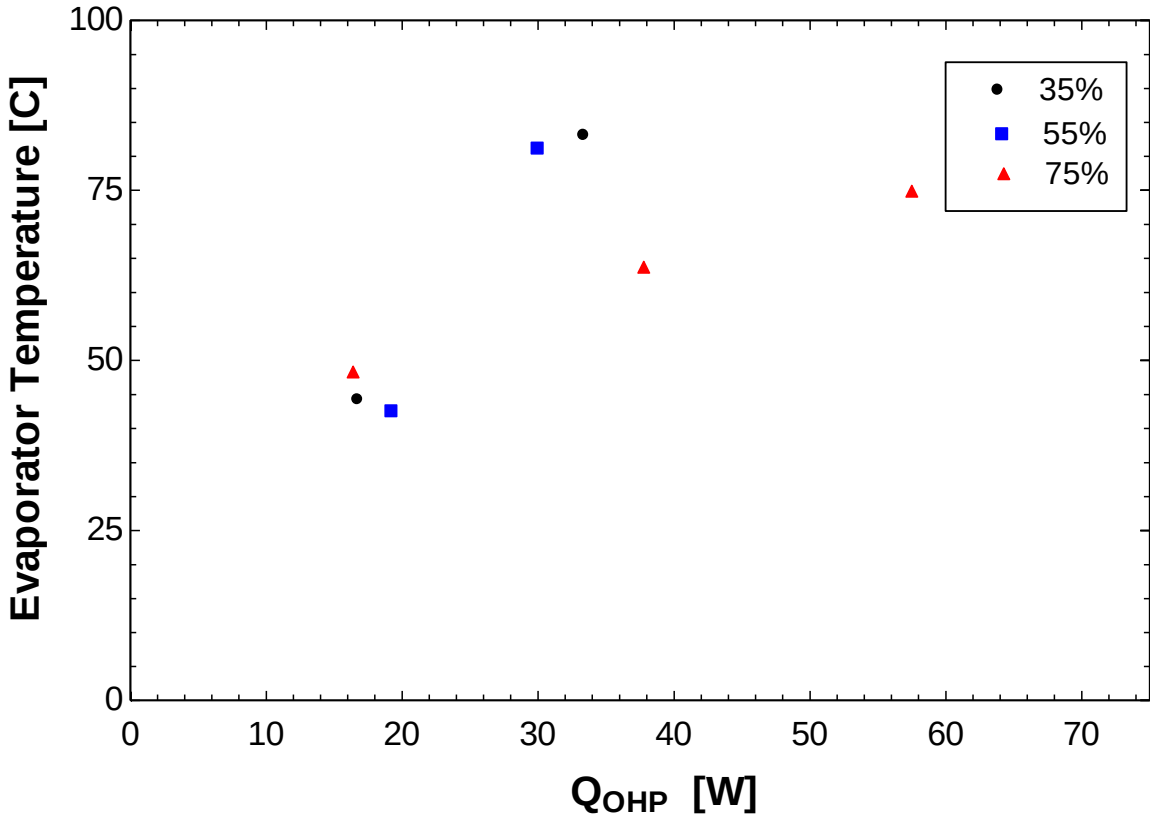

Figure 25: Straight-channel OHP evaporator temperature, 0° inclination angle.

For the straight-channel OHP at the 45° inclination angle (Figure 26) oscillation did occur, and the thermal resistance decreased exponentially to a nearly constant value. At all three fill ratios, when the heater power was approximately 25W, there was little oscillation and thus a high thermal resistance. However, once 50-W heater power was supplied, there was a subsequent decrease in the thermal resistance. The 35% fill ratio performed the best overall. It started operating at very low heater power input levels. It also approached its thermal resistance plateau at the lowest heating value. The 55% fill ratio also performed well, having similar start-up characteristics to that of 35%. The 75% fill ratio performed the worst. It had the highest evaporator temperature and the highest thermal resistance over nearly the entire range of heater power. It is possible that by having a high percentage of working fluid in the channels, the fluid acted as a damper to

the oscillating motion, thus limiting oscillating frequency and amplitude, which in turn negatively affected performance.

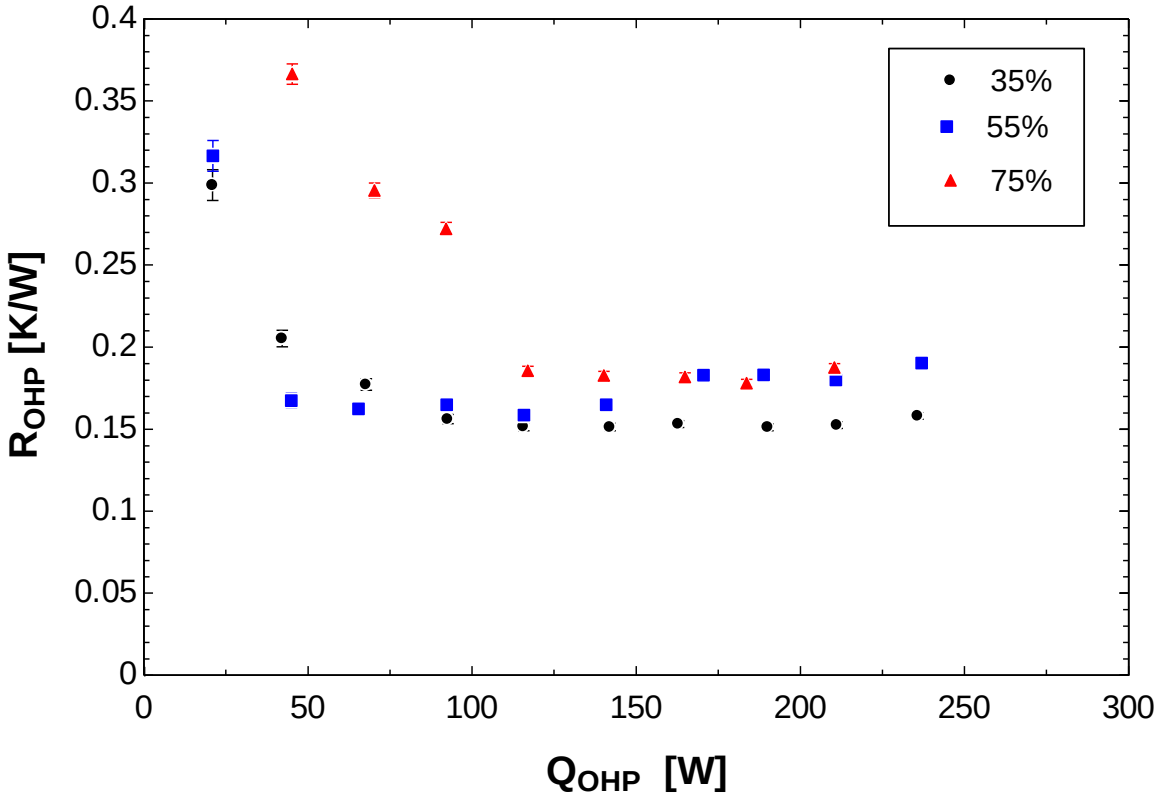

Figure 26: Straight–channel OHP performance, 45° inclination angle.

With the straight-channel OHP in the vertical orientation (Figure 27), the performance of the 35% and 55% fill ratios was nearly identical. The thermal resistance followed nearly the same pattern except at high heater power values, where the 35% fill ratio performed slightly better. There is also an inflection point for both 35% and 55% at approximately 125W. It was observed that around this power level, the flow transitioned from slug-and-plug flow to annular flow, which has been cited to improve performance at higher heating levels [50]. The 75% fill ratio was again the worst performer, especially at the lower heater powers. The critical evaporator temperature was reached earlier for the 75% then for 35% and 55%.

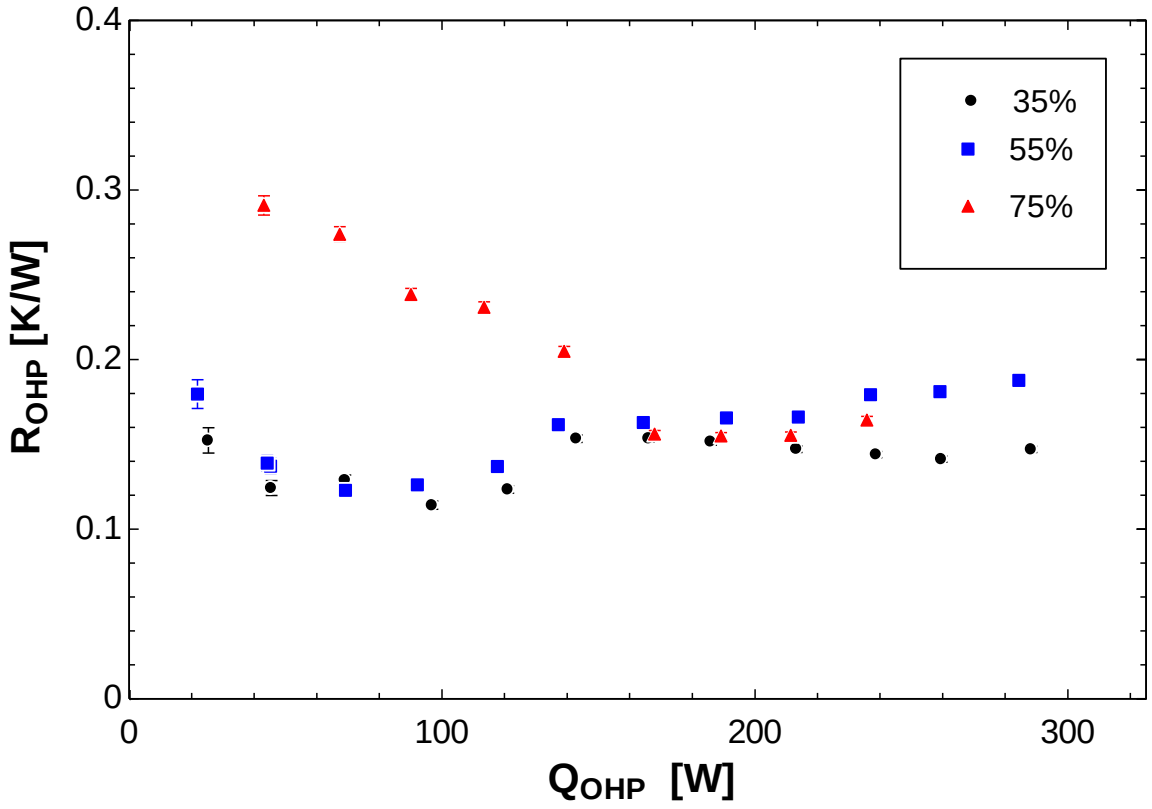

Figure 27: Straight-channel OHP performance, 90° inclination angle.

3.1.2 – Pin-and-Cavity OHP

The pin-and-cavity OHP is a modified OHP geometry that contained pins center in the channel in the evaporator section. These modifications were meant to increase turbulence, thus improving heat transfer performance.

For this device in the horizontal orientation (Figure 28), similar to the straight-channel OHP, no oscillations occurred and a rapid increase in evaporator temperature occurred. There was no observable pattern of thermal resistance with heater power input. Thermal resistance for 35% increased as the heating value increased. The thermal resistance of the 55% and 75% fill ratios fluctuated with increased heater power input, but flow oscillations were not observed at all in these tests.

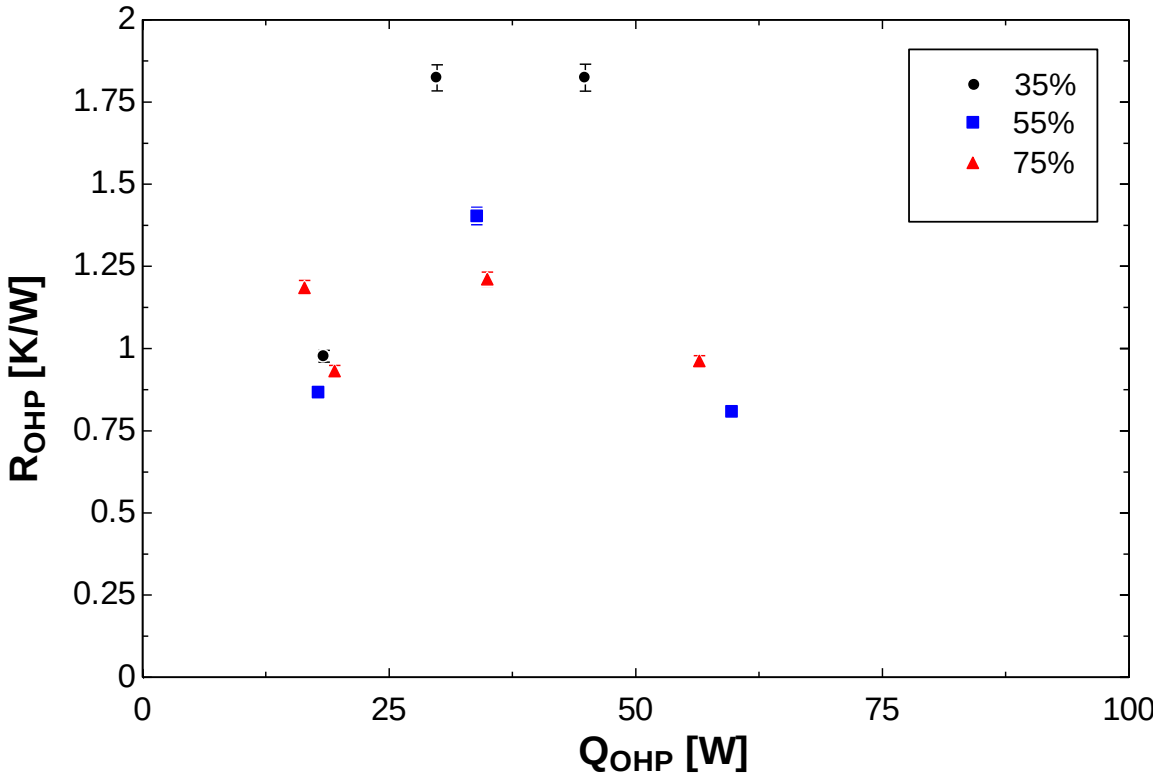

Figure 28: Pin-and-cavity OHP performance, 0° inclination angle.

The pin-and-cavity OHP performance at a 45° inclination angle (Figure 29) had more distinct trends then in the horizontal inclination angle. In this case the thermal resistance for the 35% and 55% fill ratios approached a thermal resistance plateau as the heating value increased. In general, it was observed that the 35% fill ratio performed better; however, as the heating value increased, the performance of 55% fill ratio and 35% fill ratio converged. The 75% fill ratio performed the worst in terms of thermal resistance and hit the maximum evaporator temperature at 175 W, compared to 250 W for 35% and 55% fill ratios.

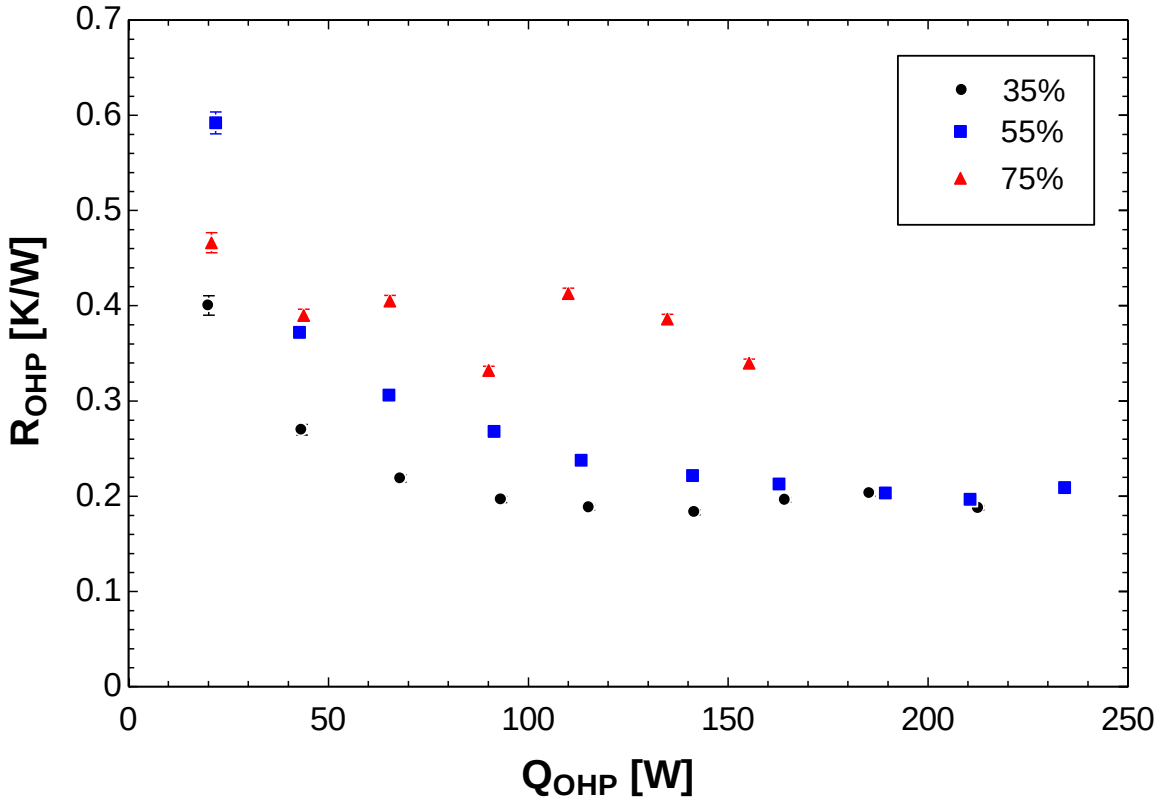

Figure 29: Pin-and-cavity OHP performance, 45° inclination angle.

The pin-and-cavity OHP performed best in the 90° inclination angle (Figure 30). All three fill ratios approached a thermal resistance plateau as heater power input increased and had nearly the same heat transfer capacity. In this case, the 35% fill ratio performed best, with 55% fill ratio being slightly worse, and 75% being the worst overall.

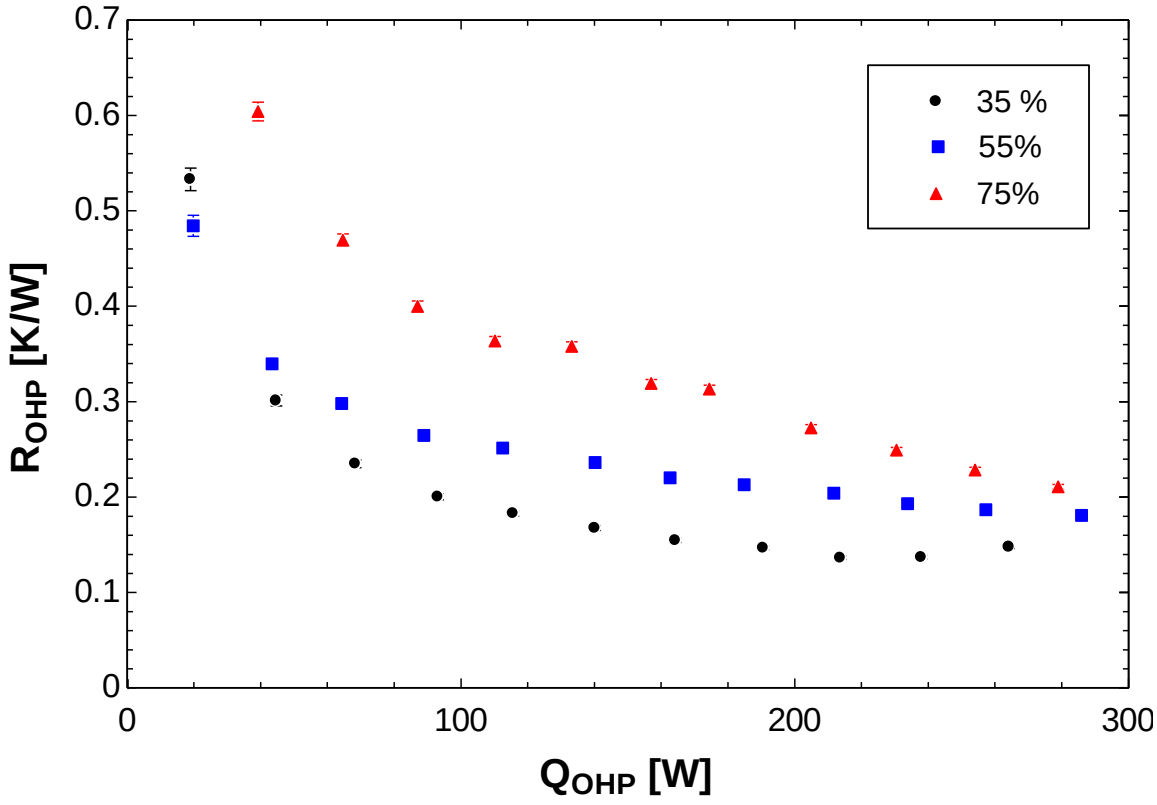

Figure 30: Pin-and-cavity OHP performance, 90° inclination angle.

3.1.3 – Recessed-Cavity OHP

The recessed-cavity OHP is a modified OHP that has small channels machined at an angle in the channel walls. This configuration is meant to promote bulk fluid flow, resulting in more stable operation.

The recessed-cavity OHP in the horizontal configuration (Figure 31) produced results unlike the straight-channel or pin-and-cavity OHPs. The 35% fill ratio was the worst performer, never oscillating. However, the 55% and 75% fill ratios did show signs of oscillation. At the 75% fill ratio, the thermal resistance plateau was observed, although at a higher thermal resistance than at other inclination angles. The 55% fill ratio performed the best, with consistent oscillations observed. As a result, it maintained a relatively low

thermal resistance up to 125 W, nearly double what the straight-channel and pin-and-cavity OHPs were capable of in this orientation.

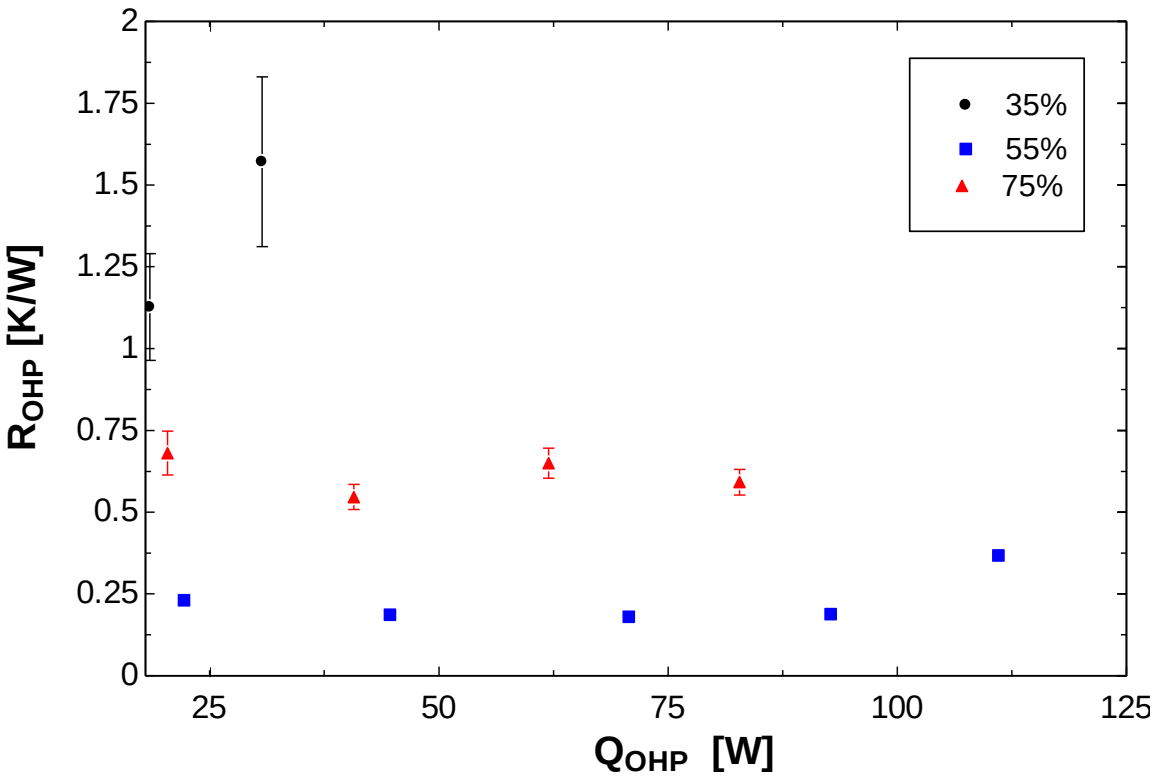

Figure 31: Recessed-cavity OHP performance, 0° inclination angle.

For the recessed-cavity OHP with a 45° inclination angle (Figure 32), the 75% fill ratio performed the worst. It had the highest thermal resistance and lowest heat transfer capacity.

The 55% fill ratio performed well up to 250 W. At this point, the flow regime was observed to change; instead of visible bubbles and liquid plugs, only a slow moving thin liquid film along the wall briefly remained with no visible liquid being transferred to the condenser section. This flow was similar to wispy annular flow, first described by

Bennett eta al. [70]. Wispy annular flow is described as a slow moving liquid film surrounding a rapidly moving gas core. This flow regime was unlike annular flow, which has been stated to decrease thermal resistance at the transition [71]. When the flow regime changed, the thermal resistance began to increase. However, full dry-out did not occur, maintaining the evaporator temperature at acceptable temperatures even when normal operation had subsided. The constant wetting of the surface is hypothesized to be responsible for maintaining the low evaporator temperature.

The 35% fill ratio performed the best. It had a nearly constant thermal resistance throughout all heating values. A small increase in thermal resistance was observed at a heater input power of 250 W. At this point, it was observed that the flow regime was beginning to change like it had for the 55% fill ratio. However, when the heater input power was increased, the regime switched back to primarily annular flow, maintaining the low thermal resistance. The 35% fill ratio was observed to transfer 400 W, the maximum heat input of the apparatus, without dry-out.

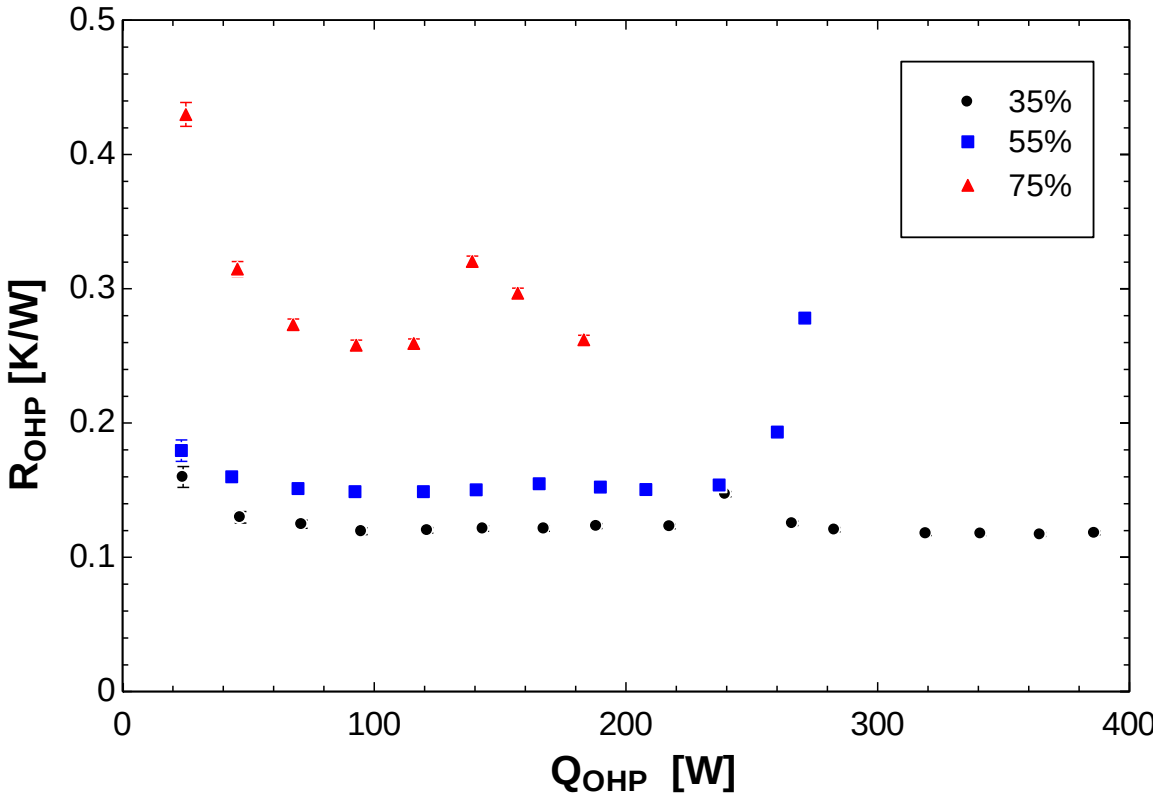

Figure 32: Recessed-cavity OHP performance, 45° inclination angle.

For the recessed-cavity OHP in the vertical orientation (Figure 33), the 75% fill ratio was the worst performer. It had a much higher thermal resistance and much lower heat transfer capacity than the 35% or 55% fill ratio. Up to 250 W heater power input, the 35% fill ratio and 55% fill ratio performed nearly the same. At 250 W, a similar trend as seen for the 45° orientation angle was observed.

The 55% fill ratio flow regime changed so only a thin film remained. When this occurred, the OHP continued to effectively transfer heat after normal oscillatory operation ceased. The OHP was no longer oscillating, but a thin film remained on the evaporator surface. It is believed that continuous wetting and subsequent vaporization of fluid allowed the OHP to maintain an allowable temperature without achieving dry-out.

Even with an increase in thermal resistance and only a thin film of fluid remaining, the 55% fill ratio continued to transfer sufficient heat to maintain the evaporator temperature below the previously defined maximum critical operating temperature. This may indicate that this geometry could provide protection against temperature spikes due to complete dry-out. Overall, the 35% fill ratio performed the best. However, it did not maintain a satisfactory evaporator temperature at heater power inputs above 300 W.

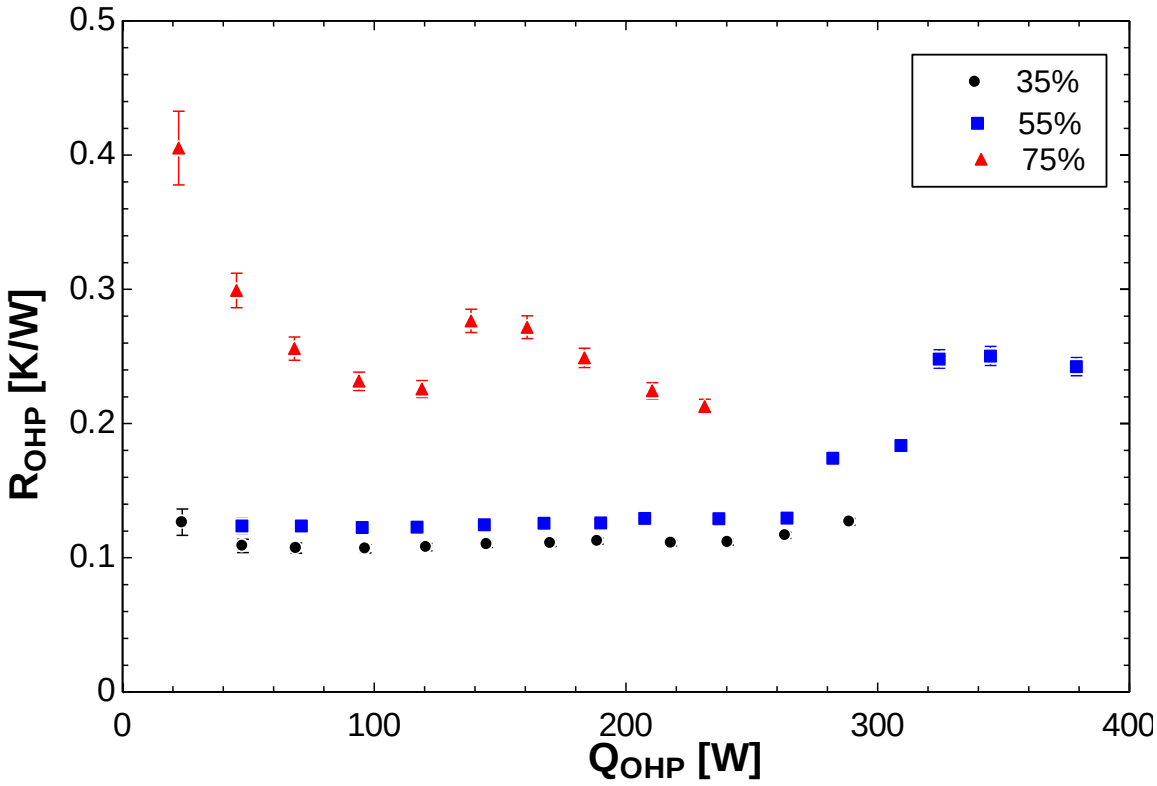

Figure 33: Recessed-cavity OHP performance, 90° inclination angle.

3.1.4 – Wavy-Channel OHP

The wavy-channel OHP is a modified OHP geometry consisting of wavy-channels in the evaporator section. The wavy-channels are meant to create turbulence to improve heat transfer between the channel walls and working fluid.

For the wavy-channel OHP in the horizontal orientation (Figure 34), the 75% fill ratio did not oscillate and had the highest thermal resistance. In contrast, the 35% and 55% fill ratios performed very well in this orientation. The OHP with both of these fill ratios had a nearly constant thermal resistance of 0.17 K/W at all heat input values. The 35% fill ratio had the highest heat transfer capacity, reaching 375 W of input power. At these fill ratios, small droplets of acetone were left on the channel walls as the liquid slugs passed through the wavy-channel evaporator section. These small droplets quickly evaporated, but instead of dry-out occurring, the system oscillated again, rewetting the surface. This wetting of the surface with small droplets was not observed in other testing, and it is believed to be a major reason why these fill ratios performed so well.

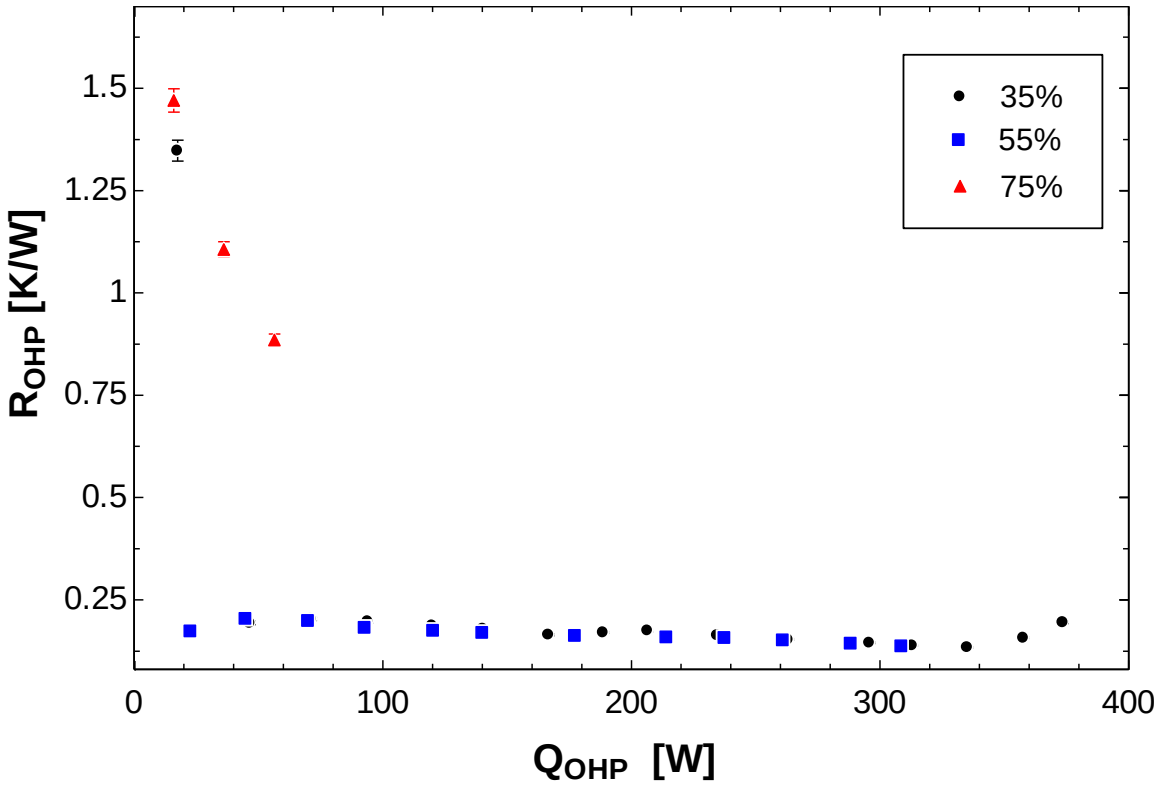

Figure 34: Wavy-channel OHP performance, 0° inclination angle.

For the wavy-channel OHP at the 45º inclination angle (Figure 35), the 75% fill ratio was the worst performer. The 75% fill ratio had a high thermal resistance at low heater power inputs, then dropped substantially as power input was increased. This was due to the OHP beginning to oscillate. At a heater power input of 150 W, the thermal resistance increased. This was due to a change in the flow regime, which at 175 W resulted in dry-out conditions. The OHP with 35% and 55% fill ratios performed well. For both fill ratios, a small inflection point was observed where the thermal resistance began to decrease as heater power input increased. It is unknown what caused this inflection. In this case, the 35% fill ratio had the largest heat transfer capacity, reaching 400 W of heater input power.

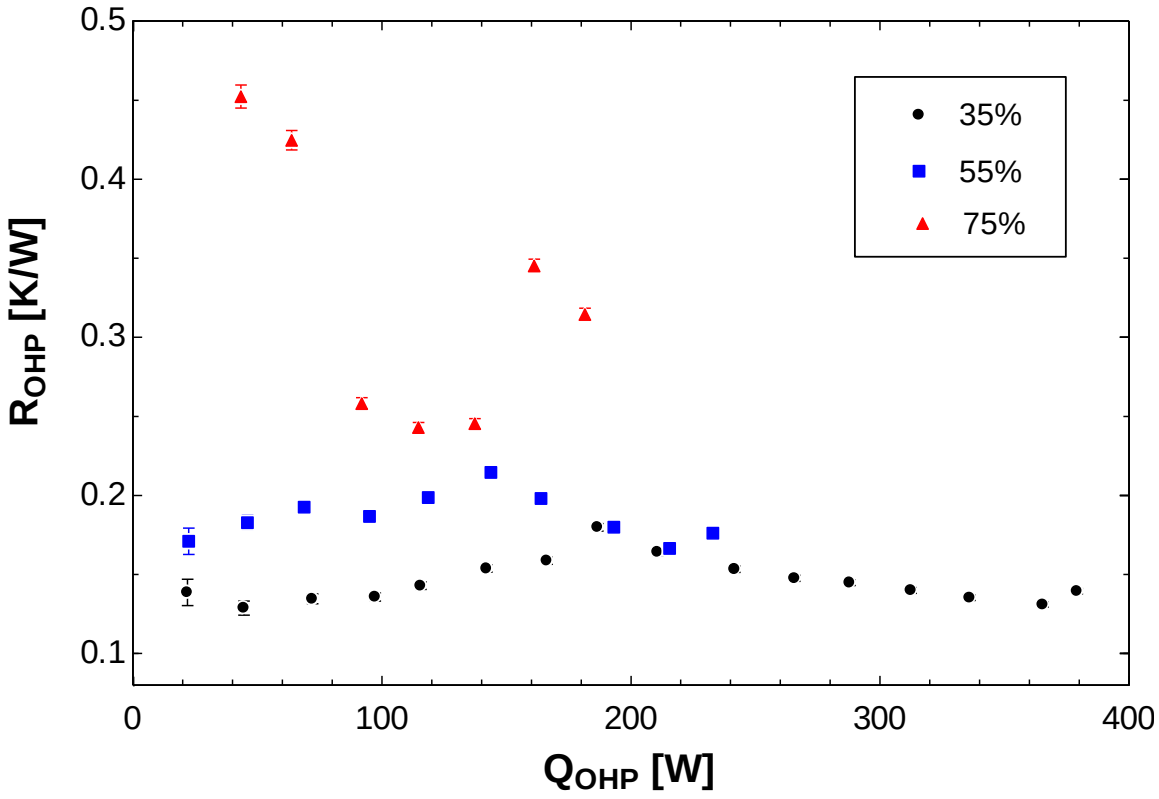

Figure 35: Wavy-channel OHP performance, 45° inclination angle.

For the wavy-channel OHP in the vertical orientation (Figure 36), the 55% and 75% fill ratio performed nearly identically. It is uncertain what caused this, since in the previous test they had performed very differently. The 35% fill ratio performed the best. As was seen for the 45° inclination angle, a small inflection point is present in the plot of thermal resistance versus heater input power. For higher heater powers, the OHP's thermal resistance decreased as heater power increased, and the OHP continued to operate up to 375 W of power input.

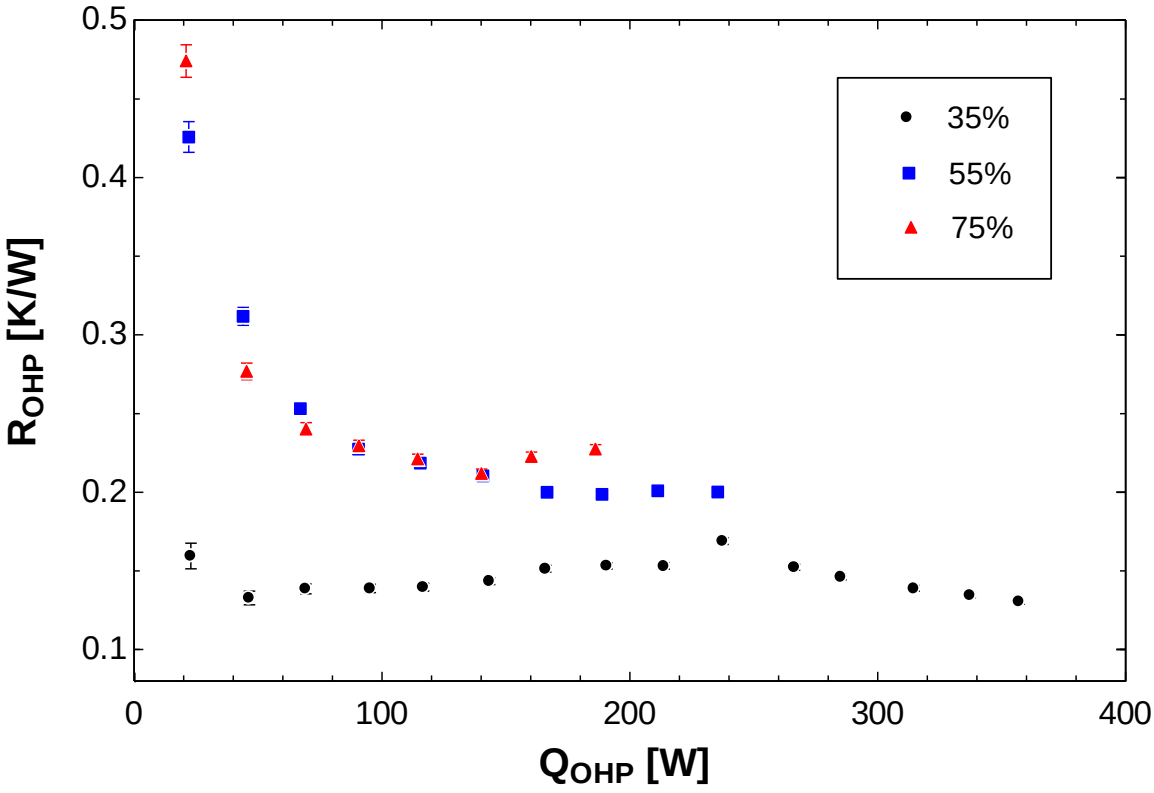

Figure 36: Wavy-channel OHP performance, 90° inclination angle.

3.2 - Geometry Comparison

A comparison was made between the heat transfer performance of each of the geometries. For the OHPs operating in the vertical position with a 35% fill ratio (Figure 37), the pin-and-cavity OHP had the highest thermal resistance and dried out at the lowest heat

input value. The wavy-channel and straight-channel OHPs performed similarly. The recessed-cavity OHP performed the best, having the lowest thermal resistance. However, even though the wavy-channel OHP had a higher thermal resistance, it also had a higher heat transfer capacity.

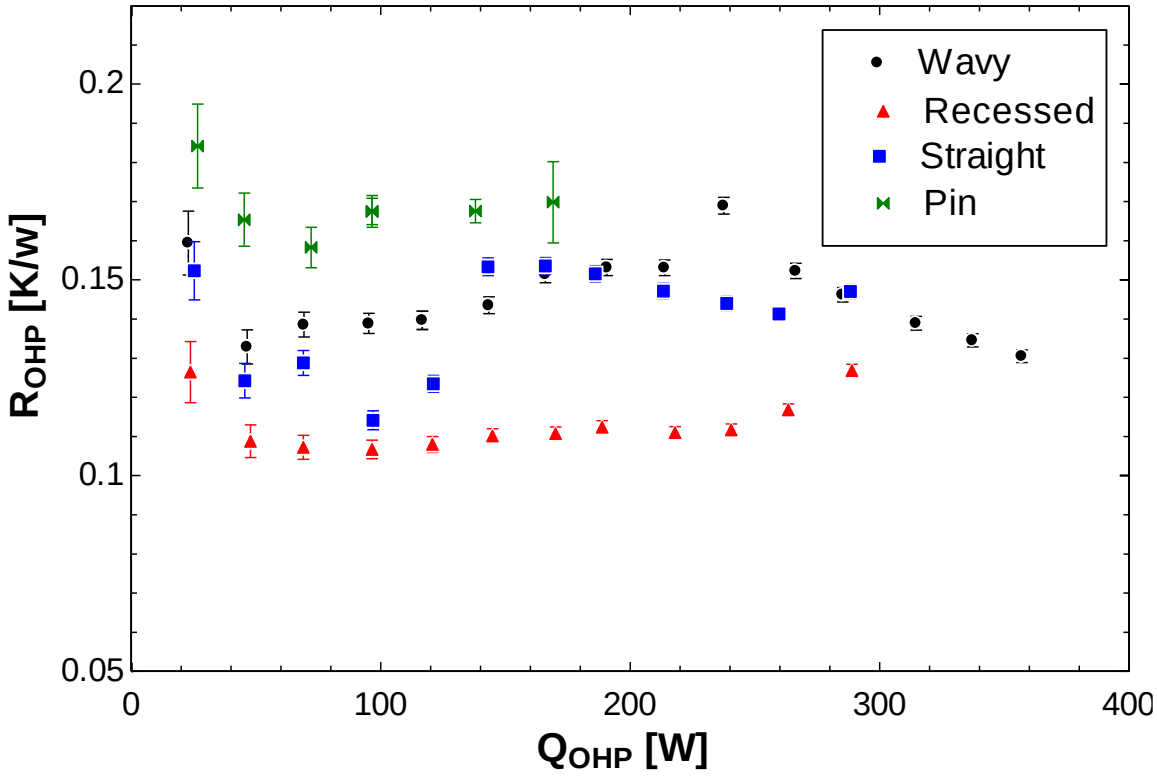

Figure 37: Performance comparison, 35% fill ratio with 90° inclination angle.

For the OHPs operating in the vertical orientation with a 55% fill ratio (Figure 38), the pin-and-cavity OHP had the highest thermal resistance, with the wavy-channel OHP performing slightly better while following a similar trend. The straight-channel OHP performed well at low input heater powers; however, after the initial heating, the thermal resistance began to trend upward towards the thermal resistance of the wavy-channel and pin-and-cavity OHPs. The recessed-cavity OHP performed the best overall. The recessed-cavity OHP's thermal resistance approached that of the other three OHPs at 275

W. However, the recessed-cavity OHP continued to operate beyond this point, although at a higher thermal resistance, due to a thin layer of working fluid being maintained at the channel surfaced as discussed in the previous section.

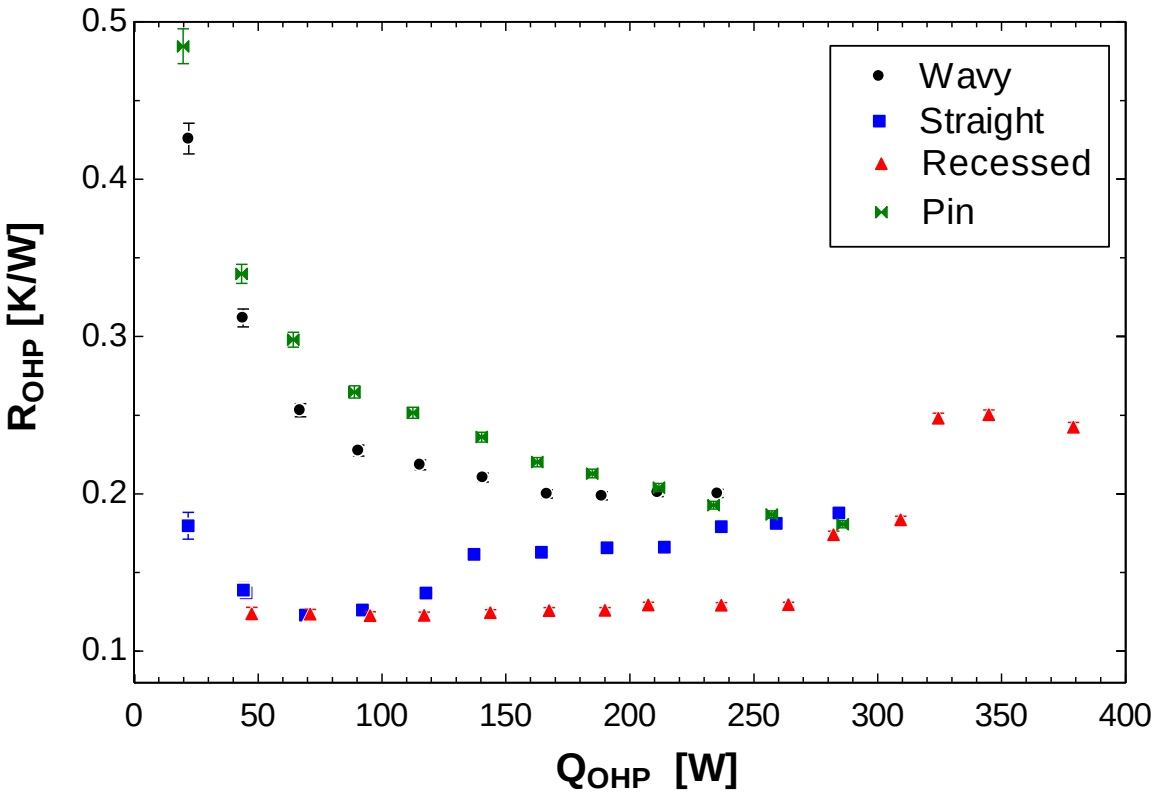

Figure 38: Performance comparison, 55% fill ratio with 90° inclination angle.

For the OHPs operating in the vertical orientation with a 75% fill ratio (Figure 39), the pin-and-cavity OHP performed worst with the highest thermal resistance. The other three OHP geometries performed very similarly. The straight-channel OHP was the only OHP for which the thermal resistance continued to decrease as the heater input power increased, with the exception of the high-thermal-resistance pin-and-cavity OHP.

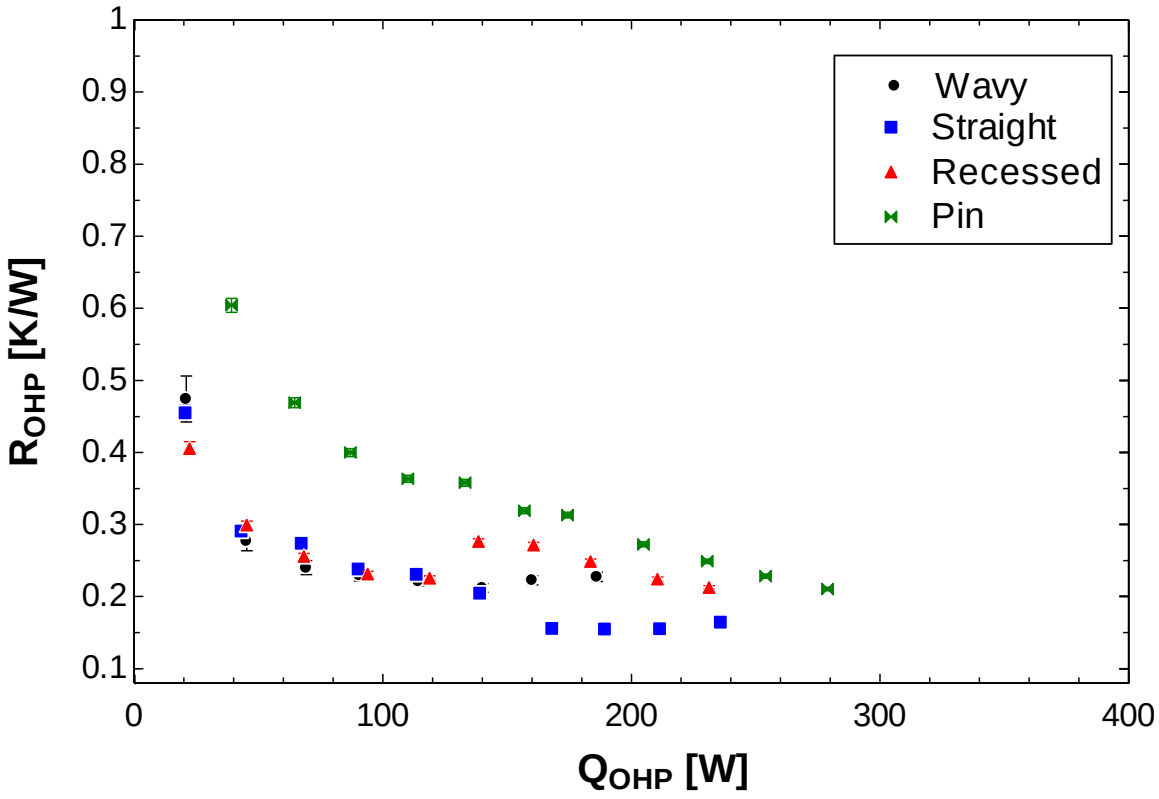

Figure 39: Performance comparison, 75% fill ratio with 90° inclination angle.

For the OHPs operating in the 45° inclination angle with a 35% fill ratio (Figure 40), the pin-and-cavity OHP had the highest thermal resistance. The wavy-channel and recessed-cavity OHPs performed the best, both having very high heat transfer rates. However, the recessed-cavity OHP had a slightly lower thermal resistance than the wavy-channel OHP. The straight-channel OHP was higher than the recessed-cavity or wavy-channel OHP and had a similar start-up trend as that of the pin-and-cavity OHP.

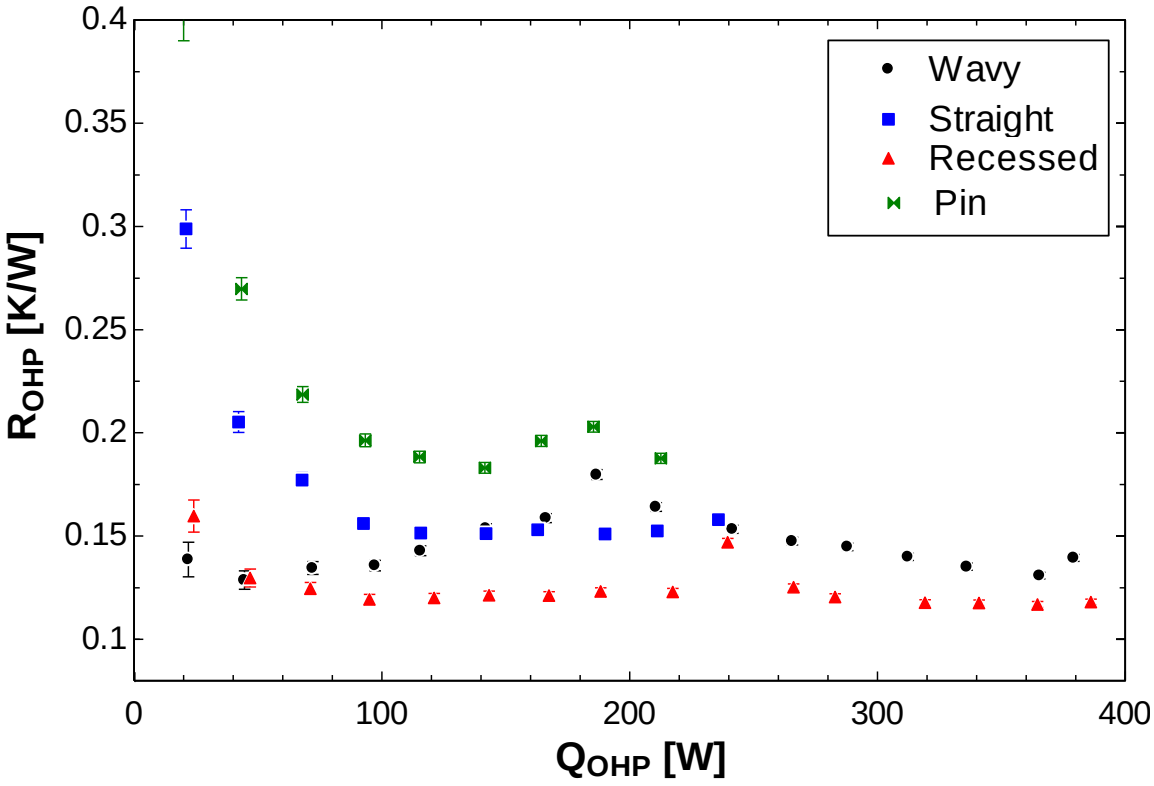

Figure 40: Performance comparison, 35% fill ratio with 45° inclination angle.

For the OHPs operating at the 45° inclination angle with a fill ratio of 55% (Figure 41), the pin-and-cavity OHP had the highest thermal resistance at lower heater input power, but converged to a similar thermal resistance of the other OHP geometries as the heating level increased. The wavy-channel, straight-channel, and recessed-cavity OHP geometries all had similar trends and thermal resistances. The recessed-cavity OHP was able to operate at a higher heat transfer level, but this was not at true OHP operation. Due to a thin film being maintained on the evaporator walls, the OHP operated at an acceptable temperature without dry-out occurring.

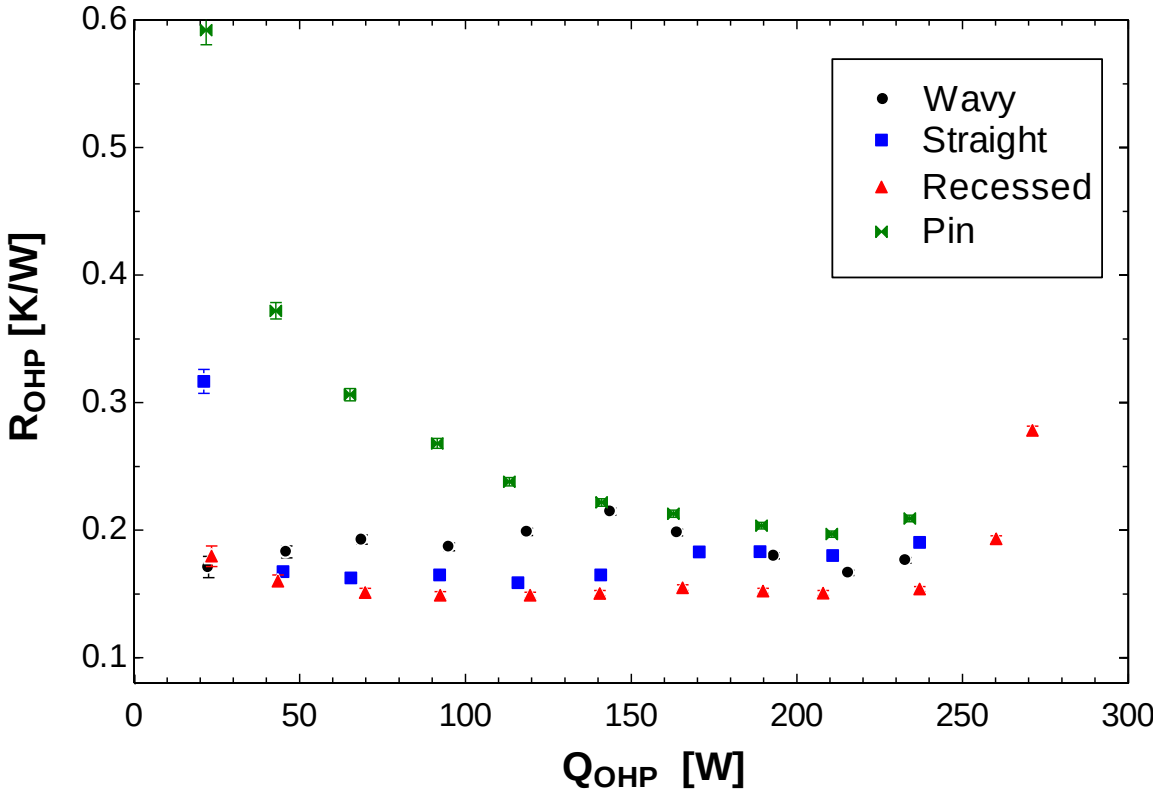

Figure 41: Performance comparison, 55% fill ratio with 45° inclination angle.

For the OHPs operating in the 45° inclination angle with a 75% fill ratio (Figure 42), each of the OHPs behaved quite differently, though the thermal resistance of the modified OHPs decreased with increased heater input power for all geometries. The straight-channel OHP had the lowest thermal resistance and maintained this low thermal resistance at a relatively constant value for each of the heater input powers.

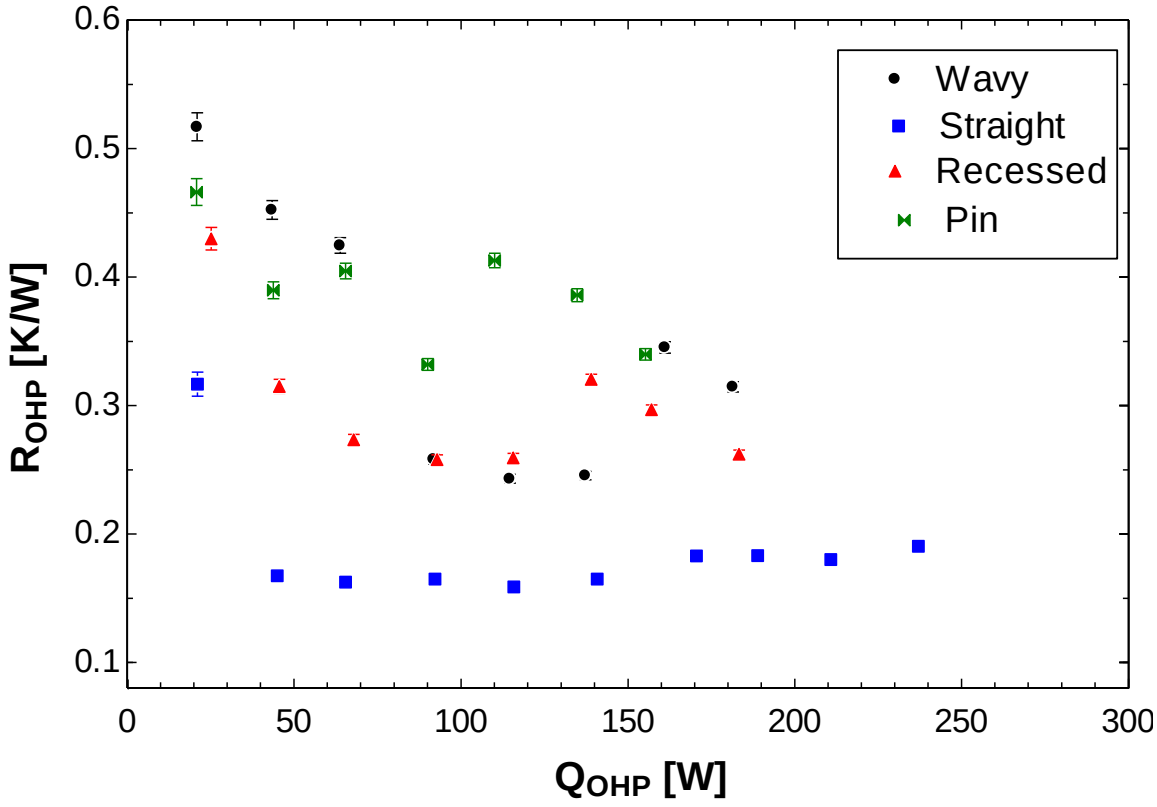

Figure 42: Performance comparison, 75% fill ratio with 45° inclination angle.

For the OHPs operating in the horizontal position with a 35% fill ratio (Figure 43), the straight-channel, recessed-cavity, and pin-and-cavity OHPs did not operate and thus had very high thermal resistances. In contrast, the wavy-channel OHP performed very well, achieving a nearly constant thermal resistance up to a heat transfer rate of 375 W before dry-out occurred in the evaporator section. The wavy-channel OHP operated well at this orientation compared to the other geometries, which may be a major advantage for this geometry. The wavy-channel OHP may be more robust in non-optimal configurations where the straight-channel or other geometries may not work properly.

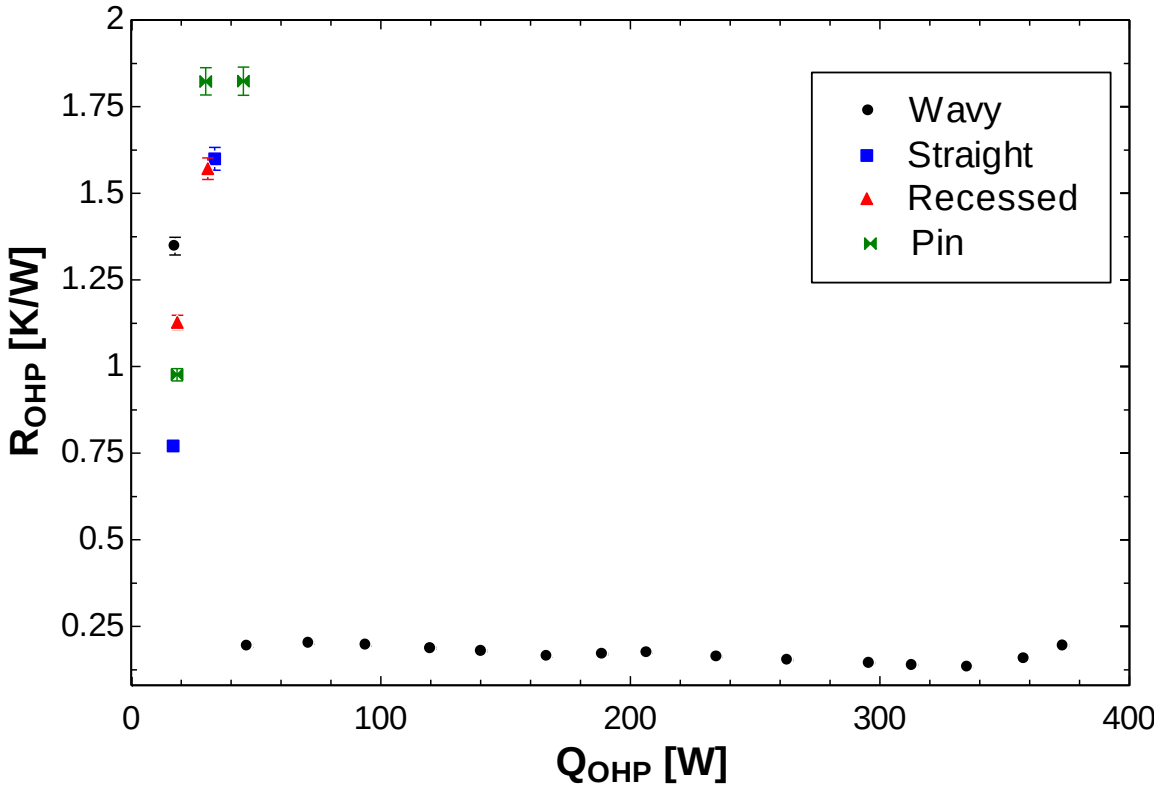

Figure 43: Performance comparison, 35% fill ratio with 0° inclination angle.

For the OHPs operating in the horizontal orientation with a 55% fill ratio (Figure 44), similar performance is observed for straight-channel and pin-and-cavity OHPs as for the 35% fill ratio. In this configuration, however, the recessed-cavity OHP did operate up to a heater input power of 125 W before dry-out occurred. This was a major improvement over the 35% fill ratio configuration. One possible explanation is that the additional working fluid in the OHP allowed the channel walls to stay wetted at higher temperatures longer, improving performance. The wavy-channel OHP again performed well, having a very low, steady thermal resistance.

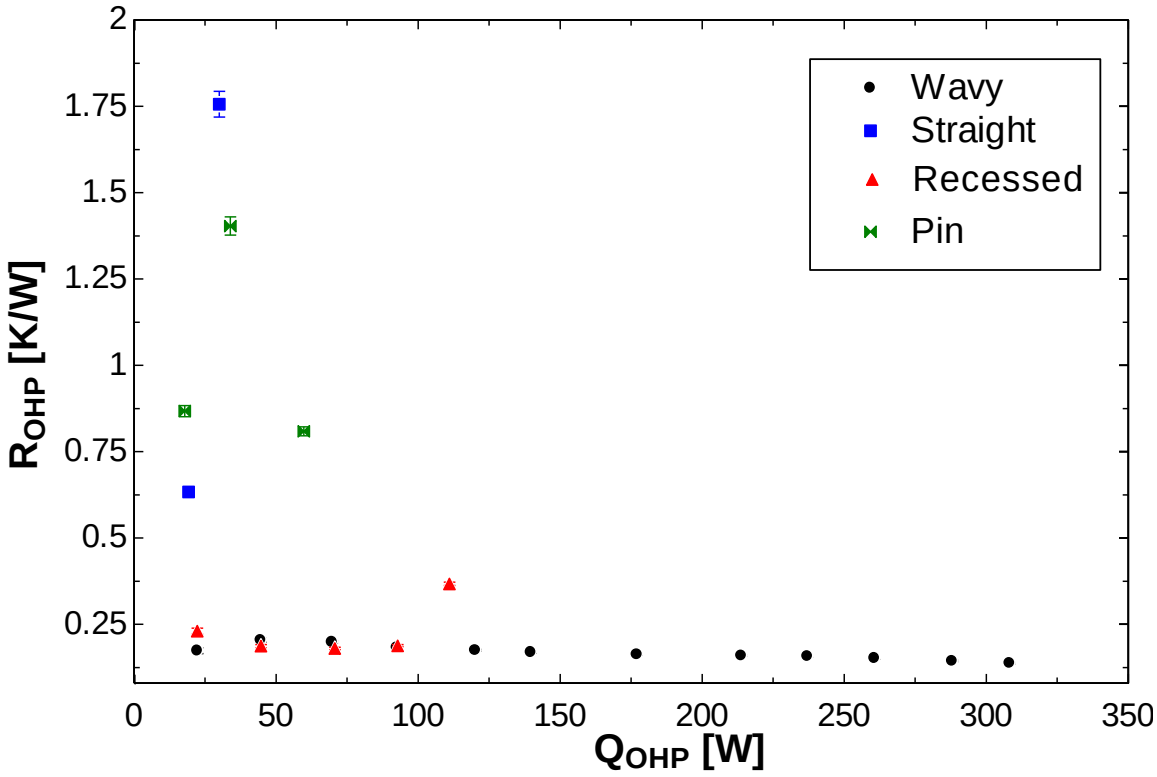

Figure 44: Performance comparison, 55% fill ratio with 0° inclination angle.

When the OHPs operated in the horizontal position with a 75% fill ratio (Figure 45), all exhibited very high thermal resistances, including the wavy-channel OHP. The additional fluid present in the OHP may have prevented fluid flow.

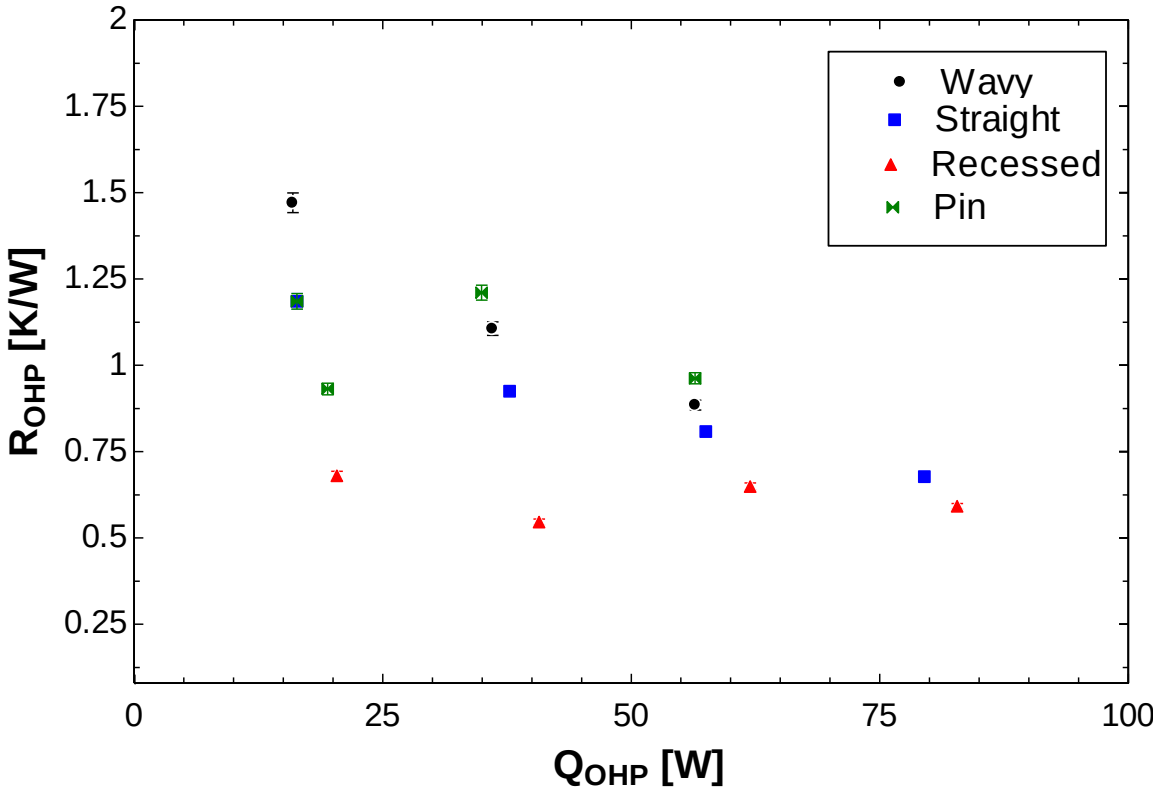

Figure 45: Performance comparison, 75% fill ratio with 0° inclination angle.

The average thermal resistance of each geometry for each test configuration is presented in Table 4. On average, the wavy-channel geometry performed the best, with the recessed-cavity OHP being second-best. The baseline straight-channel OHP was the third-best geometry, and the pin-and-cavity geometry had the worst overall performance.

Table 4: Average thermal resistance for each case, averaged over all heating input levels.

	K/W				
	Wavy	**Straight**	**Recessed**	**Pin**	**Average**
35%/90°	0.145	0.140	0.113	0.213	0.153
55%/90°	0.245	0.157	0.157	0.256	0.204
75%/90°	0.263	0.232	0.265	0.401	0.290
35%/45°	0.146	0.175	0.125	0.227	0.168
55%/45°	0.187	0.187	0.168	0.282	0.206
75%/45°	0.350	0.258	0.302	0.390	0.325
35%/0°	0.244	1.185	1.349	1.541	1.080
55%/0°	0.169	1.195	0.231	1.027	0.655
75%/0°	1.154	0.899	0.617	1.073	0.936
Average	0.322	0.492	0.370	0.601	

The average thermal resistance for each of the geometries is shown in Figure 46. The wavy-channel and recessed-cavity OHPs performed on average 40% and 27.6% better than the traditional straight-channel OHP, respectively. The pin-and-cavity OHP performed 22.7% worse than the straight-channel OHP.

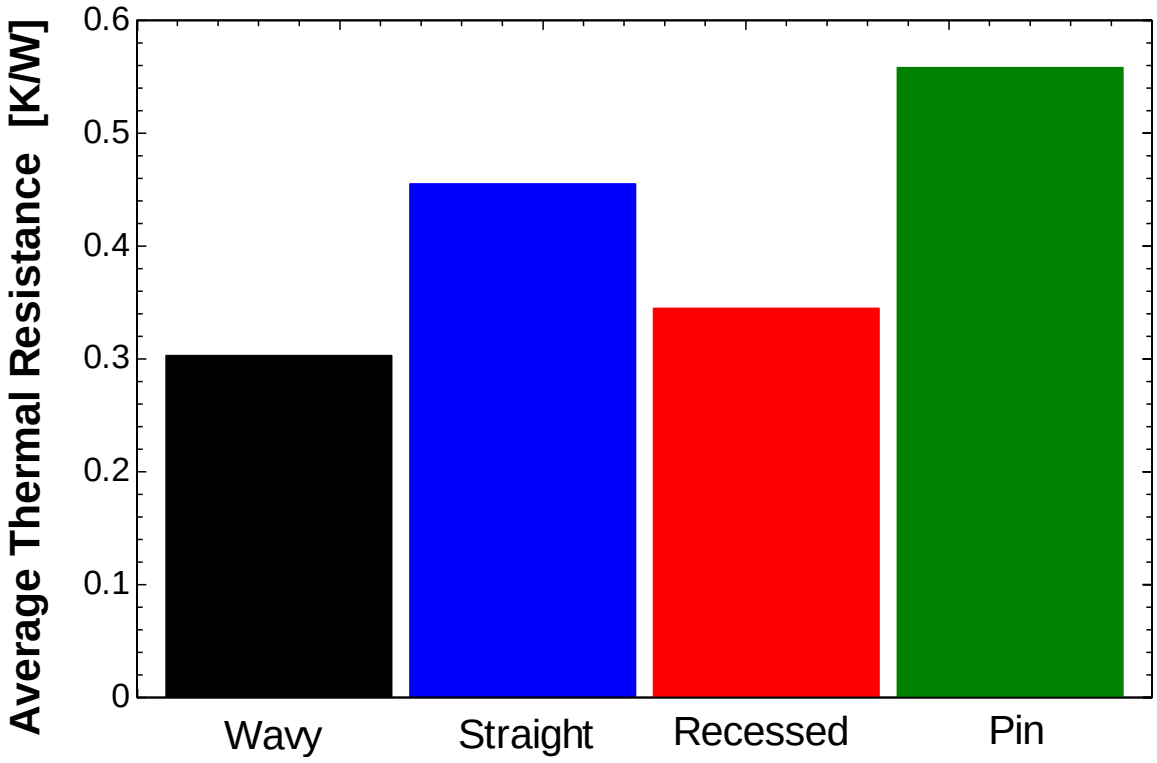

Figure 46: Average thermal resistance of each geometry.

Figure 47 presents the average thermal resistance for each geometry in each orientation and fill ratio. As the fill ratio increases, the thermal resistance increases for all four geometries. It is also apparent that the 0° inclination angle had the largest thermal resistances, with the exception of the wavy-channel geometry and the recessed-cavity geometry for one fill ratio. The pin-and-cavity geometry had a slightly greater thermal resistance than the other geometries. Figure 47 excludes the horizontal data in order to show the other orientations in greater detail.

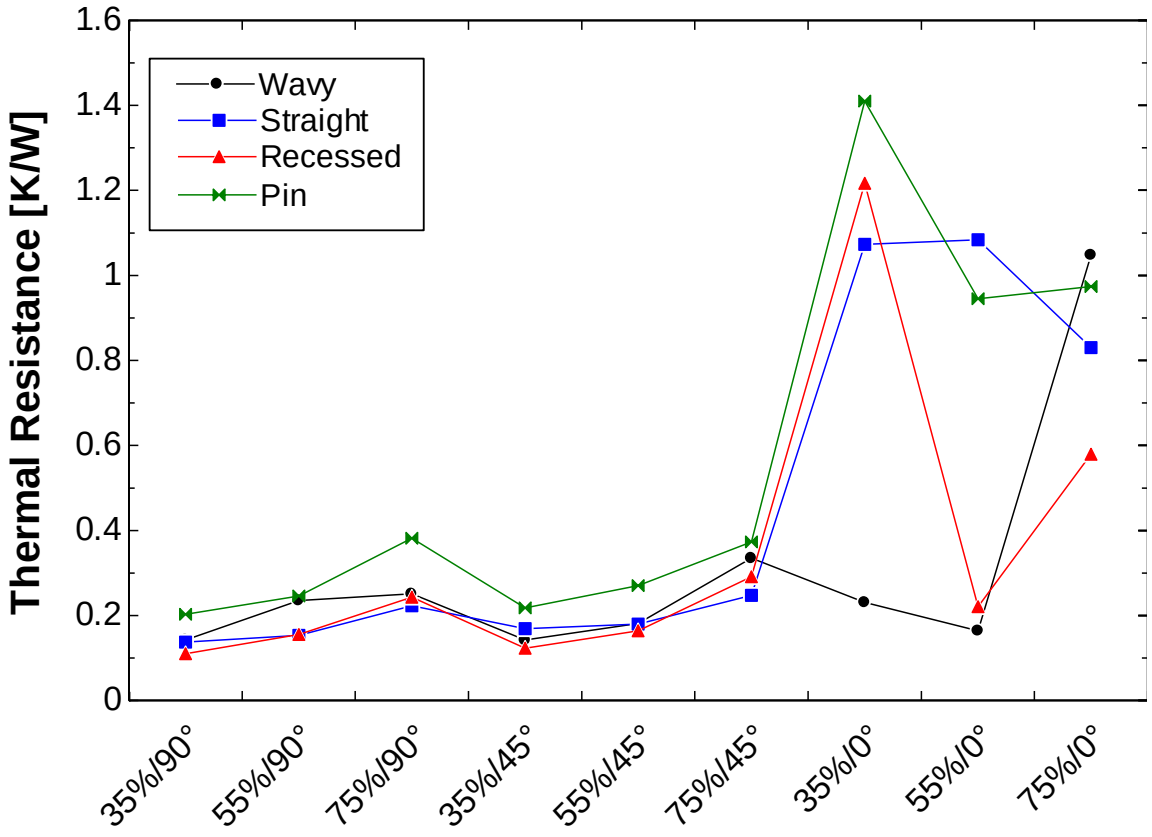

Figure 47: Average thermal resistance comparison for each geometry in each case.

The pin-and-cavity geometry had the highest thermal resistance for the non-horizontal orientation angles. The relative performance of the other three geometries varied between each case. The recessed-cavity OHP performed the best, and the wavy-channel and straight-channel OHPs performed nearly the same. If the analysis from above is repeated, excluding the horizontal data, then wavy-channel performs 14.9% worse, recessed-cavity 2.2% better, and pin-and-cavity 45.0% worse than the straight-channel OHP.

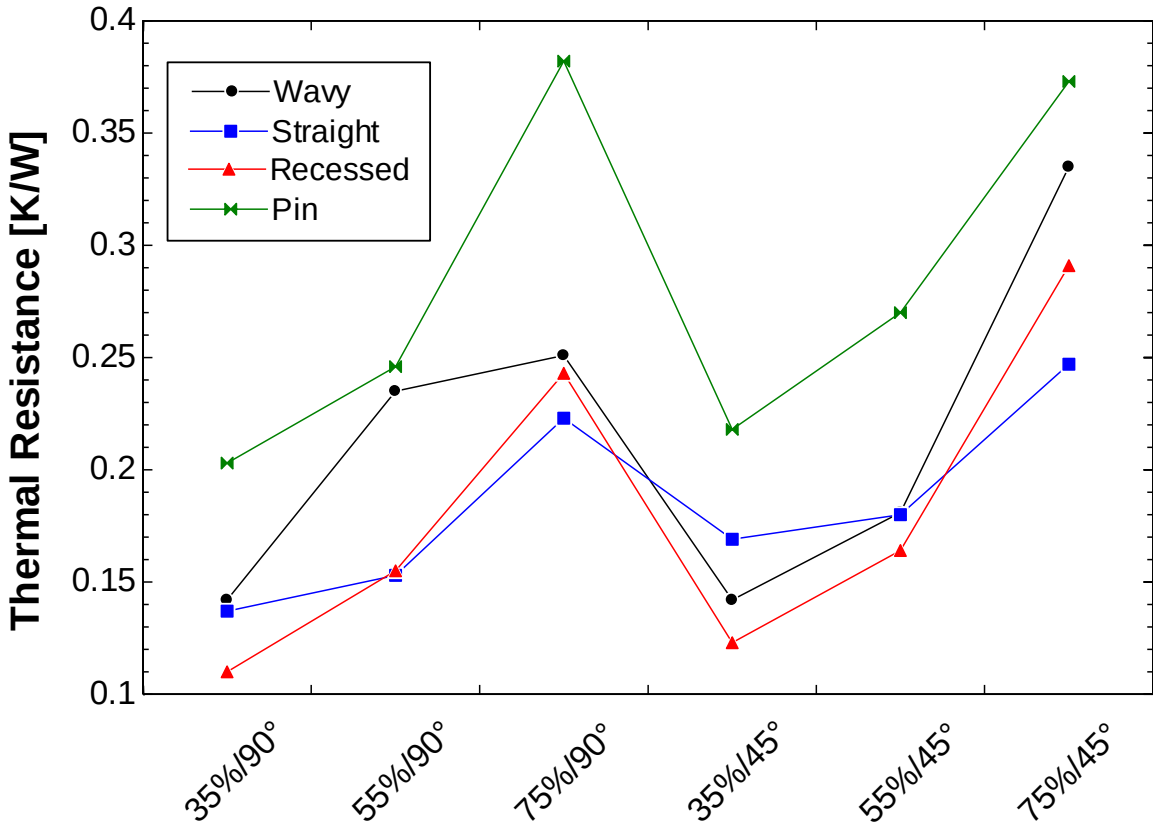

Figure 48: Average thermal resistances, excluding 0° inclination angle.

The maximum heat transfer rate is also an important properties to consider. The maximum rate of heat transfer for heat case is presented in Table 5. Trends for the maximum heat transfer rate are comparable to those made for thermal resistance. The best heat transfer rate is at the 90° inclination angle, and the best fill ratio is 35% overall. The wavy-channel OHP had the best overall performance at 256.4 W and recessed-cavity OHP was 218.2 W. The straight-channel OHP and pin-and-cavity OHP were similar at 178.8 and 176.9 W, respectively. The maximum heat transfer rate was 386 W for the recessed-cavity OHP at a 45° inclination angle and 35% fill ratio.

Table 5: Maximum heat transfer rate for each case.

Case	Wattage				
	Wavy	Straight	Recessed	Pin	Average
35%/90°	354.2	288.3	288.8	264.1	298.9
55%/90°	235.4	259.1	379.0	285.9	289.9
75%/90°	186.2	235.7	231.2	278.9	233.0
35%/45°	379.2	235.8	386.0	212.6	303.4
55%/45°	232.8	237.0	271.1	234.1	243.8
75%/45°	181.5	210.4	183.3	155.2	182.6
35%/0°	373.5	33.4	30.7	44.9	120.6
55%/0°	308.3	29.9	111.0	59.7	127.2
75%/0°	56.5	79.5	82.8	56.4	68.8
Average	256.4	178.8	218.2	176.9	

3.3 – Effective Heat Transfer Coefficient

An attempt to compare the performance of the OHP geometries investigated in this study with other cooling methods commonly used for electronic thermal management is presented in Figure 49. The OHP has definite thermal advantages compared with some of the cooling techniques. The OHPs are orders of magnitude better at cooling than the common air heat sink. Even when a fan is introduced, creating forced convection, the OHP has much better heat transfer coefficient. Water with natural convection also does not perform as well as the OHPs, but when water is pumped to create forced convection, the heat transfer coefficient is similar to that of the OHP. However, water with forced

convection requires external power input which may not be possible for certain applications. It is not until jet impingement, boiling, and condensation are used that greater heat transfer coefficients are achieved. These technologies also have drawbacks, such as noise, size requirements, and external power input.

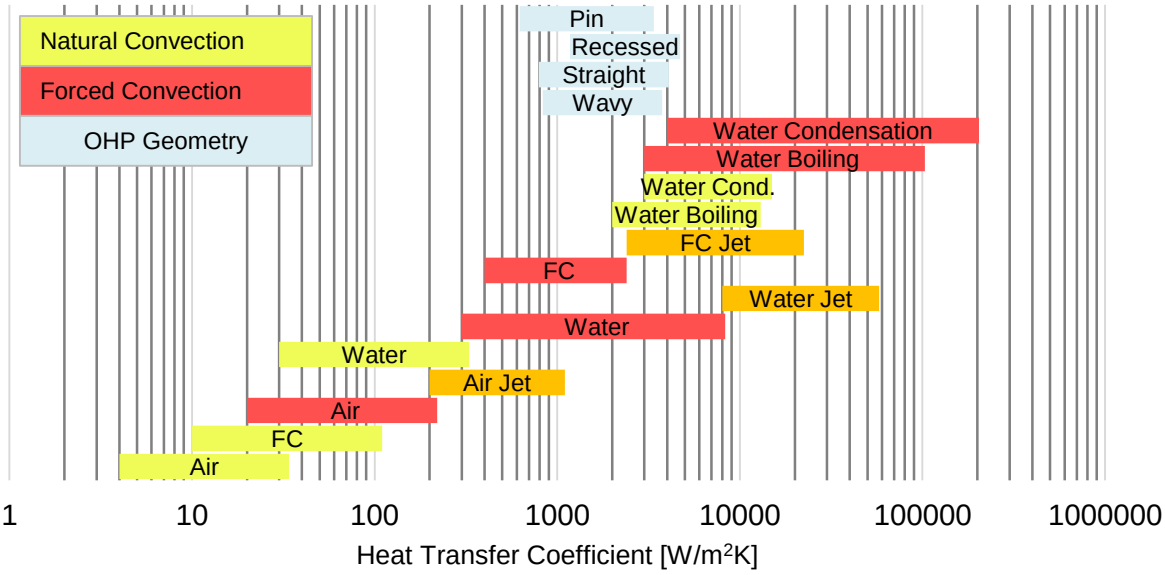

Figure 49: Heat transfer coefficient comparison of various cooling technologies [3].

Although the type of cooling technique employed will vary with each application, Figure 49 shows that OHPs can be very competitive with other techniques while being passive. Although some technologies do have higher heat transfer coefficients, such as jet impingement, the ability of the OHP to maintain acceptable temperatures in a passive environment means that it will have several unique advantages for cooling applications.

CHAPTER 5 – CONCLUSIONS

Four evaporator geometries were constructed and tested under similar conditions. From these tests, several conclusions can be made about each geometry and the overall operation of OHPs.

It has been found that for acetone the lower the fill ratio, the better the performance. This can only be stated for acetone, as other working fluid properties will affect how the fluid performs in an OHP. In each orientation, with the exception of horizontal, the 35% fill ratio was the best performer with an average overall thermal resistance of 0.161 K/W. The 55% and 75% fill ratios had an average thermal resistance of 0.205 K/W and 0.308 K/W, respectively. At the horizontal inclination angle the 55% fill ratio was found to be the best at 0.655 K/W; however, at this orientation the OHP was non-operational for nearly all cases.

Overall, the OHP's performance in the horizontal inclination angle was reduced. Pulsating flow was not observed in the straight-channel, pin-and-cavity, and some configurations of the recessed-cavity OHP. In these cases, the fluid was stagnant in the evaporator section. This indicates that there is some gravity dependence in the operation of the OHP. However, this was not the case for the wavy-channel configuration.

The wavy-channel OHP had an average thermal resistance of 0.244 K/W in the horizontal position. This is a 55% increase in thermal resistance over the averages of the vertical and 45° inclination. This increase, however, is small compared to the over 200%

increase in thermal resistance found for the other geometries. The high level of performance for the wavy-channel OHP was attributed to small droplets of acetone that were deposited on the surface of the OHP channels. These small droplets prevented dry-out from occurring, because the bubbles would boil off, taking advantage of heat removal from latent heat transfer. This then resulted in a varying pressure differential that would drive the condensed fluid to the evaporator section. The significant improvement found over the other geometries indicates that the wavy-channel configuration is highly effective in horizontal applications.

The results of this study show that geometry does have an effect on the performance of the OHP. The pin-and-cavity geometry was the worst performing, with an average thermal resistance of 0.601 K/W. This is believed to be due to the larger pressure drop through the evaporator section. This increased pressure drop resisted the fluid flow between the evaporator and condenser sections that ultimately reduced flow. The recessed-cavity and wavy-channel OHPs both performed better than the straight-channel geometry, which had an average thermal resistance of 0.492 K/W. This is believed to be due to an increase in the surface area coupled with only a slight increase in pressure drop. The recessed-cavity OHP was the best performer when the horizontal results are neglected, with an average thermal resistance of 0.188 K/W. The increase in performance could be a result of the increase in surface area in the evaporator section. The wavy-channel OHP was the best overall performer, with an average thermal resistance of 0.322 K/W. This was largely due to the highly effective performance in the horizontal inclination angle.

From this study, it can be concluded that variations in geometry can have both positive and negative contributions to an OHP. The recessed-cavity and wavy-channel OHPs both showed improvements of 41.7% and 28.4%, respectively, over the baseline straight-channel OHP. However, these geometries do add complexity to the design that can add to overall system cost. However, the wavy-channel configuration is a simple variation of the straight-channel geometry and wavy-channels are used widely in other applications. The simplicity and improved performance may make it a superior design option over the straight-channel OHP. Conversely, the pin-and-cavity OHP showed negative performance, increase in thermal resistance by 22.3% over the straight-channel OHP, and increased complexity. This geometry may not be ideal for OHP operation, though variations in cavity density should be explored further to determine if varying the pressure drop through the evaporator can improve its performance.

CHAPTER 6 – FUTURE WORK

Suggested work on current apparatus:

- Conduct a thorough flow analysis using high speed video to identify and understand the mechanisms that are causing flow regime changes.
- Determine pressure drop for each geometry, determine significance of pressure drop to performance.
- Conduct study using a different working fluid, such as R-141b or FC-72.

Work for future development:

- Develop geometry optimization methods by further investing the effects of pressure drop on performance using known two-phase flow correlations for simple geometry.
- Develop alternative geometries for testing.
- Study a straight-channel OHP with small springs inserted into channels in evaporator sections, and evaluate performance.

LITERATURE CITED

[1] Garimella, S. V., Fleischer, A. S., Murthy, J. Y., Keshavarzi, A., Prasher, R., Patel, C., Bhavnani, S. H., Venkatasubramanian, R., Mahajan, R., Joshi, Y., Sammakia, B., Myers, B. A., Chrosinski, L., Baelmans, M., Sathyamurthy, P. and Raad, P.E., 2008, "Thermal Challenges in Next-Generation Electronic Systems," IEEE Thransactions on Components and Packaging Technologies, 31(4), pp. 801-815.
[2] Mudawar, I., 2001, "Assessment of High-Heat-Flux Thermal Management Schemes," Ieee Transactions on Components and Packaging Technologies, 24(2), pp. 122-141.
[3] Lasance, C. J., and Simons, R. E., 2005, "Advances in High-Performance Cooling for Electronics," Electronics Cooling, 11(4).
[4] Simons, R. E., 1996, "Direct Liquid Immersion Cooling for High Power Density Microelectronics," Electronics Cooling, 2, pp. 24-29.
[5] 2016, "Cold Plate," http://www.lytron.com/Cold-Plates.
[6] Mudawar, I., and Maddox, D., 1989, "Critical Heat Flux in Subcooled Flow Boiling of Fluorocarbon Liquid on a Simulated Electronic Chip in a Vertical Rectangular Channel," International Journal of Heat and Mass Transfer, 32(2), pp. 379-394.
[7] Kim, J., 2007, "Spray Cooling Heat Transfer: The State of the Art," International Journal of Heat and Fluid Flow, 28(4), pp. 753-767.
[8] Chrysler, G., Chu, R., and Simons, R., "Jet Impingement Boiling of a Dielectric Coolant in Narrow Gaps," Proc. Thermal Phenomena in Electronic Systems, 1994. I-THERM IV. Concurrent Engineering and Thermal Phenomena., InterSociety Conference on, IEEE, pp. 1-8.
[9] 2014, "Spray Cooling of Electronics," http://mscweb.gsfc.nasa.gov/msctech/spraycooling.htm.
[10] Zuo, Z. J., North, M. T., and Wert, K. L., 2001, "High Heat Flux Heat Pipe Mechanism for Cooling of Electronics," Ieee Transactions on Components and Packaging Technologies, 24(2), pp. 220-225.
[11] 2014, "Heat Pipe Solutions: Copper-Water."
[12] Khrustalev, D., and Faghri, A., 1995, "Thermal Characteristics of Conventional and Flat Miniature Axially Grooved Heat Pipes," J. Heat Transf.-Trans. ASME, 117(4), pp. 1048-1054.
[13] Nadgauda, O., 2006, "Fabrication, Filling, Sealing and Testing of Micro Heat Pipes."
[14] Akachi, H., 1990, "Structure of a Heat Pipe," U. S. Patent, ed.
[15] Ahachi, H., Polasek, F., & Stulc, P.,, "Pulsating Heat Pipes," Proc. Proceedings of the 5th Inernational Heat Pipe Symposium
[16] Taft, B. S., Williams, A. D., and Drolen, B. L., 2012, "Review of Pulsating Heat Pipe Working Fluid Selection," J Thermophys Heat Tr, 26(4), pp. 651-656.
[17] Rittidech, S., Dangeton, W., and Soponronnarit, S., 2005, "Closed-ended Oscillating Heat-Pipe (CEOHP) Air-Preheater for Energy Thrift in a Dryer," Appl. Energy, 81(2), pp. 198-208.
[18] Shafi, M., Faghri, A., and Zhang, Y., 2001, "Thermal Modeling of Unlooped and Looped Pulsating Heat Pipes," Journal of Heat Transfer, 12(6), pp. 1159-1172.
[19] Khandekar, S., 2004, "Therm-Hydrodynamics of Closed Loop Pulsating Heat Pipes," Ph. D., Universitat Stuttgart, Stuttgart, Germany.

[20] Thompson, S. M., Ma, H. B., and Wilson, C., 2011, "Investigation of a Flat-Plate Oscillating Heat Pipe with Tesla-type Check Valves," Exp. Therm. Fluid Sci., 35(7), pp. 1265-1273.
[21] Gu, J., Kawaji, M., and Futamata, R., 2004, "Effects of Gravity on the Performance of Pulsating Heat Pipes," J Thermophys Heat Tr, 18(3), pp. 370-378.
[22] Xu, J., Li, Y., and Wong, T., 2005, "High Speed Flow Visualization of a Closed Loop Pulsating Heat Pipe," International Journal of Heat and Mass Transfer, 48(16), pp. 3338-3351.
[23] Charoensawan, P., and Terdtoon, P., 2008, "Thermal Performance of Horizontal closed-Loop Oscillating Heat Pipes," Appl. Therm. Eng., 28(5-6), pp. 460-466.
[24] Yang, H., Kandekar, S., and Groll, M.,, "Operational Characteristics of Flat Plate Closed Loop Pulsating Heat Pipes," Proc. Precedings of the 13th International Heat Pipe Conference.
[25] Khandekar, S., Charoensawan, P., Groll, M., and Terdtoon, P., 2003, "Closed Loop Pulsating Heat Pipes - Part B: Visualization and Semi-Empirical Modeling," Appl. Therm. Eng., 23(16), pp. 2021-2033.
[26] Zhang, X. M., Xu, J. L. and Zhou, Z. Q.,, 2004, "Experimental Study of a Pulsating Heat Pipe Using FC-72, Ethonal, and Water as Working Fluids," Experimental Heat Transfer, 17(1), pp. 47-67.
[27] Yin, D., Rajab, H., and Ma, H.,, 2014, "Theoretical Analysis of Mazimum Filling Ratio in an Oscillating Heat Pipe," International Journal of Heat and Mass Transfer, 74, pp. 353-357.
[28] Groll, M., and Khandekar, S., "State of the Art on Pulsating Heat Pipes," Proc. ASME 2004 2nd International Conference on Microchannels and Minichannels, American Society of Mechanical Engineers, pp. 33-44.
[29] Pachghare, P., Borkar R., 2012, "State of The Art on Closed Loop Pulsating Heat Pipe," International Journal of Emerging Technology and Advanced Engineering, 2(10), pp. 202-207.
[30] Mito, T., Natsume, K., Yanagi, N., Tamura, H., Tamada, T., Shikimachi, K., Hirano, N., and Nagaya, S., 2010, "Development of Highly Effective Cooling Technology for a Superconducting Magnet Using Cryogenic OHP," Applied Superconductivity, IEEE Transactions on, 20(3), pp. 2023-2026.
[31] Jiao, A. J., Ma, H. B., and Critser, J. K., 2009, "Experimental Investigation of Cryogenic Oscillating Heat Pipes," International Journal of Heat and Mass Transfer, 52(15-16), pp. 3504-3509.
[32] Hathaway, A. A., Wilson, C. A., and Ma, H. B., 2012, "Experimental Investigation of Uneven-Turn Water and Acetone Oscillating Heat Pipes," J Thermophys Heat Tr, 26(1), pp. 115-122.
[33] Maydanik, Y. F., Dmitrin, V. I., and Pastukhov, V. G., 2009, "Compact Cooler for Electronics on the Basis of a Pulsating Heat Pipe," Appl. Therm. Eng., 29(17-18), pp. 3511-3517.
[34] Han, H., Cui, X. Y., Zhu, Y., and Sun, S. D., 2014, "A Comparative Study of the Behavior of Working Fluids and their Properties on the Performance of Pulsating Heat Pipes (PHP)," Int. J. Therm. Sci., 82, pp. 138-147.

[35] Cui, X. Y., Zhu, Y., Li, Z. H., and Shun, S. D., 2014, "Combination Study of Operation Characteristics and Heat Transfer Mechanism for Pulsating Heat Pipe," Appl. Therm. Eng., 65(1-2), pp. 394-402.
[36] Qu, J., and Wu, H. Y., 2011, "Thermal Performance Comparison of Oscillating Heat Pipes with SiO2/water and Al2O3/water Nanofluids," Int. J. Therm. Sci., 50(10), pp. 1954-1962.
[37] Ma, H. B., Wilson, C., Yu, Q., Park, K., Choi, U. S., and Tirumala, M., 2006, "An Experimental Investigation of Heat Transport Capability in a Nanofluid Oscillating Heat Pipe," J. Heat Transf.-Trans. ASME, 128(11), pp. 1213-1216.
[38] Ma, H. B., Wilson, C., Borgmeyer, B., Park, K., Yu, Q., Choi, S. U. S., and Tirumala, M., 2006, "Effect of Nanofluid on the Heat Transport Capability in an Oscillating Heat Pipe," Appl. Phys. Lett., 88(14), p. 3.
[39] Cheng, P., Thompson, S., Boswell, J., and Ma, H. B., 2010, "An Investigation of Flat-Plate Oscillating Heat Pipes," J. Electron. Packag., 132(4), p. 6.
[40] Mameli, M., Marengo, M., and Zinna, S., 2012, "Thermal Simulation of a Pulsating Heat Pipe: Effects of Different Liquid Properties on a Simple Geometry," Heat Transfer Eng, 33(14), pp. 1177-1187.
[41] Lin, Z., Wang, S., Huo, J., Hu, Y., Chen, J., Zhang, W., and Lee, E.,, 2011, "Heat Transfer Characterisitics and LED Heat Sink Application of Aluminum Plate Oscillating Heat Pipes," Appl. Therm. Eng., 31(14-15), pp. 2221-2229.
[42] Khandekar, S., and Groll, M.,, 2006, "Insights into the Performance Modes of Closed Loop and Pulsating Heat Pipes and some Design Hints," Proceeding of the 18th National & 7th ISHMT-ASME Heat and Mass Transfer ConferenceGuwahtl, India.
[43] Hu, C. F., and Jia, L., 2011, "Experimental Study on the Start Up Performance of Flat Plate Pulsating Heat Pipe," J. Therm. Sci., 20(2), pp. 150-154.
[44] Lin, Z. R., Wang, S. F., Huo, J. P., Hu, Y. X., Chen, J. J., Zhang, W., and Lee, E., 2011, "Heat Transfer Characteristics and LED Heat Sink Application of Aluminum Plate Oscillating Heat Pipes," Appl. Therm. Eng., 31(14-15), pp. 2221-2229.
[45] Hansen, N., VerSteeg, J., and Michna, G. J., "Effect of Condenser Temperature on Pulsating Heat Pipe Performance," Proc. ASME 2013 Heat Transfer Summer Conference collocated with the ASME 2013 7th International Conference on Energy Sustainability and the ASME 2013 11th International Conference on Fuel Cell Science, Engineering and Technology, American Society of Mechanical Engineers, pp. V002T004A019-V002T004A019.
[46] Wang, J. S., Wang, Z. C., and Li, M. J., 2014, "Thermal Performance of Pulsating Heat Pipes with Different Heating Patterns," Appl. Therm. Eng., 64(1-2), pp. 209-212.
[47] Qu, W., and Ma, T.-Z., 2002, "Experimental Investigation on Flow and Heat Transfer of Pulsating Heat Pipe," Journal of Engineering Thermophysics, 23(5), pp. 596-598.
[48] Lee, W. H., Jung, H., Kim, J., and Kim, J., "Flow Visualization of Oscillating Capillary Tube Heat Pipe," Proc. Proceedings of the 11th International Heat Pipe Conference, Tokyo, Japan, pp. 131-136.
[49] Hoesing, M. P., and Michna, G. J., "Geometric Evaporator Enhancements of an Oscillating Heat Pipe," Proc. ASME 2015 13th International Conference on Nanochannels, Microchannels, and Minichannels collocated with the ASME 2015 International Technical Conference and Exhibition on Packaging and Integration of

Electronic and Photonic Microsystems, American Society of Mechanical Engineers, pp. V001T007A002-V001T007A002.
[50] Khandekar, S., Groll, M., Charoensawan, P., Rittidech, S., and Terdtoon, P., "Closed and Open Loop Pulsating Heat Pipes," Proc. K-4, Proceedings of 13th International Heat Pipe Conference, China Academy of Space Technology, Shanghai, China, pp. 38-51.
[51] Mameli, M., Araneo, L., Filippeschi, S., Marelli, L., Testa, R., and Marengo, M., 2014, "Thermal Response of a Closed Loop Pulsating Heat Pipe Under a Varying Gravity Force," Int. J. Therm. Sci., 80, pp. 11-22.
[52] Groll, M., and Khandekar, S., 2002, "Pulsating Heat Pipes: A Challenge and Still Unsolved Problem in Heat Pipe Science," Archives of Thermodynamics, 23(4), pp. 17-28.
[53] Liu, S., Li, J. T., Dong, X. Y., and Chen, H. Z., 2007, "Experimental Study of Flow Patterns and Improved Configurations for Pulsating Heat Pipes," J. Therm. Sci., 16(1), pp. 56-62.
[54] Wilson, C., Borgmeyer, B., Winholtz, R. A., Ma, H. B., Jacobson, D., and Hussey, D., 2011, "Thermal and Visual Observation of Water and Acetone Oscillating Heat Pipes," J. Heat Transf.-Trans. ASME, 133(6), p. 5.
[55] Bhuwakietkumjohn, N., and Rittidech, S., 2010, "Internal Flow Patterns on Heat Transfer Characteristics of a Closed-Loop Oscillating Heat-Pipe with Check Valves using Ethanol and a Silver Nano-Ethanol Mixture," Exp. Therm. Fluid Sci., 34(8), pp. 1000-1007.
[56] Rittidech, S., Pipatpaiboon, N., and Terdtoon, P., 2007, "Heat-Transfer Characteristics of a Closed-Loop Oscillating Heat-Pipe with Check Valves," Appl. Energy, 84(5), pp. 565-577.
[57] Supirattanakul, P., Rittidech, S., and Bubphachot, B., 2011, "Application of a Closed-Loop Oscillating Heat Pipe with Check Valves (CLOHP/CV) on Performance Enhancement in Air Conditioning System," Energy Build., 43(7), pp. 1531-1535.
[58] Thompson, S. M., Cheng, P., and Ma, H. B., 2011, "An Experimental Investigation of a Three-Dimensional Flat-Plate Oscillating Heat Pipe with Staggered Microchannels," International Journal of Heat and Mass Transfer, 54(17-18), pp. 3951-3959.
[59] Thompson, S. M., Tessler, B. S., Ma, H. B., Smith, D. E., and Sobel, A., 2013, "Ultrahigh Thermal Conductivity of Three-Dimensional Flat-Plate Oscillating Heat Pipes for Electromagnetic Launcher Cooling," Ieee Transactions on Plasma Science, 41(5), pp. 1326-1331.
[60] Smoot, C. D., and Ma, H. B., 2014, "Experimental Investigation of a Three-Layer Oscillating Heat Pipe," J. Heat Transf.-Trans. ASME, 136(5).
[61] Holley, B., and Faghri, A., 2005, "Analysis of Pulsating Heat Pipe with Capillary Wick and Varying Channel Diameter," International Journal of Heat and Mass Transfer, 48(13), pp. 2635-2651.
[62] Chien, K. H., Lin, Y. T., Chen, Y. R., Yang, K. S., and Wang, C. C., 2012, "A Novel Design of Pulsating Heat Pipe with Fewer Turns Applicable to all Orientations," International Journal of Heat and Mass Transfer, 55(21-22), pp. 5722-5728.
[63] Tseng, C. Y., Yang, K. S., Chien, K. H., Jeng, M. S., and Wang, C. C., 2014, "Investigation of the Performance of Pulsating Heat Pipe Subject to Uniform/Alternating Tube Diameters," Exp. Therm. Fluid Sci., 54, pp. 85-92.

[64] Smoot, C. D., Ma, H. B., Winholtz, R. A., Jacobson, D. L., and Hussey, D. S., 2013, "Thermal and Visual Observation of a Hybrid Heat Pipe," Heat Transfer Research, 44(1), pp. 31-42.
[65] Lin, Z. R., Wang, S. F., Zhang, W., Lee, E., Zeng, X. Y., and Tang, Y., 2011, "A Feasibility Study of Applying Pulsating Heat Pipe in Heat Sink," Journal of Enhanced Heat Transfer, 18(6), pp. 527-536.
[66] Iwata, N., Ogawa, H., and Miyazaki, Y., 2011, "Temperature-Controllable Oscillating Heat Pipe," J Thermophys Heat Tr, 25(3), pp. 386-392.
[67] Taslimifar, M., Mohammadi, M., Afshin, H., Saidi, M. H., and Shafii, M. B., 2013, "Overall Thermal Performance of Ferrofluidic Open Loop Pulsating Heat Pipes: An Experimental Approach," Int. J. Therm. Sci., 65, pp. 234-241.
[68] Ma, H. B., Borgmeyer, B., Cheng, P., and Zhang, Y., 2008, "Heat Transport Capability in an Oscillating Heat Pipe," J. Heat Transf.-Trans. ASME, 130(8), p. 7.
[69] Zhang, Y., and Faghri, A., 2002, "Heat Transfer in a Pulsating Heat Pipe with Open End," International Journal of Heat and Mass Transfer, 45(4), pp. 755-764.
[70] Bennett, B., Hewitt, G., Kearsey, H., Keeys, R., and Lacey, P., "Paper 5: Flow Visualization Studies of Boiling at High Pressure," Proc. Proceedings of the Institution of Mechanical Engineers, Conference Proceedings, SAGE Publications, pp. 260-283.
[71] Spinato, G., Borhani, N., and Thome, J. R., 2016, "Operational Regimes in a Closed Loop Pulsating Heat Pipe," Int. J. Therm. Sci., 102, pp. 78-88.

APPENDIX A – ERROR PROPAGATION

$$s_f = \sqrt{\left(\frac{\partial f}{\partial x}\right)^2 s_x^2 + \left(\frac{\partial f}{\partial y}\right)^2 s_y^2 + \left(\frac{\partial f}{\partial z}\right)^2 s_z^2 + \cdots}$$

where

s_f = Uncertainty of function f

s_x= Uncertainty of variable x

s_y= Uncertainty of variable y

s_z= Uncertainty of variable z

Thermal Resistance of Oscillating Heat Pipe

$$R_{OHP} = \frac{T_E - T_C}{Q} = \frac{\Delta T_{E\rightarrow C}}{Q}$$

where

R_{OHP} = Thermal Resistance of OHP, K/W

T_E = Average temperature of evaporator, °C

T_C = Average temperature of condenser, °C

Q = Heat transfer rate of OHP, W

Uncertainty Analysis of R_{OHP}

$$s_{R_{OHP}} = \sqrt{\left(\frac{\partial R_{OHP}}{\partial \Delta T_{E\rightarrow C}}\right)^2 s_{\Delta T_{E\rightarrow C}}^2 + \left(\frac{\partial R_{OHP}}{\partial Q}\right)^2 s_Q^2}$$

where

$$\frac{\partial R_{OHP}}{\partial \Delta T_{E\to C}} = \frac{1}{Q}$$

$$\frac{\partial R_{OHP}}{\partial Q} = -\frac{\Delta T_{E\to C}}{Q^2}$$

Calculating $s^2_{\Delta T_{E\to C}}$

First, the uncertainty of each thermocouple must be calculated, then the uncertainty in the evaporator and condenser sections.

$$s_{TC} = 0.2°C$$

Due to the thermocouples having a bias error, the uncertainty of the temperature measurement in the evaporator and condenser section is the following.

$$s_{T_E} = s_{T_C} = 0.2°C$$

Uncertainty in temperature difference

$$\Delta T_{E\to C} = T_E - T_C$$

$$s_{\Delta T_{E\to C}} = \sqrt{\left(\frac{\partial \Delta T_{E\to C}}{\partial T_E}\right)^2 s^2_{T_E} + \left(\frac{\partial \Delta T_{E\to C}}{\partial T_C}\right)^2 s^2_{T_c}}$$

$$\frac{\partial \Delta T_{E\to C}}{\partial T_E} = 1$$

$$\frac{\partial \Delta T_{E\to C}}{\partial T_C} = -1$$

$$s_{\Delta T_{E\to C}} = \sqrt{(1)^2(0.2°C)^2 + (-1)^2(0.2°C)^2} = 0.2828°C$$

Now, the uncertainty for heat transfer rate must be determined.

$$Q = P_{in} - Q_{loss}$$

where

Q = Heat transfer rate, W

P_{in} = Power input, W

Q_{loss} = Heat loss from OHP, W

$$s_Q = \sqrt{\left(\frac{\partial Q}{\partial P_{in}}\right)^2 s_{P_{in}}^2 + \left(\frac{\partial Q}{\partial Q_{loss}}\right)^2 s_{Q_{loss}}^2}$$

$$\frac{\partial Q}{\partial P_{in}} = 1$$

$$\frac{\partial Q}{\partial Q_{loss}} = -1$$

$$P_{in} = VI$$

where

P_{in} = Power input, W

V = Voltage, V

I = Current, A

$$s_{P_{in}} = \sqrt{\left(\frac{\partial P_{in}}{\partial V}\right)^2 s_V^2 + \left(\frac{\partial P_{in}}{\partial I}\right)^2 s_I^2}$$

$$\frac{\partial P_{in}}{\partial V} = I$$

$$\frac{\partial P_{in}}{\partial I} = V$$

$$s_V = 0.5\% = 0.005V$$

$$s_I = 1\% = 0.01I$$

$$s_{P_{in}} = \sqrt{(I)^2(0.005V)^2 + (V)^2(0.01I)^2}$$

$$s_{P_{in}} = \sqrt{(VI)^2(0.005)^2 + (VI)^2(0.01)^2}$$

$$s_{P_{in}} = \sqrt{(P_{in})^2((0.005)^2 + (0.01)^2)}$$

$$s_{P_{in}} = P_{in}\sqrt{(0.005)^2 + (0.01)^2}$$

$$s_{P_{in}} = 0.011P_{in}$$

The uncertainty of Q_{loss} is determined next.

$$Q_{loss} = UA(\Delta T_{E\to\infty})$$

where

UA = Overall heat transfer coefficient, W/K

$\Delta T_{E\to\infty}$= Temperature difference between evaporator and ambient conditions, °C

$$s_{Q_{loss}} = \sqrt{\left(\frac{\partial Q_{loss}}{\partial UA}\right)^2 s_{UA}^2 + \left(\frac{\partial Q_{loss}}{\partial \Delta T_{E\to\infty}}\right)^2 s_{\Delta T_{E\to\infty}}^2}$$

$$\Delta T_{E\to\infty} = T_E - T_\infty$$

$$s_{\Delta T_{E\to\infty}} = \sqrt{\left(\frac{\partial \Delta T_{E\to\infty}}{\partial T_E}\right)^2 s_{T_E}^2 + \left(\frac{\partial \Delta T_{E\to\infty}}{\partial T_\infty}\right)^2 s_{T_\infty}^2}$$

$$\frac{\partial \Delta T_{E\to\infty}}{\partial T_E} = 1$$

$$\frac{\partial \Delta T_{E\to\infty}}{\partial T_\infty} = -1$$

$$s_{T_E}^2 = 0.2°C$$

$$s_{T_\infty}^2 = 0.2°C$$

$$s_{\Delta T_{E\to\infty}} = \sqrt{(1)^2(0.2°C)^2 + (-1)^2(0.2°C)}$$

$$s_{\Delta T_{E\to\infty}} = 0.28°C$$

UA was found during the heat loss experiment using the method of least squares.

$$m = \frac{N\sum_{i=1}^{N} X_i Y_i - \sum_{i=1}^{N} X_i \sum_{i=1}^{N} Y_i}{N\sum_{i=1}^{N} X_i^2 - \left(\sum_{i=1}^{N} X_i\right)^2}$$

$$s_{\mathrm{m}} = \sqrt{\sum_{i=1}^{N}\left(\frac{\partial \mathrm{m}}{\partial Y_i}\right)^2 s_{Y_i}^2 + \sum_{i=1}^{N}\left(\frac{\partial \mathrm{m}}{\partial X_i}\right)^2 s_{X_i}^2}$$

$$s_{\mathrm{UA}} = \sqrt{\sum_{i=1}^{N}\left(\frac{\partial \mathrm{UA}}{\partial q_{loss,m}}\right)^2 s_{q_{loss,m}}^2 + \sum_{i=1}^{N}\left(\frac{\partial \mathrm{UA}}{\partial \Delta T_{E\to\infty}}\right)^2 s_{\Delta T_{E\to\infty}}^2}$$

$$s_{\mathrm{UA}} = 0.093$$

$$\frac{\partial Q_{loss}}{\partial UA} = \Delta T_{E\to\infty}$$

$$\frac{\partial \mathrm{UA}}{\partial \Delta T_{E\to\infty}} = UA$$

$$s_{Q_{loss}} = \sqrt{(\Delta T_{E\to\infty})^2 0.093^2 + (UA)^2 0.28^2}$$

Next, the uncertainty of the heat transfer through the OHP is determined.

$$s_Q = \sqrt{\left(\frac{\partial \mathrm{Q}}{\partial P_{in}}\right)^2 s_{P_{in}}^2 + \left(\frac{\partial \mathrm{Q}}{\partial Q_{loss}}\right)^2 s_{Q_{loss}}^2}$$

$$\frac{\partial \mathrm{Q}}{\partial P_{in}} = 1$$

$$\frac{\partial \mathrm{Q}}{\partial Q_{loss}} = -1$$

$$s_{P_{in}} = 0.011 P_{in}$$

$$s_Q = \sqrt{(1)^2 0.011 P_{in}^2 + (-1)^2((\Delta T_{E\to\infty})^2 0.093^2 + (UA)^2 0.28^2)}$$

Finally, the uncertainty of the thermal resistance can be determined.

$$s_{R_{OHP}} = \sqrt{\left(\frac{\partial R_{OHP}}{\partial \Delta T_{E\to C}}\right)^2 s_{\Delta T_{E\to C}}^2 + \left(\frac{\partial R_{OHP}}{\partial Q}\right)^2 s_Q^2}$$

$$\frac{\partial R_{OHP}}{\partial \Delta T_{E\to C}} = \frac{1}{Q}$$

$$\frac{\partial R_{OHP}}{\partial Q} = -\frac{\Delta T_{E\to C}}{Q^2}$$

$s_{R_{OHP}}$

$$= \sqrt{\left(\frac{1}{Q}\right)^2 0.2828°C^2 + \left(-\frac{\Delta T_{E\to C}}{Q^2}\right)^2 (1)^2 0.011 P_{in}^2 + (-1)^2((\Delta T_{E\to\infty})^2 0.0930^2 + (UA)^2 0.2828^2)}$$

Range of uncertainty for data is from 1.75% to 19.2%. The highest uncertainty is in the horizontal inclination angle, where there are lower power inputs but high temperature differences.